

The Amundsen Sea Expedition 2017 – 2018
(ANA08B)

Chief Scientist: SangHoon Lee

IBRV Araon, 21 December 2017 – 13 February 2018
(Christchurch to Christchurch, New Zealand)

Contents

- 1. Physical Oceanography..... 3**
 - 1.1. Hydrographic Survey 4
 - 1.2. Long-term Mooring Systems..... 9
 - 1.3. Ocean Robots Beneath Ice Shelf (ORBIS)..... 20
 - 1.4. Aero-geophysical Survey 27
 - 1.5. Autonomous Phase-sensitive Radio Echo Sounders (ApRES) 32
 - 1.7. Surface Drifter Deployment 37
 - Appendix 1.1. ANA08B cruise log spreadsheet..... 40
 - Appendix 1.2. All design diagrams of moorings..... 47
 - Appendix 1.3. Triangulation results 55
 - Appendix 1.4. ADCP deployment files..... 61

- 2. Chemical Oceanography..... 64**
 - 2.1. Nutrient measurements..... 64
 - 2.2. Observations of dissolved and particulate matters 65
 - 2.3. Observations of sulfur species in marine aerosols..... 67
 - 2.4. Noble gases as tracers of glacial meltwaters: sample collection and onboard measurements in the Amundsen Sea 69
 - 2.5. Underway measurements of net community production and dimethylsulfide in the Amundsen Sea 73
 - 2.6. Inorganic Carbon System 77

3. Biological Oceanography	80
3.1. Biodiversity of phytoplankton community.....	80
3.2. Phytoplankton ecology in the Amundsen Sea	85
3.3. Phytoplankton physiology (photochemistry)	90
3.4. Primary production and macromolecular composition of phytoplankton	92
3.5. Acoustics	96
3.6. Grazing impacts and community structure of heterotrophic protists.....	100
3.7. Mesozooplankton community	102
4. Biogeochemical Oceanography	110
4.1. Sediment trap.....	110
4.2. Sediment coring.....	113
5. Trace metals.....	117
5.1. Sampling using the Titan sampling system for trace metals	117
5.3. Trace Metal Biogeochemistry and Proteomics.....	122
5.4. Viral ecology	125
Appendix I. Cruise participants and contact information	130
Appendix II. Group photo	131

Chapter 1

Physical Oceanography

T.W. Kim¹, K.H. Cho¹, T.W. Park¹, H.W. Yang¹, Y. Kim¹, K.M. Assmann², J. Rolandsson², P. Dutrieux³, J. Gobat⁴, L. Beem⁵, T. Richter⁵, D. Buhl⁵, I. Durand⁶,

¹Korea Polar Research Institute (KOPRI), Incheon 406-840, Korea

²University of Gothenburg (UGOT), Gothenburg, Sweden

³Lamont-Doherty Earth Observatory of Columbia University, Palisades, NY, USA

⁴Applied Physics Laboratory, University of Washington, Seattle, USA

⁵University of Texas Institute for Geophysics (UTIG), Austin, TX, USA

⁶ LOCEAN/USM 402, National Museum of Natural Histories, Paris, France

요약문

2017/18년 겨울, 쇄빙연구선 아라온호를 이용하여 남극 아문젠 해에서 5번째 종합적인 해양 탐사를 실시하였다. 해양물리 분야의 주된 연구주제는 남극 순환 심층수(circumpolar deep water) 분포의 시공간적인 변동성을 규명하고 빙봉 용해수의 분포 및 해양 순환에 미치는 영향을 규명하는 것이다. 이를 위해 아문젠 해(Amundsen Sea)와 우딘체프 (Udintsev Fracture Zone)에서 총 53개의 CTD정점에서 수리적 자료와 해수 샘플을 획득하였다. 2016년도에 갯츠 빙봉(Getz Ice Shelf) 동쪽과, 폴리냐 (Polynya) 설치된 5기의 계류시스템을 성공적으로 회수하여 닷슨 빙봉(Dotson Ice Shelf), 갯츠 빙봉 전면과 폴리냐에 4기를 다시 계류하였다. 갯츠 빙봉 서쪽에 2016년 설치하였던 UGOT (University of Gothenburg)와 UIB (University of Bergen)의 계류 장비 전부를 성공적으로 회수 3기를 다시 계류하였다. 한편, ORBIS (Ocean Robots Beneath Ice Shelves) 프로그램의 일환으로 닷슨 빙봉 전면과 하부에 수온, 염분 및 수심 평균 유속의 장기 관측을 위한 3기의 Seaglider를 설치하였다. 그리고 아문젠 해 연안을 따른 해양 기원 열 수송에 따른 빙봉 변동을 파악하기위한 항공지구물리를 실시하였으며, 갯츠 빙봉 동쪽에는 빙봉의 속도와 변동성을 관측하기위해 빙봉 상부에 ApRES 두기를 설치하였다. 마지막으로 저층수온관측을 위한 총 6개의 T-Pops를 아문젠 해 연안에 설치하였으며 총 20개의 표층 부이를 우딘체프와 아문젠 해사이 이동시 투하하였다.

Abstract

In order to monitor the temporal and spatial variation of circumpolar deep water (CDW) and its effect on the rapid melting of glaciers in the Amundsen Sea and Udintsev Fracture Zone (UFZ), an extensive oceanographic survey was conducted on the 2018 expedition (ANA08B). The overall aims in the field of physical oceanography were: (1) to identify the temporal and spatial variation of Circumpolar Deep Water (CDW) and (2) to estimate the effect of meltwater from glaciers on the ocean circulation. During

the 2018 cruise (ANA08B) by IBRV Araon, a total of 53 CTD stations were visited. In UFZ, two moorings which installed in 2016 were recovered but one mooring was lost. Five KOPRI moorings were successfully recovered and 4 moorings were deployed again on the shelf troughs and near the ice shelf fronts. UGOT and UIB moorings placed at the western side of Getz Ice Shelf between Siple and Dean Islands and Siple and Carney Island during ANA06B was installed and recovered during ANA08B. Three moorings of UGOT was installed again at the western side of Getz Ice Shelf to study the ocean circulation in the Getz Ice Shelf cavity. Another element of the cruise was The Ocean Robots Beneath Ice Shelves (ORBIS) program, funded by the Paul G. Allen Family Foundation, and involving the University of Washington and Columbia University. This program aimed at developing technologies to observe the ocean cavities beneath the ice shelves over long periods of time (few months to one year), using Seagliders, float profilers and RAFOS beacons for under ice acoustic navigation. Preliminary results are exceptionally encouraging. In order to understand the evolution of West Antarctic Ice Sheet and assess glacier sensitivity to ocean warming and climate change, the aero-geophysical observations was operated during ANA08B over floating and grounded glacier ice along the Amundsen Sea Coast. On the other hand, two ApRES units were deployed on ANA08B, on the eastern side of Getz Ice Shelf and a total of six T-POP units were deployed at two separate sites on ANA08B. Additional, a total of 20 drifters were deployed between Urdintsev Fracture Zone and Amundsen Sea.

1.1. Hydrographic Survey

1.1.1. Introduction

The widespread thinning of the West Antarctic Ice Sheet and its floating ice shelves along the Amundsen Sea coast has been recorded in recent decades and recently attributed to intrusions of warm circumpolar deep water (CDW) onto the continental shelf (Jenkins et al., 2010). The intrusion of relatively warm CDW supplies heat to the ice shelves and has led to increased ice shelf melting (Walker et al., 2007; Wåhlin et al., 2010). The spreading of meltwater from the glaciers probably influences water mass properties and ocean circulation in the polynya. Despite the importance of the spatial-temporal variability of CDW in the continental shelf, vital knowledge for assessing the role of various forcing mechanisms is very limited, primarily due to a lack of in-situ data in this remote area with harsh weather, sea and ice conditions. In order to understand the CDW's role in the hydrodynamics in the Amundsen Sea, shipborne measurements were conducted during the 2017/18 expedition (ANA08B). The overall aims of the physical oceanography group are:

- To identify the temporal and spatial distribution of CDW on the Amundsen shelf,
- To reveal the main forcing that affects the flow rate of CDW onto the Amundsen shelf, and
- To identify the spreading of meltwater from ice shelves and its effect on the ocean circulation.

From these measurements, the oceanic heat transport to the glacier and its effect on the meltwater production will be estimated. The spreading of glacier meltwater to the adjacent sea will cause changes in water mass properties and ocean circulation patterns.

1.1.2. Materials and methods

An intensive oceanographic survey was conducted in the period of December 27, 2017 – February 2, 2018 using the IBRV Araon to understand the spatial and temporal variability of CDW on the Amundsen Shelf and poleward heat flux across the ACC in Urdintsev Fracture Zone (Figure 1.1). A total of 53 CTD stations were visited to collect hydrographic data as well as water samples. At each hydrographic station, at least one cast of the CTD/Rosette system with additional probes (e.g., dissolved oxygen, fluorometer, transmissometer, PAR, etc.) was conducted to measure the vertical profiles of temperature, salinity and other related biochemical parameters. The serial numbers and calibration information of each sensor are

given in Table 1.1. During the CTD upcasts, water samples were collected at several depths. For improved accuracy, the salinities of collected water samples were further analyzed by an Autosal salinometer (Guildline, 8400B). The measurement was performed when the temperature of water samples was stabilized to a laboratory temperature, usually within 48h after the collection. A lowered acoustic Doppler current profiler (LADCP, RDI, 300 kHz) was attached to the CTD frame to measure the full profile of current velocities. The bin size was chosen as 5 m, and the number of bins was 20. On the cruise track, the vessel-mounted ADCP (RDI, 38 kHz) was continuously operated.



Figure 1.1. Map of study area. Red dots denote the stations visited during ANA08B expedition.

Table 1.1. Configuration of CTD (SBE 911plus) sensors used during ANA08B cruise.

Sensor	S/N	Calibration date
Temperature 1	5191	Jun. 24, 2017
Temperature 2	5378	Jun. 24, 2017
Conductivity 1	3801	Jun. 20, 2017
Conductivity 2	4415	Jun. 20, 2017
Pressure	0932	Jul. 6, 2017
(Changed sensor on Dec. 29, 2017)	1241	Jul. 7, 2017
Oxygen	1984	Jun. 16, 2017
Fluorometer	FLRTD-3854	Jun. 27, 2017
Transmissometer	CST-1343DR	Jul. 19, 2017
PAR	1023	Jul. 2015
Altimeter	51306	Nov. 15, 2010
(Changed sensor on Jan. 15, 2018)	51676	Nov. 15, 2010

1.1.3. Preliminary results

In January 2018, a total of 7 CTD stations were visited along the Dotson trough to investigate the spatial CDW variability along the trough (Figure 1.2). Offshore of the Amundsen Shelf (St.53) the CDW was observed to be warmer than 1.6 °C, and the salinity was 34.7 psu. As the CDW enters onto the shelf region, CDW is modified (colder and fresher) by mixing with cold surface water as well as meltwater from glaciers and sea ice. The maximum temperature and salinity of MCDW at mouth of trough (St. 52) were 0.85 °C and 34.659 psu in Jan. 2018. The maximum temperature was slightly increased but salinity was decreased compared with in Jan. 2016 (0.78 °C and 34.664 psu). The strong inter-annual variability of MCDW was found in front of Dotson Ice Shelf (DIS). The isohaline has been deepened in front of DIS due to the strong Ekman down-welling by south flows at surface under the easterly wind field (Kim et al., 2016). Especially, the strong positive gradient of isohaline in meridional direction was found in Jan 2018. Probably, it will be accompanying with strong westward coastal current nearby surface. The transect across the Dotson Trough show the intrusion of warm CDW, tilting toward the eastern side of the trough (Figure 1.3). The existence of the warm, salty water mass suggests that the trough bathymetry plays an important role in defining the inflow/outflow pattern of CDW. Warm and salty southward MCDW inclines toward the eastern flank of the trough by the effect of the Coriolis force and local cyclonic circulation pattern along the east boundary of the polynya. The gradient of isohalines across the trough was steepest in 2016 and slightly decreased in 2018.

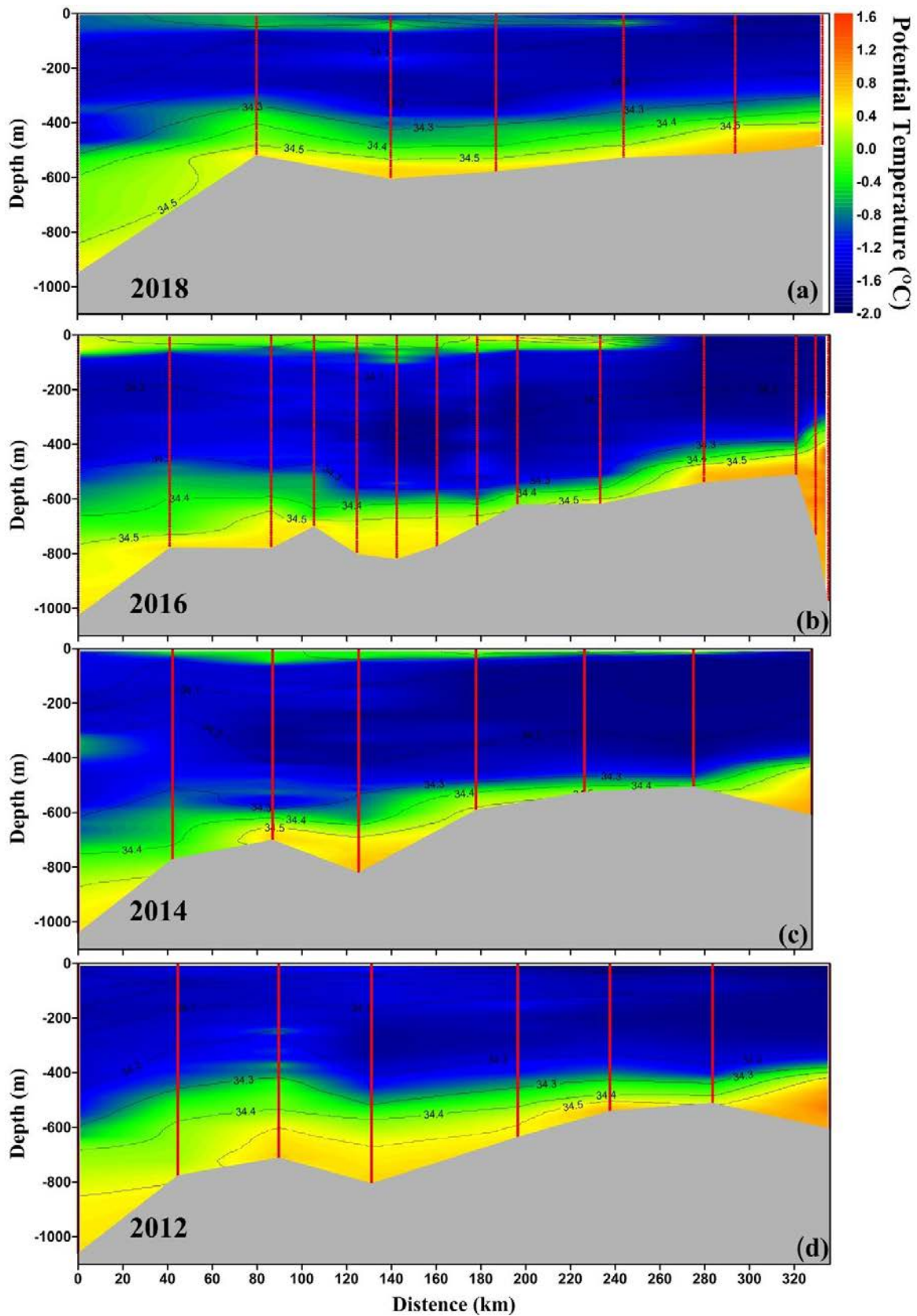


Figure 1.2. Vertical distribution of water mass properties along the Dotson Trough: (a) 2018 expedition, (b) 2016 expedition, (c) 2014 expedition, and (d) 2012 expedition. The color indicates the potential temperature, and the contour indicates the isohaline.

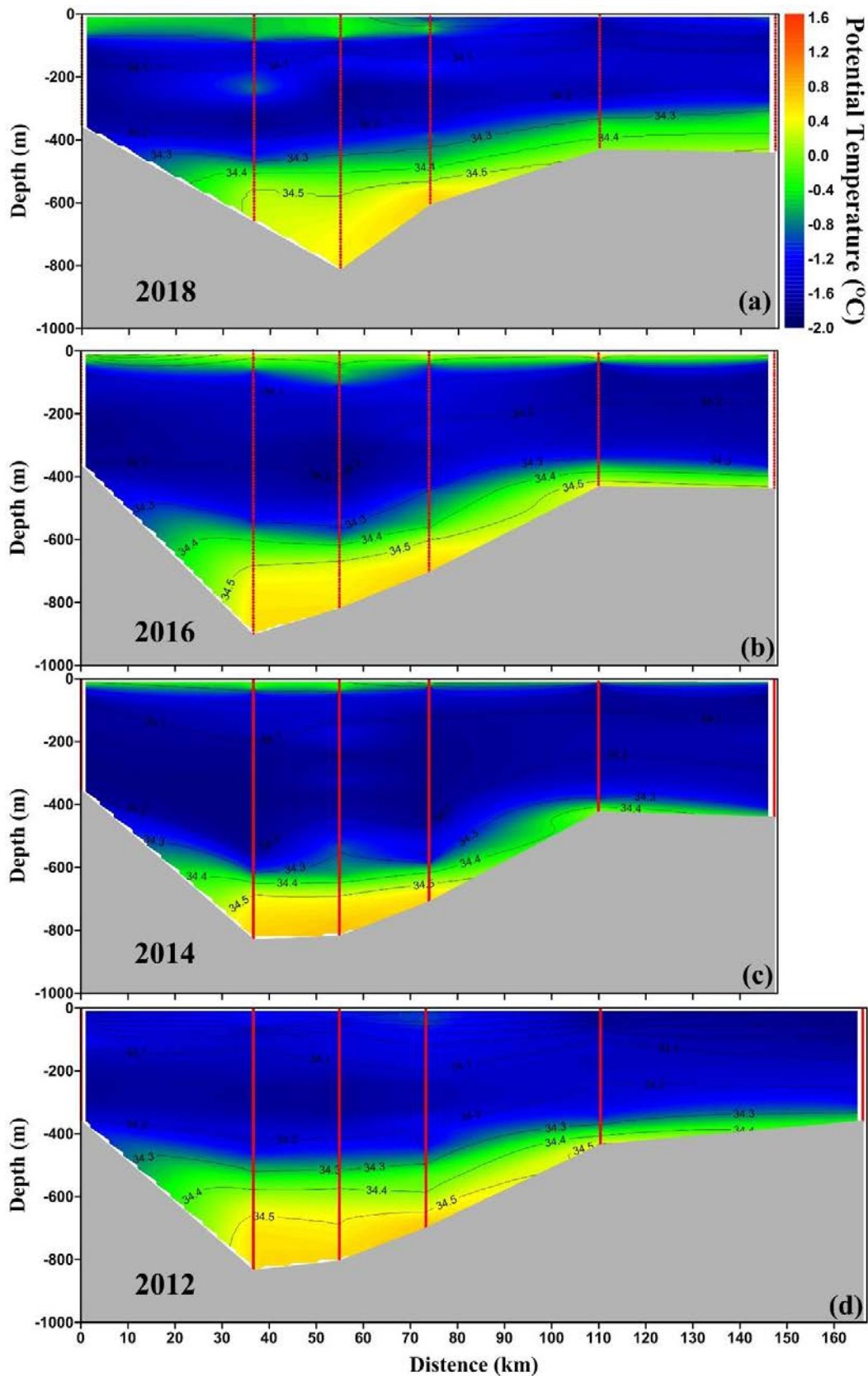


Figure 1.3. Vertical distribution of water mass properties across the Dotson Trough: (a) 2018 expedition, (b) 2016 expedition, (c) 2014 expedition, and (d) 2012 expedition. The color indicates the potential temperature, and the contour indicates the isohaline.

1.2. Long-term Mooring Systems

1.2.1. UFZ moorings

The main objective is to evaluate the cross-stream poleward heat flux across the Antarctic Circumpolar Current (ACC) in the Udintsev Fracture Zone (UFZ), South Pacific sector of the Southern Ocean. It is also intended to monitor the ACC transport at this choke point where the ACC is most strongly steered through the UFZ. For this ends, the LOCEAN and KIOST teams have installed in February 2016 three lines of current meters and Microcat-CTDs along a Jason satellite ground track. The February 2018 cruise consisted of recovering the mooring lines and making a CTD section (Fig. 1).

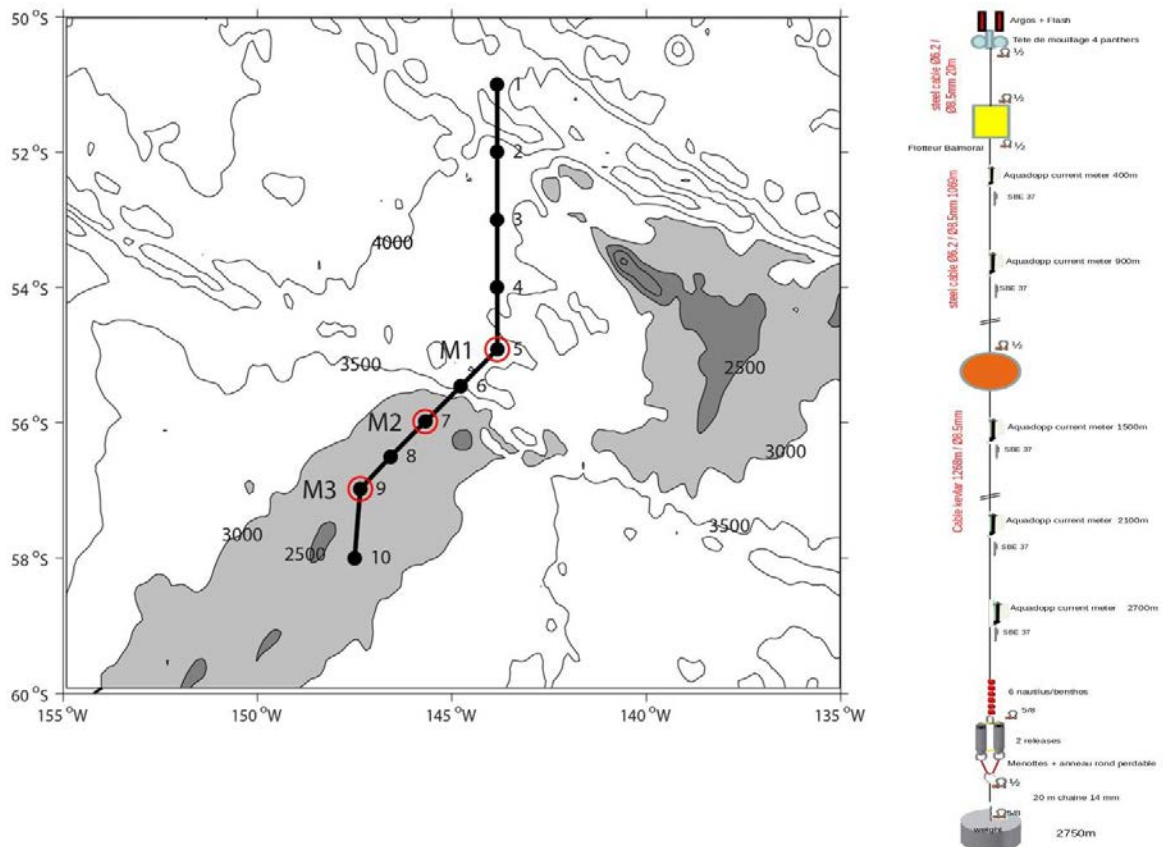


Figure 1.4. Recovery cruise plan on the Araon in the Udintsev Fracture Zone (27/12/2017-01/01/2018).

Recovery of mooring lines

M1 mooring was recovered on 30 December 2017 without any difficulty. The retrieved data have been communicated via email to the KIOST team (Drs. J.-H. Lee and C.-S. Hong).

M2 mooring was failed to recover on 31 December 2017 because the mooring line ceased to rise after it had risen for about 1000 m during the first 15 minutes and then stopped there forever. After about four hours of attempt to re-localize the mooring line, the PI and his team judged that the uppermost “Balmoral” float installed at a nominal depth of 450 m must have lost its floatability for unknown reasons, so it was useless to continue the recovery operations and left the station (c.f., Report loss and recovery attempt).

M3 mooring was recovered on 1 January 2018 after some difficulty with the releasers which did not respond to the first attempt of continuous calls on arriving at the station. After four hours of trials for re-localizing the mooring line within the nearby area, the Araon came back to the initial mooring position and the releasers responded to the first call, which was very fortunate but rests still mysterious. The recovered data indicate strongly that the “Balmoral” float indeed had lost its floatability and the first two current meters installed at nominal depths of 540 m and 1040 m, respectively, must have abruptly submerged over 1000 m since 17 January 2017, about one year before the recovery cruise (Figure. 1.5). This is probably the same reason why the M2 mooring did not have risen.

Preliminary results

Current meter data at M3 The pressure time series for the first two upper current meters clearly show a level off by about -1000 m from 17 January 2017 (Figure. 1.5a), indicative of the failure of the floatability of the “Balmoral” float, as already mentioned. Nevertheless, the recording seems correct for these current meters (Figure. 1.5b).

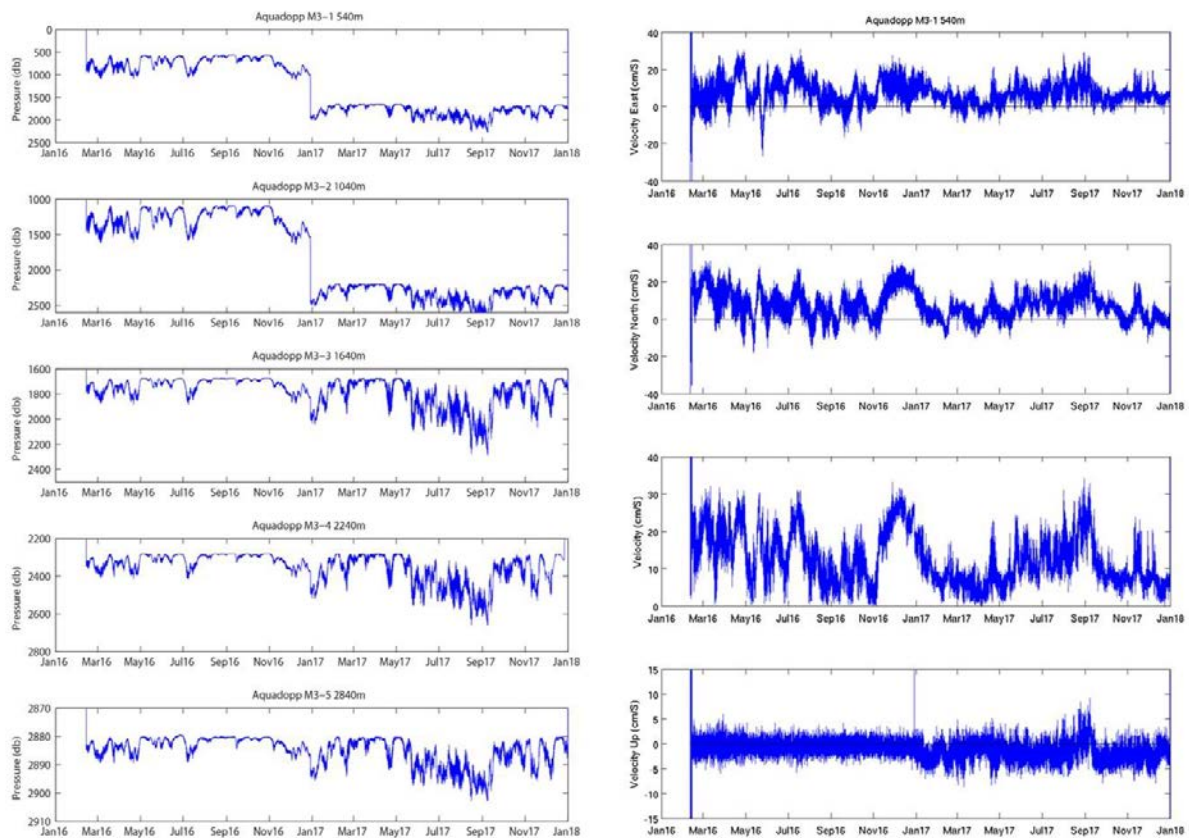


Figure 1.5. Timeseries variation of current velocity at M3

Salinity calibration The salinity of a total of 60 water samples (12 x 5 stations) was analyzed on board using an Autosol salinometer. The analyzed salinity was compared with the CTD salinity for two salinity sensors. Compared to the salinometer salinity, the first sensor (red) showed no significant difference of only +0.0001 ppt, while the second sensor (blue) did not work well with a mean difference of +0.013 ppt, especially at station 3 (Figure. 1.6a). The first sensor shows a nearly perfect superposition with the analyzed salinity (Figure. 1.6b). Therefore we conclude that the first sensor should be used and no salinity correction is necessary for the cruise.

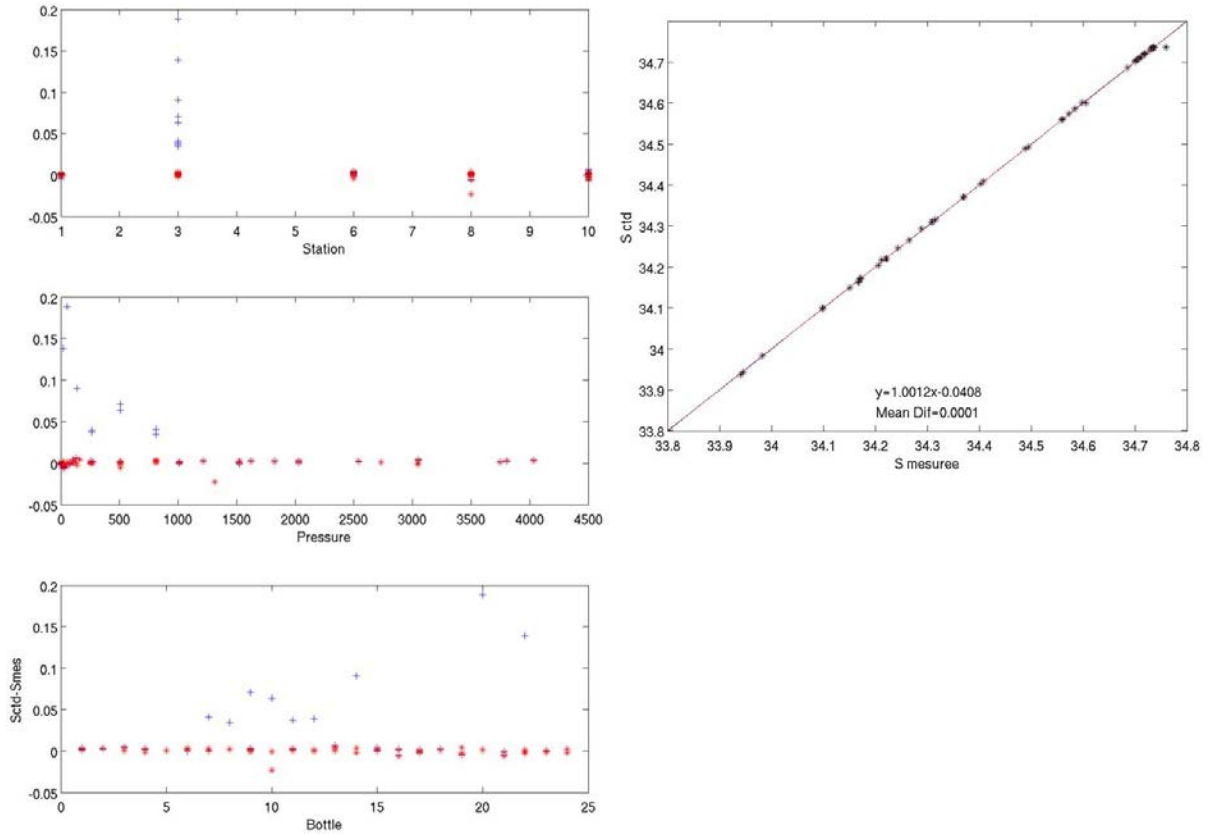


Figure 1.6. (a) Salinity difference ($S_{CTD} - S_{salinometer}$) as a function of station, depth, and bottle number. Red (blue) stands for the first (second) salinity sensor. (b) Linear regression of S_{CTD} from the first sensor with $S_{salinometer}$.

CTD data The T/S diagrams of the CTD data indicate no apparent errors in data acquisition and that the cruise covered entire breadth of the ACC, from the Subantarctic Front near the northernmost station to the Southern ACC Front at the southernmost station. More detailed analyses will be carried out in the future.

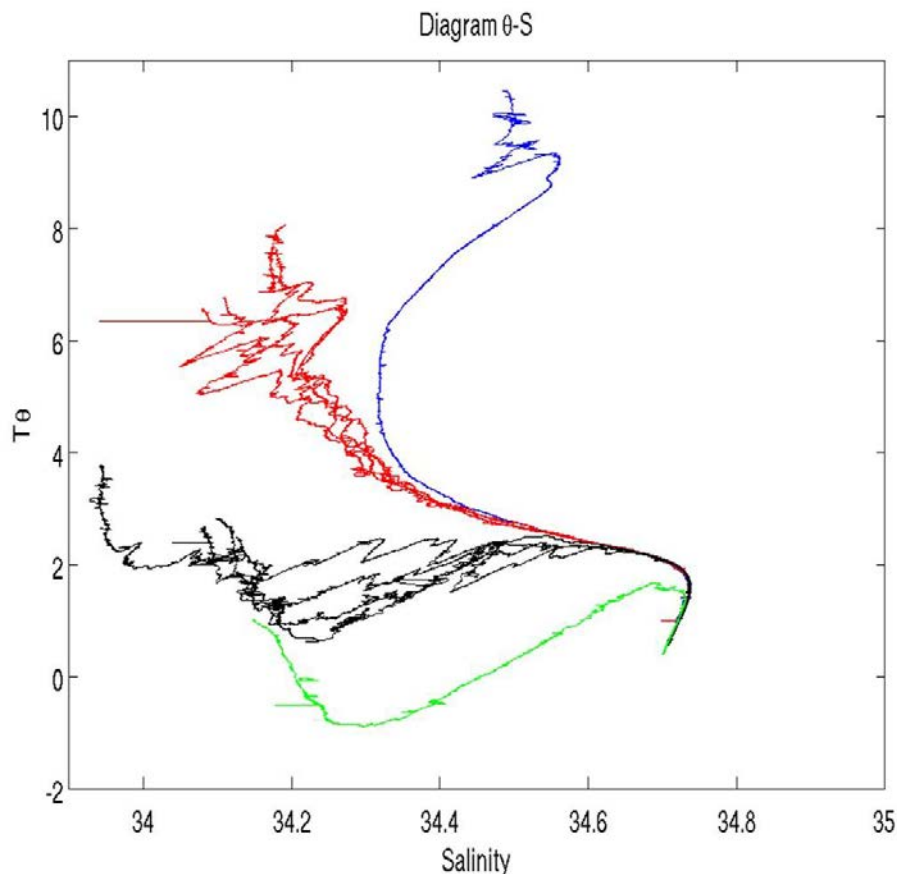


Figure 1.7. T/S diagrams for 10 stations shown in Figure 1.4, with blue for St. 1, red for Sts. 2-5, black for Sts. 6-9, and green for St. 10.

1.2.2. KOPRI moorings

Five mooring systems, installed in 2016 at the center of polynya (K2_2016), north of Martin Peninsula (K3_2016), in front of Getz Ice Shelf (K4_2016, K5_2016, K6_2016) were successfully recovered during ANA08B. Detailed information on the time table for recovery is given in Table 1.2. Four recovered moorings were redeployed in front of Getz and Dotson Ice Shelf and center of polynya to reveal the circulation pattern and pathways of CDW and meltwater from the glacier.

Recovery

The mooring positions were visited in sequence from west to recovery. For recovery and redeployment of the K4_2016 mooring system (western slope of Getz Ice Shelf east), Araon arrived at the mooring location on January 21 2018. Although, moorings were recovery and no lost sensors but some MicroCat were damaged by Icebergs. In additional, a numerous Icebergs were scattered around mooring position. The redeployment plan were abandon at this mooring position. Similar with K4_2016, some recovered MicroCat were damaged by Icebergs at two mooring stations (K5_2016, K6_2016) where located at eastern slope of Get Ice Shelf east. Therefore, we decided to maintain the eastern slope of Getz Ice Shelf east mooring changing the target depth of redeployment system to 800 m to protect the mooring from icebergs. Other moorings (K2_2016, K3_2016) were successfully recovered and measured the time series variation of temperature, salinity and current over more than two years. Detailed information on the recovered mooring contents was given in Table 1.2.

Table 1.2. Time table for recovery of mooring systems in ANA08B

Mooring Recovery	K2_2016	K3_2016	K4_2016	K5_2016	K6_2016
Date	01/23/2018	01/24/2018	01/21/2018	01/22/2018	01/22/2018
Latitude (S)	73° 16.6154'	73° 42.547'	73° 53.412'	73° 56.211'	73° 53.8805'
Longitude (W)	114° 56.7169'	114° 12.535'	118° 43.2182'	117° 15.981'	117° 15.8991'
Arrive station	19:25	17:59	0:28	23:54	17:15
Wakeup AR	19:27	18:00	0:34	(01/23) 0:04	18:00
Release	19:28	18:02	0:59	0:29	19:03
Find a Buoy	19:37	18:16	1:12	1:00	19:18
Finish recovery	03:48	19:17	3:24	2:05	20:36

Deployment

Total four mooring systems were installed in front of Getz Ice Shelf east (eastern slope: K4_2018) and Dotson Ice Shelf (eastern slope: K2_2018 and western slope: K3_2018) and center of polynya (K1_2018). K1_2018 is a key position for improving the understanding on the biochemical process in Amundsen Sea Polynya. K2_2018 and K3_2018, installed eastern and western slope in front of Dotson Ice Shelf to monitoring the intrusion of circumpolar deep water (CDW) and outflows of glacier meltwater. K4_2018 was installed at eastern slope of Getz Ice Shelf east for monitoring the circumpolar deep water (CDW) and associated rapid melting of glaciers in front of Getz Ice Shelf with installed three UGOT mooring systems at Getz Ice shelf west. The setups for MicroCats, ADCP and Aquadopp were summarized in Table 1.3 (MicroCat), Table 1.4 (ADCP), and Table 1.5 (Aquadopp). Detailed information on the deployment is given in Table 1.6. After the deployment, the triangulation was made to confirm the settlement status of moorings and record the exact GPS location for future recovery. The design diagrams and triangulation results for individual moorings are given in Appendix II and III.

Table 1.3. Summary of setups for moored MicroCat.

MicroCat		
	37-SM	37-SMP
Sample Interval	10 min	60 min
Deployment Endurance Calculator	1.5	1.5
Model Name	SBE 37 SM RS-232	SBE 37 SMP RS-232
Firmware	Firmware 3.0 and Higher	Firmware 1.0 and Higher
Pressure Sensor	Strain gauge	Strain gauge
Sample Interval (sec)	600	3600
Sampling Type	Autonomous	Autonomous
Transmit Real time	Not Enabled	Not Enabled
Deployment Temperature	-	-1
Deployment Pressure	-	500
Oxygen Time Constant (tau 20)	-	5.5
Battery Type	AA Lithium	AA Lithium
Battery Capacity	8.8 Amp-Hours	257040 Joules
Battery Endurance	5670 Days	
	Batteries are not expected to last longer 2 years	Pump on before sampling 110.2 seconds

Table 1.4. Summary of setups for moored ADCP.

ADCP			
		150 kHz	300 kHz
Deployment Timing Setup	Duration(days)	800	800
	Ensemble interval	15 min	30 min
	Ping int.	2 sec	2 sec
Profiling Setup	Pings Per	20	20
	Number of Depth	44	37
	Depth Cell size	8	4
Environmental Setup	Transducer Depth	450	560
	Salinity (ppt)	35	35
	Transducer Variation	0	0
	Temperature	-1	-1
Deployment Consequences	First cell range	12.21	6.17
	Last cell range	356.21	150.17
	Max range	355.47	105.61
	Standard deviation	1.59	0.79
	Ensemble size	1034	894
	Storage required	75.73	32.74
	Power usage	1568.77	401.68
	Battery usage	3.5	0.9
	Processing Bandwidth (BW)	Narrow BW	Narrow BW
	Power	Low	

Table 1.5. Summary of setups for moored Aquadopp.

Deployment	ANA08B
Current time	2018-01-24 5:38
Start at	2018-01-24 6:00
Comment	K1 2018 station
Measurement interval (s)	1800
Average interval (s)	60
Blanking distance (m)	0.5
Measurement load (%)	22
Power level	HIGH
Diagnostics interval(min)	1440:00:00
Diagnostics samples	20
Compass upd. Rate (s)	120
Coordinate System	ENU
Speed of sound (m/s)	MEASURED
Salinity (ppt)	35
Analog input 1	NONE
Analog input 2	NONE
Analog input power out	DISABLED
Raw magnetometer out	OFF
File wrapping	OFF
TellTale	OFF
AcousticModem	OFF
Serial output	OFF
Baud rate	9600
Assumed duration (days)	800
Battery utilization (%)	79
Battery level (V)	11.2
Recorder size (MB)	9
Recorder free space (MB)	8.973
Memory required (MB)	2.2
Vertical vel. prec (cm/s)	0.6
Horizon. vel. prec (cm/s)	0.4
Instrument ID	AQD13828
Head ID	A3L 8836
Firmware version	3.39

Table 1.6. Detail information on deployed KOPRI moorings. GPS location was determined by triangulation after finishing the deployment.

St.	Latitude (s)	Longitude (w)	Depth(m)	Release Date & Time (UTC)		CTD St.
				Date (YYYY/MM/DD)	Time (UTC)	
K1_2018	73° 16.764'	114° 56.968'	830	2018/01/24	12:21	33
K2_2018	74° 9.873'	112° 10.698'	800	2018/01/27	12:37	42
K3_2018	74° 10.253'	113° 19.107'	650	2018/01/26	14:08	36
K4_2018	73° 55.315'	117° 17.485'	800	2018/01/23	06:42	30

1.2.3. UGOT and UIB moorings

The array of UGOT and UIB moorings placed at the western side of Getz Ice Shelf between Siple and Dean Islands and Siple and Carney Island during ANA06B was designed to study the ocean circulation in the Getz Ice Shelf cavity. These moorings were complemented by three KOPRI moorings at the eastern opening of this part of the cavity between Wright and Duncan Islands to compare and contrast the two sides of the cavity and to investigate the existence of a possible connection between the two parts. The locations of mooring UiB1 (710 m depth) and Mooring UiB4 (600 m depth) were chosen to study the inflow of warm water towards the Getz ice shelf between Siple and Dean Island, while mooring UiB2 (600 m depth) was meant to capture the outflow of warm water-melt water mixture on the southwestern side of the same front. The inflow moorings are complemented by UGOT mooring S6, which was placed along the same isobath as UiB4, but much closer (within a Rossby radius) to the ice shelf front. By comparing the moorings it will be made clear how much of the water flowing towards the ice shelf front actually enters into the ice shelf cavity in a process study. UiB3 was placed at 650 m depth along the eastern slope leading into the ice shelf front between Siple Island and Carney Island to study the flow of water towards the Getz ice shelf through one of the minor openings into the ice shelf cavity.

On ANA08B we replaced this mooring array with three moorings between Siple and Dean Island. Two of the moorings, S7 and S8, were placed at a distance of 3nm to the ice shelf edge on the northeastern inflow side at 600m and 700m, respectively. The third mooring, S9, was placed on the southwestern outflow side of the cavity at a depth of just over 600m also around 3nm from the ice shelf edge. The other focus of the UGOT mooring work in the Amundsen Sea is the S1 site on the eastern side of the Getz-Dotson Trough on the outer shelf at a depth of around 550m. This site has been occupied by a mooring since 2010 monitoring the warm CDW inflow to the deep basin north of Dotson and eastern Getz Ice Shelves.

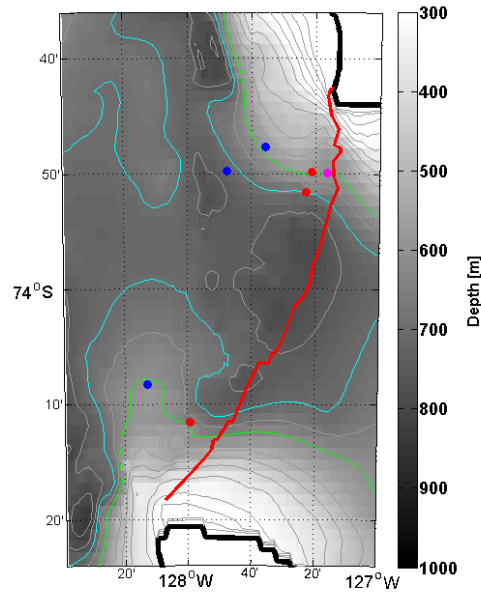


Figure 1.8. Map detail of the moorings at the western side of Getz Ice Shelf recovered and deployed during ANA08B. The bathymetry is from IBCSO. The green and cyan lines mark the 600 and 700m isobaths, respectively. The bold red line marks the late 2015 ice shelf edge.

UGOT Moorings

At the western Getz Ice Shelf, S6 was recovered at 20180118 17:21 (UTC) close to the front of the ice shelf without any particular issues. The top SBE37 #8016 had moved down the rope to the next instrument SBE56 #5815. Inspection of the data record revealed that the change in pressure coincides with a pressure spike presumably caused by an iceberg passing over the mooring. This event appears to have caused the instrument to move. SBE37 #8016 was undamaged and the data record is fine. We deployed three moorings at the western Getz Ice Shelf. Locations were chosen from the IBCSO bathymetry. The location of S7 was kept at the planned location, since the Multibeam depth was 600 m as planned. S8 was moved slightly into deeper water, as it turned out that the IBCSO depth was around 20 m too shallow and S9 was moved northeast along the ice shelf edge into deeper water, since the Multibeam indicated that the depth at the planned site was only around 570m instead of 600m. Details about mooring deployment and triangulation are given in Table 1.7 For mooring designs and results from triangulation, see Appendix II and III.

Table 1.7. Information about deployed UGOT moorings and positions.

	S1	S7	S8	S9
<u>Anchor Release</u>				
Latitude	72°26.636'S	73°49.7444'S	73°51.4953'S	74°11.5423'S
Longitude	116°26.919'W	127°20.9205'W	127°22.8781'W	127°59.4117'W
Depth (Multibeam)	554	604 m	705 m	639m
Time (UTC)	20180131 07:54	20180119 01:58	20180119 04:42	20180119 17:54
<u>Triangulation</u>				
Sound velocity	1453	1453	1453	1453
Lat1	72°26.6969'S	73°49.5562'S	73°51.3339'S	74°11.6613'S
Lon1	116°27.5737'W	127°20.5735'W	127°23.0244'W	127°58.5227'W
Range1	663 m	869 m	894 m	791 m
Lat2	72°26.4188'S	73°50.0257'S	73°51.6943'S	74°11.2718'S
Lon2	116°26.7400'W	127°20.4848'W	127°21.8355'W	127°59.5368'W
Range2	692 m	756 m	903 m	824 m
Lat3	72°26.7306'S	73°49.8172'S	73°51.7751'S	74°11.6998'S
Lon3	116°26.4908'W	127°21.9698'W	127°23.5600'W	128°00.3528'W
Range3	633 m	753 m	835 m	851 m
<u>Mooring Position</u>				
Latitude	72°26.633'S	73°49.852'S	73°51.623'S	74°11.551'S
Longitude	116°26.950'W	127°21.107'W	127°22.885'W	127°59.377'W
2-D error	8 m	10 m	11m	17 m
Depth, triangulation	544 m	591 m	691 m	617 m
<u>Acoustic release</u>				
SN	54247 (865)	72636 (R12K)	72637 (R12K)	50774 (866, 2yr)
Address/Release	A/C	36/39868	37/39869	E/F
Rx/Tx (kHz)	10.5/12.0	N/A	N/A	15.0/13.0
SN	54244 (865)	N/A	N/A	55011 (866, 4yr)
Address/Release	D/F	N/A	N/A	F/C
Rx/Tx (kHz)	9.0/12.0	N/A	N/A	11.0/12.0
Station Number	50	16	17	21

An unsuccessful attempt to recover S1 was made on 29 Jan 2018. We tried to wake up and range the ARU at two locations around 300 m from the deployment location and then 3-4 km to the west of the site in the direction of iceberg drift. At no point during the operation did we manage to contact the ARU. A Multibeam and EK60 survey of the vicinity of the deployment site did not show the mooring either. By this time an iceberg had moved over the mooring location damming the sea ice upwind of it, so that we did not blind-release the mooring due to the high chance of it surfacing under the sea ice or iceberg. We deployed an altered mooring design of S1 at a site 1 nm from the previous site on 31 Jan 2018. The change in position was necessary because the original site was covered in 100% sea ice and several icebergs. The deployment was performed in a small pool of open water without incident. Due to the heavy sea ice cover we did not attempt to release the old mooring on this occasion either.

The moorings are all equipped with SBE37 and SBE56. S7, S8, and S1 have in addition an RDI ADCP (150kHz/75 kHz). S7 and S8 have single Benthos R12K releases with an estimated lifetime of 4 years. S9 has a double Benthos 866A release with a standard 2-year release and a long-life 4-year release. S1 is equipped with a pair of Benthos 865A releases on loan from KOPRI with a battery life of 2 years. All SBE37 are pumped and measure temperature, conductivity and pressure. The following SBE37 have oxygen sensors in addition: 16262 to 16267, 11214, and 11213. These were set to measure every 7200 sec. The remaining SBE37 on S7, S8, and S9 are set to measure every 1800 sec, those on S1 every 900 sec. All SBE56 were set to a measurement interval of 120 sec. The downward-facing 75 kHz RDI ADCP on S8 has an ensemble interval of 7200 sec. The upward-facing 150kHz ADCPs on S7 and S1 have an ensemble interval of 1800 sec. The ADCP command files can be found in Appendix IV.

Table 1.8. Table summarizing the times and positions of the UGOT and UIB mooring recoveries.

	UIB4	UIB1	S6	UIB2	S1	UIB3
Date	20180118	20180118	20180118	20180119	20180129	20180131
Latitude (S)	73°47.671'	73°49.800'	73°49.895'	74°8.296'	72°27.250'	73°41.159'
Longitude (W)	127°35.807'	127°47.578'	127°16.682'	128°12.916'	116°21.270'	123°35.048'
Arrival at station	10:00	12:46	16:17	12:40	06:40	21:30
First contact AR	10:11	12:47	16:20	12:43		21:35
Released	10:16	unclear	16:21	12:48		unclear
At surface	10:20	13:10	16:25	12:50		21:53
Recovered	11:14	14:02	17:21	13:31		22:36

UIB Moorings

All four moorings belonging to the University of Bergen (UIB) that were deployed in 2016 during ANA06B were recovered during ANA08B. UIB1, UIB4 and UIB2 on the western side of Getz Ice Shelf (see Figure 1.8 and Figure 1.1 for locations) were recovered 18-19 January 2018 in calm seas and fine weather together with UGOT mooring S6. A first attempt was made to recover UIB3 at the central Getz Ice Shelf on 21 Jan 2018. The mooring location had been under fast ice or heavy sea ice cover for most of the cruise duration. When we reached the station position, the mooring position was in open water about 130m from the sharp edge of heavy sea ice. Strong winds and surface currents were both directed towards the sea ice edge. We ranged the mooring on 20180121 23:18 at 73° 40.9080' S and 123° 34.7115' W. The range of 797 m was found to be consistent with the mooring being at the triangulated position at deployment. After considering various options we decided not to attempt to recover the mooring, because of the danger of it drifting into the sea ice cover after release. We returned to the UIB3 location on 31 January 2018, found the site to be ice-free in calm weather and recovered the mooring. Positions and times of recovery are summarized in Table 1.8.

The releases on UIB1 and UIB3 did not give positive confirmation that they had been released, but the moorings eventually appeared at the surface, as specified in Table 1.8. We thus have no definitive time of release. The order of instruments on UIB4 was in the order that was marked on the diagram in the ANA06B cruise report, i.e., SBE56 #4592 was above SBE56 #4594. The 75kHz ADCP #21396, SBE56 #4590, SBE56 #4594 and 7 glass spheres were re-deployed on the UGOT moorings as specified in the mooring diagrams.

1.3. Ocean Robots Beneath Ice Shelf (ORBIS)

1.3.1. Motivation

The ocean cavities beneath polar ice shelves hundreds of meters thick are among the last uncharted and unexplored frontiers on Earth. Current knowledge, from a few, very costly data points retrieved by range-limited autonomous underwater vehicles (Dutrieux et al., 2014a; Dutrieux et al., 2014b; Jacobs et al., 2011; Jenkins et al., 2010) or through logistically demanding, costly ice-shelf drilling campaigns (Stanton et al., 2013) suggests that glacier–ocean interactions vary over a wide spectrum of scales in time and space. Only long-term observations in the ice-shelf cavity, resolving the thermohaline circulation and oceanic mixing from the seabed to the glacier–ocean interface, and their seasonal to inter-annual variability, will ultimately clarify how the varying ocean heat is actually transferred to the ice. Such deeper understanding is necessary to build improved parameterizations that could be exploited in coupled glacier–ocean models and used to significantly improve predictions of ice-flow behavior and future ice-sheet contribution to sea level.

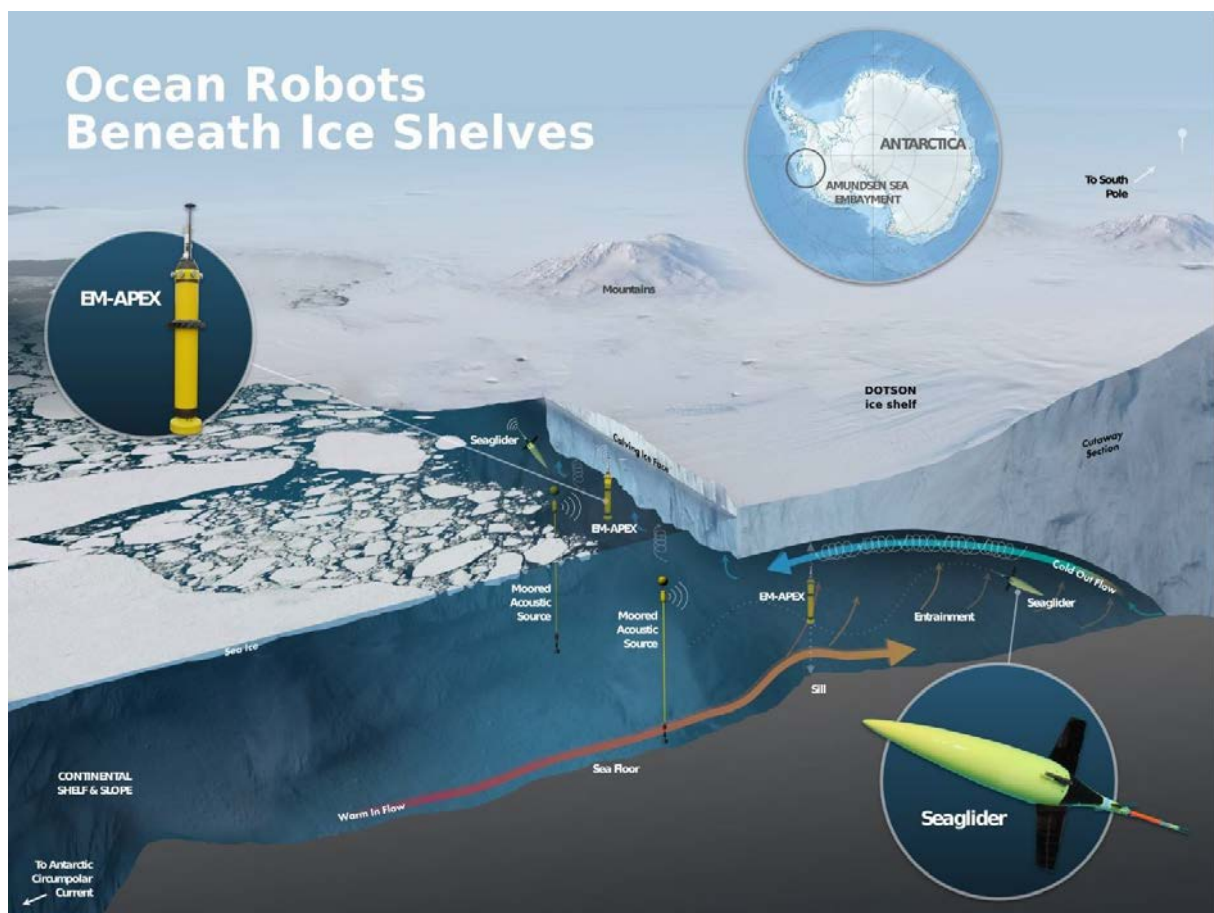


Figure 1.9. Schematic showing the assets deployed during the ORBIS program.

1.3.2. Objectives

Observation near and beneath ice shelves is logistically challenging. The ice geometry, which is carved by and drives oceanic melt, moves over the ocean at speeds reaching more than 10 m/day (or 4 km/yr). Although the glacier's bottom geometry can be mapped at multi-kilometer-scale using satellite observations, such highly dynamic environments limit the use of traditional propeller driven robotic submarines to short missions (1-3 days) with large logistical requirements (for example, the presence of an icebreaker for the duration of the mission). The observations, though informative, are inadequate to understand the glacier–ocean system due to their limited duration. Glacier–ocean interactions occur on

multiple timescales, from hourly to inter-annually and longer. In order to understand the glacier's response to the changing ocean forcing, we must observe the coupled interaction of the glacier and ocean throughout the entire ice-shelf cavity on all timescales.

The main objective of this project is to build on mature autonomous platforms with track records for under-sea-ice exploration and provide platforms for future, long term under-ice shelf explorations. Sea ice is a relatively thin sheet that has areas of open waters at the surface and a deep ocean beneath. In contrast, ice shelves are tens-of-kilometers long slabs of glacier ice that are hundreds of meters thick, and the ocean cavity beneath them has a very irregular, potentially entrapping, and constantly evolving geometry. For example, the undersides of the few ice shelves explored, instead of being smooth, are largely crevassed in places, and harbor inverted hills and valleys 100 to 400 m high and 1 to 4 km wide (Dutrieux et al., 2014a). The flanks of these hills are not smooth, but consist of terraces connected by 10 to 50 m high near vertical walls. The seabed beneath, carved by past glacier motion, can also feature large (hundreds-of-meters) topographic features (Jenkins et al., 2010). As a result of this complex geometry, the ocean water column thickness under the ice shelf can vary from 200 m to 0 m within a kilometer of horizontal distance. Sound propagation, reflections, and environmental noise are also unknown, making it difficult to assess the reliability of available technology for acoustic tracking and navigation in the ocean under the ice shelf.

To achieve long-term, spatially-distributed observations that resolve seasonal to inter-annual variability in ocean properties and circulation beneath ice shelves, we tested a network of relatively inexpensive, long-endurance, easily deployable robots (Figure 1.9). Our new approach exploits the complementary strengths of two platforms already working under sea ice: autonomous Seagliders, which can navigate between predefined targets, and EM-APEX floats that drift freely with horizontal ocean currents, to create an observational network within an ice-shelf cavity. Both technologies profile the cavity in three dimensions and relay observations via satellite upon exiting the ice-shelf cavity and surfacing at the ice-shelf front. Acoustic transmissions between elements of the network and moored sources at the ice-shelf front enable geolocation of the platforms under the ice shelf and/or sea ice. Seagliders are sampling the region near the cavity entrance, transiting repeatedly between ice-covered and open water, and transmitting scientific and operational data via satellite when clear of ice cover. Floats are using the dominant ocean circulation patterns in the cavity (relatively warm water entering at depth melts the ice and generates a buoyant fresh return flow at the ice-shelf base) to collect observations deep in the interior of the ice-shelf cavity. The network provides an evolving three-dimensional view of the under-ice environment.

1.3.3. Methodology and Deployments

Seagliders

Due to our limited knowledge of sound propagation under ice shelves and to verify general performance in the cavity, we are initially programming the Seagliders for a series of incrementally longer forays along the deep central trough beneath Dotson Ice Shelf (Figure 1.13). Mission complexity will be added over time, sending the glider deeper under the shelf along different transit lines. Present endurance capabilities should allow one-year of observations with periodic loitering at depth between scheduled sections. Seagliders can be equipped with a fairly wide range of scientific sensors, but for these initial missions and to save on energy consumption, they are measuring temperature, salinity and pressure by default, and dissolved oxygen and WetLabs optics (fluorometer, two channel backscatter) sporadically.

Autonomous floats

The under-ice ocean temperature structure with colder, fresher water overlying warmer, saltier water implies an exchange circulation driven by melting at the underside of the ice. The simplest way to get under the ice shelf, then, is simply to follow the inflow of warmer water. The EM-APEX control software

has been developed to allow an autonomous drifting vehicle to track a specific isotherm (e.g. 0.5°C or a value near the local near-bottom temperature determined from vertical profiles). After a pre-determined time span (15 days), the vehicle will switch to following a cold outflowing near-ceiling isotherm until it reaches open water, at which time all observations will be sent via satellite telemetry. The path followed will be reconstructed after the fact, using the same RAFOS navigation technology used on the gliders, as well as known cavity geometry, magnetic field anomalies, and measured current velocities. Eventually, we want to test the possibility of inferring float positions without the need for acoustic sources, which would open prospects of using this technology via air-deployments, hence significantly expanding their reach and usability. The EM-APEX measures temperature, salinity, pressure, and horizontal velocity when profiling. They are also equipped with sensors to measure turbulent mixing. The profiler drifts horizontally with the water velocity and moves vertically through active buoyancy adjustment, collecting up to 300 round-trip profiles from the surface to 2000 m depth on a single set of batteries. Upon surfacing, position is determined via GPS, and data are sent via Iridium satellite phone.

Table 1.9. Detail of ORBIS instrument deployments location and time

Asset	Deployment time	Deployment position
Seaglider SG221	2018-01-24 1626UT	73° 41.228'S, 114° 15.382'W
Seaglider SG222	2018-01-24 1632UT	73° 41.271'S, 114° 15.194'W
Seaglider SG223	2018-01-24 1637UT	73° 41.306'S, 114° 15.031'W
Sound source west	2018-01-26 2310UT	74° 11.786'S, 112° 43.106'W
Sound source central	2018-01-27 0316UT	74° 03.778'S, 112° 24.650'W
Sound source east	2018-01-27 1425UT	74° 12.485'S, 112° 07.679'W
EM-APEX 7495	2018-01-27 1543UT	74° 07.648'S, 112° 05.410'W
EM-APEX 7493	2018-01-27 1547UT	74° 07.681'S, 112° 05.964'W
EM-APEX 7494	2018-01-27 1550UT	74° 07.708'S, 112° 04.592'W
EM-APEX 7800	2018-01-27 1553UT	74° 07.734'S, 112° 04.245'W

Field Deployment

Dotson ice shelf and the neighboring Amundsen Polynya, West Antarctica, have been a major focus for investigations over past decades. The seasonal opening of the polynya in front of the ice shelf makes it an ideal candidate for testing the ORBIS platforms. Three types of instruments were deployed in front of the Dotson ice shelf: three Seagliders, three moorings hosting RAFOS sound sources, and four EM-APEX floats. Table 1.9 summarizes the locations and times for each deployed asset. Seagliders and EM-APEX floats were all deployed via the stern A-frame using a “slip stick” arrangement. With the ship moving ahead slowly at 1-2 knots, each vehicle was lifted off the deck via the lifting line as the A-frame was extended outboard. With the A-frame fully extended, the vehicles were lowered to the water. Just as they touched the water, the stick was pulled to release lift line. In good weather the deployments went quickly (about 3-4 minutes per vehicle) and without any problems.

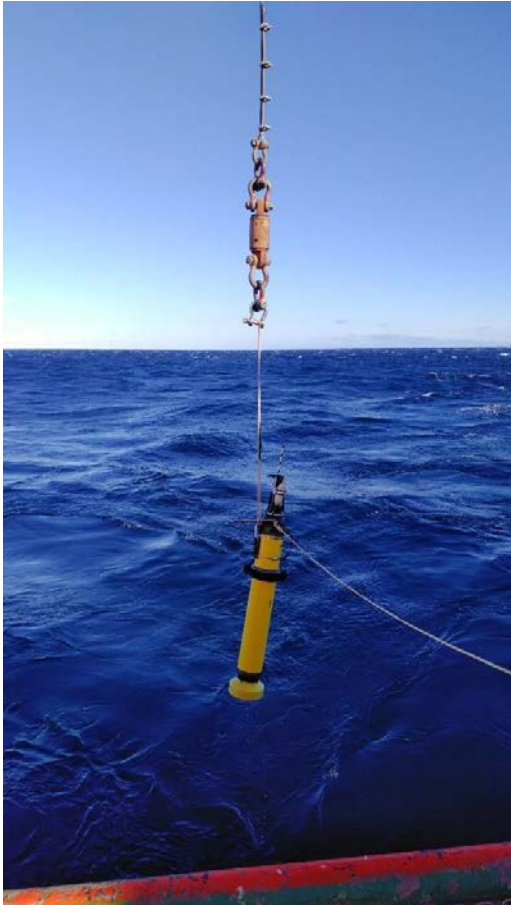


Figure 1.10. EM-APEX float being lowered to the water from the stern A-frame.



Figure 1.11. Detail of slip stick arrangement on the EM-APEX lifting handle.



Figure 1.12. Seaglider being lowered to the water via slip stick lifting line looped around the rudder.

1.3.4. Initial Results

Seagliders: As of the writing of this report, each glider has performed well, accomplishing up to 95 dives per platform. Initially launched to the north-west of the Dotson ice shelf, they were piloted in the deep portion of the Dotson trough and have since realized a series of sections both along the Dotson trough and along the Dotson ice front at varying distance (~35km, ~16km, ~7km), with some of the later being repeated multiple times (Figure 1.13). One glider (SG222) successfully performed 2 forays under the central portion of the ice shelf, extending ~5km (Figure 1.14) and ~15km from the ice front, respectively, and reporting good navigational abilities using acoustics. We plan to continue exploring the cavity as much as possible before the sea-ice closes in on satellite communications. After that, we will reduce the number of under-ice shelf incursions and along-ice shelf front sections to ~one per month, using loitering in the interim, to save energy and allowing the glider batteries to last until the following boreal Spring, the reopening of the polynya and satellite communications. Seaglider data is available and updated in real time at the following address: http://iop.apl.washington.edu/seaglider/index.php?mission=ORBIS_Jan18.

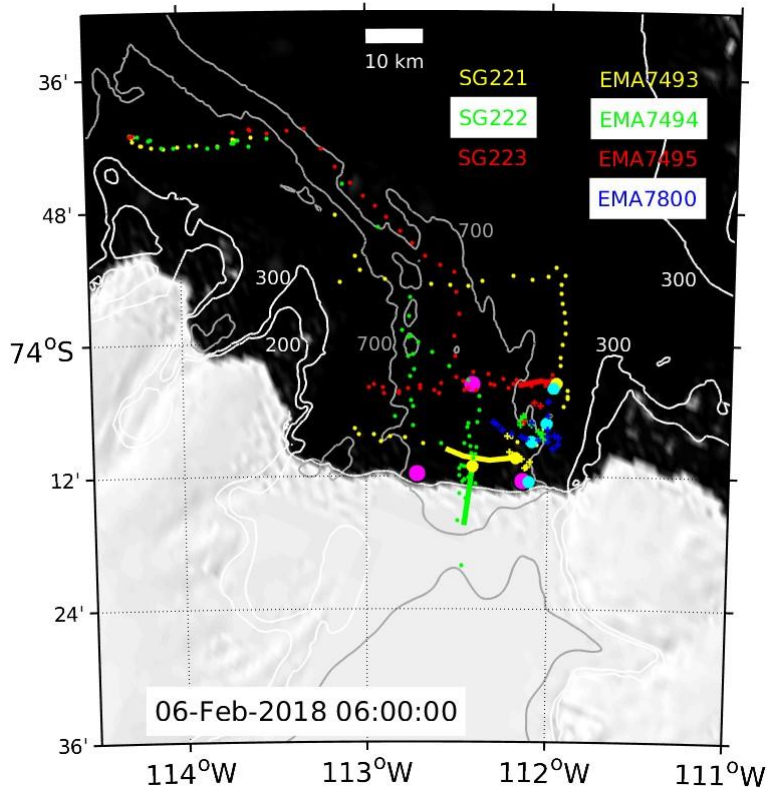


Figure 1.13. ORBIS color-coded Seagliders (dots) and EM-APEX floats (crosses) sampling in front of and under Dotson ice shelf as of February 6th, 2018. Gliders/Floats last recorded positions are denoted by the yellow/cyan disks, and the last day of Seaglider track highlighted by a color-coded line. Sound beacons location are marked by magenta disks. Background is a MODIS photo at 1km resolution. Contours indicate 200 and 300m isobath (white) and the 700m isobath (gray) from the Millan *et al.*, 2017 gravimetry inversion.

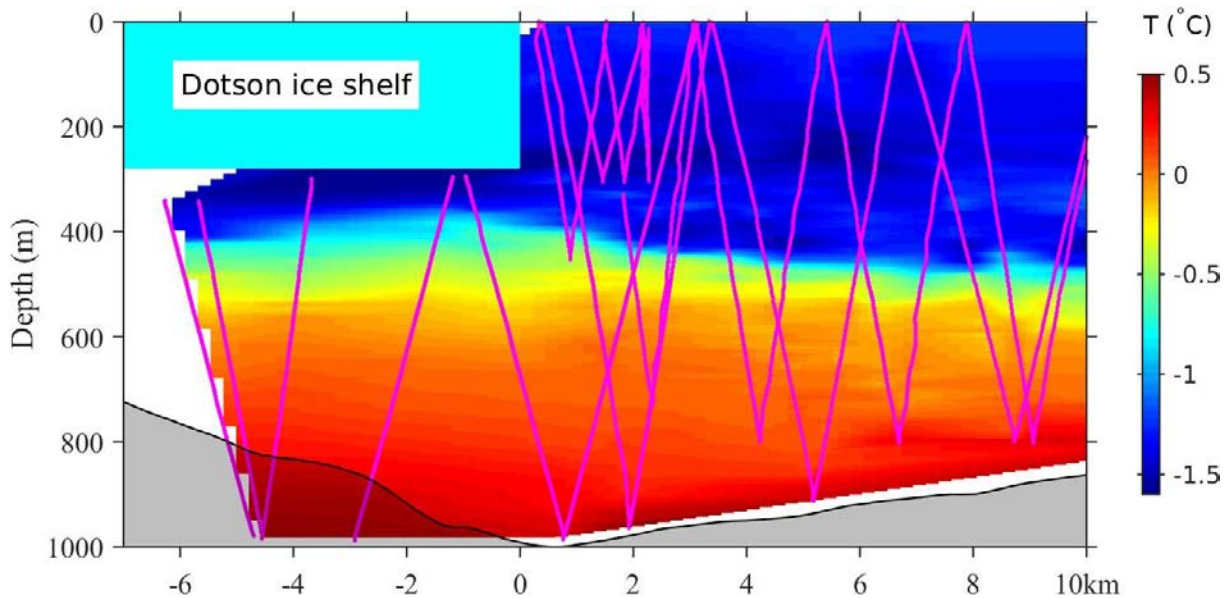


Figure 1.14. Surface referenced potential temperature along the first (ever!) acoustically tracked Seaglider under-ice-shelf survey. Magenta dots indicate the sampling location. The Dotson ice shelf is represented by an ad-hoc cyan rectangle, while the seabed (grey shading) is interpolated along a median glider line using the Millan *et al.*, 2017 gravimetry inversion.

Autonomous floats

All 4 floats are active, and most systems are working on most floats. All project float data is available and updated in real time at the following address: <https://ohm.apl.uw.edu/~emapex/> . Here is a brief summary of the results so far.

→ 7493 has a CTD temperature bias, cascading into a bias in conductivity observations. Velocity, microstructure, and RAFOS positions are all working well (see second figure below, especially the bottom two panels showing the comparison between GPS and RAFOS). The last call was at 03:42 GMT on Jan 31, from about 1 km north of the ice face. This float has now very likely managed to go under the ice shelf.

→ 7494 is probably the best performing EM-APEX overall (Figure 1.15), but hasn't managed to make much southward progress yet. EM velocity, CTD, and microstructure systems are working well, but RAFOS positions are off and needs to be worked on.

→ 7495 is calling in very infrequently (only 4 round-trip profiles, in contrast to 8, 11, and 16 in the other 3 floats so far) and not providing EM velocity data after the first profile. There may be a problem with the electronics. It does seem to be going all the way to the bottom and drifting at 625m (at least some of the time), but the large gaps in the record make it difficult to analyze progress. It has also been hearing the RAFOS sources, just not recording them very often. Some of the CTD and microstructure profiles seem reasonable when they occur, so at the very least we will obtain those observations in spite of its problems.

→ 7800, after initial latency in calls, is now calling in frequently (every 4.5 hours) because it has moved into water shallower than its intended drift depth. We are working on correcting this. Microstructure seems to have broken after the first profile, but everything else (velocity, CTD, RAFOS) is working as intended.

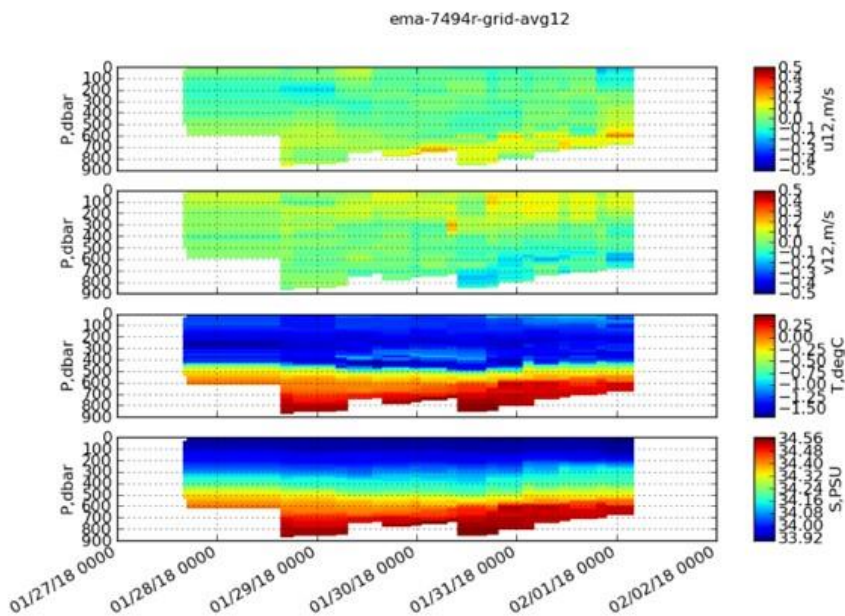


Figure 1.15. **EM-APEX observations.** A little more than 4 days of profile observations of zonal and meridional component of velocity, temperature, and salinity realized by float 7494.

1.4. Aero-geophysical Survey

1.4.1. Summary

A collaboration between Korea Polar Research Institute (KOPRI) and the University of Texas Institute for Geophysics (UTIG) collected aero-geophysical observations over floating and grounded glacier ice along the Amundsen Sea Coast. The goal of the season was to collect data to understand the evolution of West Antarctic Ice Sheet and assess glacier sensitivity to ocean warming and climate change, as well as to further the technological and logistical development of a helicopter based aero-geophysical platform. Primary science targets were Thwaites Glacier, Getz Ice Shelf, and Dotson Ice Shelf, but due to logistical constraints and helicopter mechanical issues only two of the five planned flight days were accomplished, one over Getz Ice Shelf and the other over Dotson Ice Shelf. Thwaites Glacier was not surveyed this year. The aero-geophysical platform collected ice sounding radar, magnetic field strength, ice surface elevation, and optical imagery over a total line distance greater than 1600 km.

The helicopter based aero-geophysical instrument suite utilized in this project is the same as first operated from Jang Bogo during the 2016-17 Antarctic summer, upgraded with the addition of a magnetometer. To the authors' knowledge this work constituted the first time scientific ice-penetrating radar has been operated from a ship-based aircraft.

1.4.2. Introduction

The goals of the season consisted of the first airborne ice penetrating radar survey of an ice sheet launched from a ship, the scientific investigation of changing conditions of the margins of the West Antarctic Ice Sheet, and the demonstration of operations of the KOPRI/UTIG helicopter geophysical platform aboard a ship. The Amundsen Sea region has a recent history of rapid changes, including glacier acceleration (Joughin et al., 2014), grounding line migration (Rignot et al., 2014), and submarine melting (Paolo et al., 2015). Each of the survey targets, Thwaites Glacier and Getz Ice Shelf, and Dotson Ice Shelf, have exhibited these changes which are potentially indicative of ocean warming and climate evolution (Pritchard et al., 2012). The observed glaciological changes in this region are consistent with the mechanisms of rapid sea level rise.

Rapid sea level rise is thought to occur from either or both processes of marine ice sheet retreat (Mercer, 1978) or ice cliff failure (Pollard et al., 2015). The progression of these feedbacks depends on geometry of the ice and bed, the bed character (geology and hydrology), and a perturbation to start the retreat feedback (potentially submarine melting at the grounding line). Aero-geophysical survey is an effective means to investigate each of these necessary conditions. Radar can evaluate ice geometry, bed shape, and bed character when ice is grounded. Observed magnetic field strength is indicative of the subglacial geology. For floating ice, the radar defines the upper geometry of the ice-shelf cavity and magnetic field strength contributes to gravimetric inversions for water column thickness by constraining bedrock density models.

Tectonic evolution of the Antarctic continent is another important scientific inquiry where aero-geophysical observations make meaningful contributions. Magnetic field strength data are used to interpret subglacial geology and the geology's link to both the tectonic evolution of the continent and the feedbacks expressed on glacial systems (e.g. Gohl et al., 2013). An international consortium, ADMAP, is compiling a mosaic of the magnetic anomalies of the Antarctic Continent (Golynsky et al., 2001) and the Amundsen Sea region has large areas without observations (including Getz Ice Shelf). Magnetic field strength data collected during ANA08B cruise will fill gaps in understanding for this important international collaboration to understand Antarctic geologic history.

The season also served to further technological and logistical developments of the helicopter based aero-geophysical platform. A new instrument, a magnetometer was added to the forward boom and since this

was the first season of flying extensive surveys from a ship, the associated logistical complexities were addressed for the first time. These developments further prove the capabilities of this geophysical instrumentation and expand the scientific possibilities and targets for the future.

1.4.3. Survey Instrumentation and Logistical Development

The primary geophysical instruments aboard the helicopter are an ice-penetrating radar sounder for profiling and characterizing the ice and bed directly below the aircraft, a scalar magnetometer to help constrain geology along the survey lines, and a laser surface profiler (see Figure 1.16). Auxiliary instrumentation consisted of inertial navigation system, geodetic GPS and down-looking camera.

Ice penetrating radar

The radar transmits and receives signals from two antennas located in booms that extend to the sides of the aircraft. A short FM pulse (chirp) centered at 60 MHz and with 15 MHz bandwidth is digitally synthesized, amplified to 8 kW and transmitted. Signal returns from the surface, within the ice and at the bed are received by the same antennas then amplified, digitized and recorded. The radar transmits and receives 6000 pulses per second. The system maintains phase coherency, and signals received by the antennas are digitized separately to allow cross-track interferometric processing.

This radar system was successfully flown aboard the same helicopter (ZK-IBH) last year (2016-17 season) from Jang Bogo Station. It is also effectively the same radar system operated by UTIG on the DC-3T platform across much of Antarctica since 2008 (Peters et al., 2007) as the High Capability Radar Sounder version 2 (HiCARS2) system and the Multi-frequency Airborne Radar-sounder for Full-phase Assessment (MARFA).

Magnetometer and Base Magnetometer

A magnetometer sensor is installed in the boom extending to the front of the aircraft. The instrument is a commercial, cesium vapor, scalar magnetometer produced by Geometrics, model G-823A. Data from the unit is time stamped and recorded by the same data system that handles the radar data. Additionally, an identical magnetometer is configured to be deployed at a fixed location on the ice surface as a “base” magnetometer. The base magnetometer is used to characterize short timescale fluctuations in the Earth’s magnetic field not related to local geology and topography.

Laser Altimeter and Optical Imagery

A commercial laser range finder is installed looking downward through a window in the cockpit. This instrument, combined with data from an inertial navigation system and geodetic GPS, provides another way to locate and characterize the surface of the ice. A digital SLR camera is installed and set to take overlapping, geo-tagged images of the ice directly below the aircraft. The images can be used to provide context for the geophysical instruments and for photogrammetry.

Logistical Development

For safety reasons two helicopters must be available at all times during flight operation. The two helicopters are i) a survey helicopter which is configured with the scientific instrument suite (see Figure 1.16) and ii) a utility helicopter which is available for Search and Rescue (SAR) and other operational needs. A typical flight day operation had the survey helicopter flying for 8 to 10 hours, while the second helicopter was engaged in supporting both the survey and other scientific operations on the ice sheet.

Building off the success of the 2016-17 survey season based out of Jang Bogo Station, the ANA08B cruise used a fuel caching system to extend the range of the survey helicopter. The utility helicopter can

simultaneously carry up to three full barrels of fuel. Establishing a fuel cache of between 4 and 6 barrels is enough to support up to 10 hours of the survey helicopter flight time (including the initial full tank when departing the ship) without necessitating a mid-day return to the ship.

Logistics of ship-based helicopter survey operations are determined by considerations of Safety / SAR needs, pilot duty day regulations, fuel consumption and availability, and additional helicopter operational requirements. Careful scheduling of helicopters was necessary to mitigate risks and optimize science and operational goals. Basic helicopter operational safety requires that two helicopters be flyable and remain within 100 nm of each other in case any SAR needs develop. An additional safety requirement is that the helicopters do not fly over more than 500 m of open water. Thick sea ice (>70 cm), ice shelf, or land can serve as suitable landing spots. It is possible for the helicopter to use multiple ice floes to reach the Antarctic coast and not violate the 500 m open water safety rule, although this option was not used in ANA08B. From a flight operations perspective having the ship be within 500 m of the Antarctic coast (grounded or floating glacier ice) is preferred. For both flight days of ANA08B the ship moved to within 500 m of an ice shelf edge. Related to safety needs is the limitation on the pilot duty day, maximum 10 hours of flight time within a 12-hour duty day, followed by 12 hours off-duty before further flights.

Flexibility of ship/flight scheduling was essential for this year's successful operations. Weather above Antarctica is notoriously variable and harsh. Allowing the ship to move into flight position when a period of flyable weather occurred maximizes the chance of flight success. We believe that without the support and flexibility of ship-time scheduling, capitalization on periods of suitable weather would have been difficult or impossible.

Ship mobility during helicopter logistics was a concern during the field season. Although during both ANA08B flight days the ship remained stationary for the entire operation, plans for ship mobility were developed during the field season. From a flight operations perspective a stationary ship is preferred and aero-geophysical success is partially due to logistical freedom of having the ship (and its fuel source) remain available during the entirety of the flight day. If on future cruises maximizing ship time for simultaneous airborne and ship-based operations are desired, there are logistical mechanisms that can be used, however these reduce the day's helicopter operational achievements. Further, ship mobility increases the risk of personnel engaged in unscheduled camping on the ice sheet and increases the risk of weather conflicts. These considerations should be weighed against the goals and priorities of the expedition.

The aero-geophysical survey flights were tightly integrated into a complete helicopter operations plan for each flying day that also included support for ApRES installations on the Getz Ice Shelf and Automatic Weather Station site reconnaissance.

1.4.4. Survey Accomplishments

Two flights were flown during the 2017-18 ANA08B cruise, one on January 22, 2018 over Getz Ice Shelf and the other on January 25, 2018 over Dotson Ice Shelf and Kohler Glacier (see Figure 1.17). Over 1600 km of survey line were flown that will further understanding of ice shelf cavity geometry and change, tectonic evolution of Antarctica, and grounding zone dynamics of the Kohler Glacier. This year's survey flights were partially conducted along existing airborne gravity observations that do not include co-located measurement of magnetic field strength.

During the first flight day, over Getz Ice Shelf, three survey legs were flown totaling about 8 flight hours and 800 km. A fuel cache was setup and used for three refueling stops. Targets were primarily re-flights of Operation Ice Bridge flight lines that do not include magnetometer data. This data can be used to improve gravimetric inversions for water column thickness beneath the ice shelf.

During the second flight day, over Dotson Ice Shelf, flew for 9 hours and totaled 850 km. Three survey legs were flown from the ship with refueling on-board between each leg. Two of the survey legs targeted existing Operation Ice Bridge lines and the third leg was flown to capture the grounding line character of Kohler glacier.

During the Dotson Ice Shelf flight day the utility helicopter established a 6-barrel fuel cache ($-75^{\circ} 13.720'$ N $-109^{\circ} 15.511'$ E) to support an anticipated flight to Thwaites Glacier. However, due to a mechanical failure on one of the helicopters, no additional flights were possible and the 6 barrels of fuel had to be left in place.



Figure 1.16. Configured survey helicopter with booms.

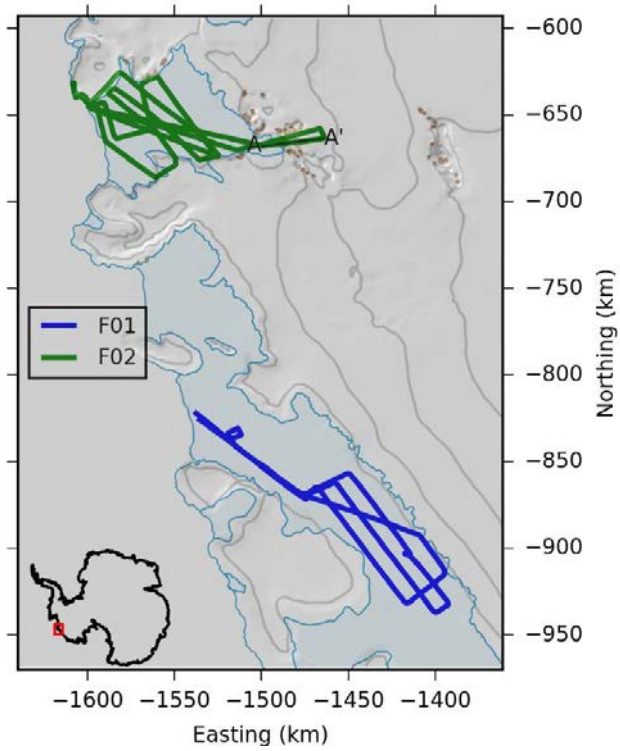


Figure 1.17. Survey lines flown. A to A' is location of radargram shown in Figure 1.18.

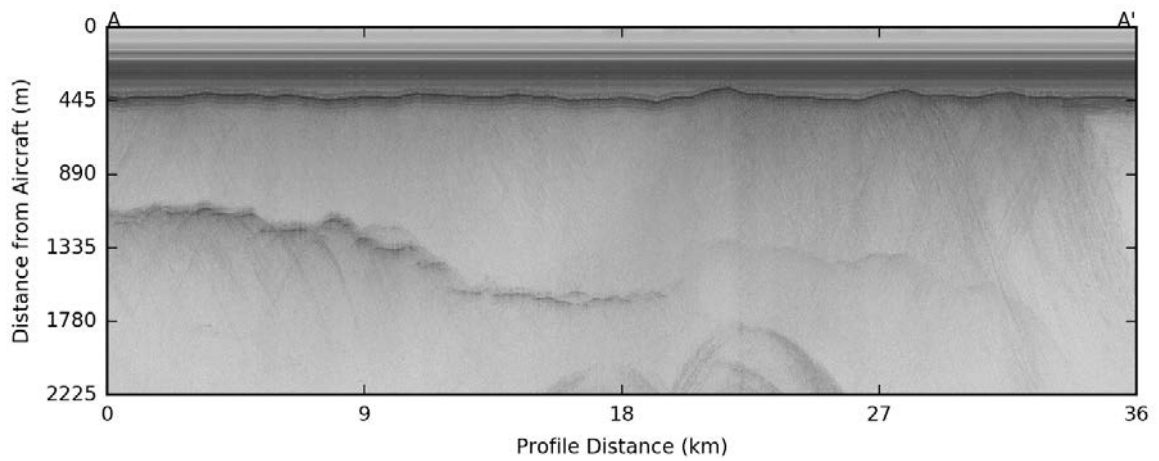


Figure 1.18. Example radargram of Dotson Ice Shelf and Kohler Glacier. See Figure 1.17 for profile location.

1.5. Autonomous Phase-sensitive Radio Echo Sounders (ApRES)

Two ApRES units were deployed on ANA08B, on the eastern side of Getz Ice Shelf. There were 10 ApRES units available for deployment on ANA08B. Three were remaining units from ANA06B (SN 37,46,47), purchased from the British Antarctic Survey in 2015, the other seven were new units from 2017 (SN 102-108). Of the 10 ApRES, four each are owned by KOPRI (SN 47, 104-106) and UIB (SN 37,46,102,103), respectively, and two by BAS/NYU (SN 107&108).

On ANA08B, ApRES deployments were planned at four areas in air operations coordinated with the Aerial Geophysics Team. These were the western and eastern Getz, Dotson and Thwaites Ice Shelves. At the western Getz Ice Shelf, we planned to recover any of the old sites deployed during ANA06B, if possible, as well as deploying new instruments. On our first visit to the western Getz, air operations did not take place due to impending inclement weather over the ice shelf. The deployments on Dotson and Thwaites had to be abandoned due to technical problems with one of the helicopters.

ApRES deployments on the Getz Ice Shelf complement the array of moorings that has been present at the eastern (Duncan-Wright) and western (Siple-Dean) fronts of the main cavity since 2016. The aim here is to link changes in water mass distribution and circulation from the moorings to variability in ice shelf basal melting. We deployed two ApRES units at sites GE1 and GE3 on 22 January 2018 (Figure 1.19). GE2 and GE4 were additional sites for potential deployments, in case we had been successful in recovering any of the old sites on the western Getz Ice Shelf. GE2 is located in a marked channel in the ice shelf. GE4 is located on the thinner front of the ice shelf.

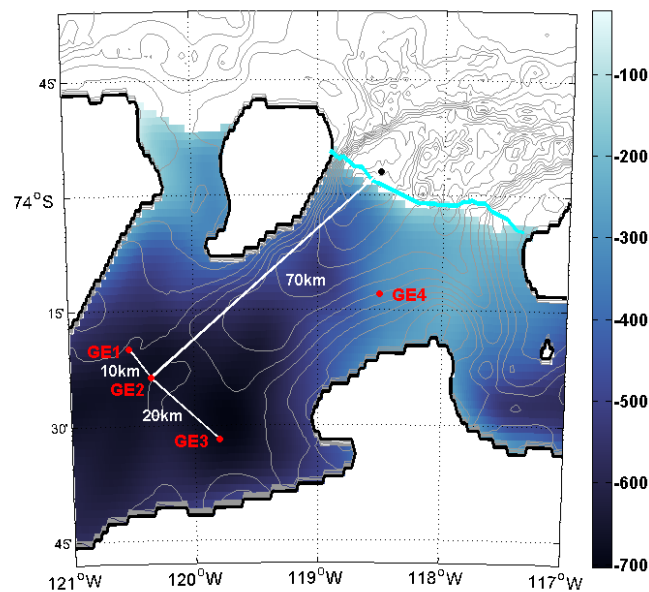


Figure 1.19. Map of the eastern Getz Ice Shelf with ApRES sites and flight distances. The coloured shading is ice draft from RTOPO. The gray lines bathymetry from IBCSO and the cyan line marks the ice shelf edge in 2015.

1.5.1. Instruments and methods

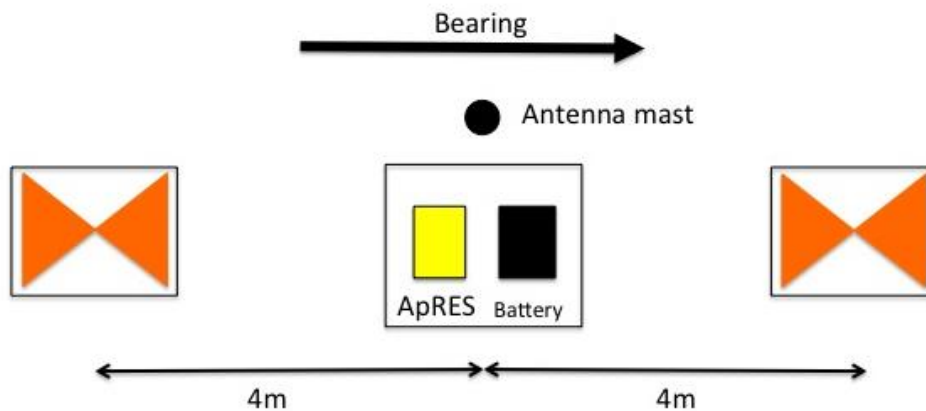


Figure 1.20. Sketch of an ANA08B ApRES site seen from above. GPS positions reported were taken at the antenna mast. Magnetic bearings were taken along the axis of the site with the antenna mast to the left.

The radars were installed into 1-m deep holes dug into the snow, with a 60x100 cm sheet of 12-mm plywood above the radar and battery. Batteries used were Sun Xtender PVX-1080T 108-Ah absorbed glass mat (AGM) batteries, charged on board before deployment. Both ApRES deployed have two Sandisk Extreme 60 MB/s 16 GB cards.

The radars were connected to two cavity-backed bowtie antennas, measuring 60x70x30 cm when assembled. The assembly consists of two copper triangles soldered to a circuit board with a balun and mounted on a polycarbonate roofing sheet using double-faced tape; this is placed in the bottom of the corrugated plastic box, with reinforcing plastic pieces above, and an aluminium reflector at the top of the box. The antennas were buried 40 cm beneath the snow, in a 90 cm deep hole, approximately 4 m from the radar, with a total separation of 8 m between the antenna centres (Figure. 1.20). The magnetic bearing along the line between the antennas with the pole to the left was measured using two hand-held GPS units and is noted below (Figure 1.20).

Each radar was connected to compact GPS and Iridium antennas mounted on a 6-m long aluminium pole, with black and red fabric flags at the top of the pole. In addition, packages of three RECCO reflectors were mounted about 0.5 m below the top of the mast to aid recovery should the poles get buried. We got successful Iridium tests from both ApRES. Please note, however, that we experienced erratic Iridium coverage on the eastern Getz Ice Shelf during the deployment day. We did not manage to get successful GPS fixes. This may be due to the fact that the field laptop only had Internet Explorer as a browser and this does not display this part of the web interface. But we also determined later back on board that the antenna connections on the bracket at the top of the mast are extremely sensitive to how tightly they are screwed into the antenna. The instrument clocks were set using the clock of a handheld GPS.

The deployment positions, settings, and other notes are given below. At each site, the radars were first turned on in attended mode, connected to a laptop. Test bursts of varying attenuation and gain were done to determine the correct settings. In both cases, an attenuation of 14 dB and gain of -4dB was most appropriate. Then one hundred bursts were fired using the chosen settings. These data were transferred to the computer to be analysed using Matlab and determine the “triples” setting, which sets the bin ranges for data to be sent back by Iridium (note that this can readily be done directly on the radar web interface). SN47 at GE1 ran the 2015 firmware and we were able to run the plot_triples.m script available

to us to find the ice shelf base and determine the triples. SN102, however, at GE3 had the 2017 firmware with a changed file format, making the available radar reading Matlab software suite unusable. Regardless, we used the same triples as for SN47 (GE1) after the altimeter reading of 260ft (79m) from the helicopter indicated that the ice was of a similar thickness as at GE1. Back on board Araon, we were able to run an updated version of the software suite to confirm that the ice base was indeed in a similar position at GE3 and the triples setting is therefore appropriate.

Once the settings were finalised, the configuration file was updated on the radar, the computer was disconnected, and the radar started in autonomous mode.

The data is presently handled by Iridium service provider Rock7 and sent to the gmail address UGOT_Iridium@gmail.com from where it can be accessed by all project partners. The IMEI numbers for the modems are also given below.

Site: GE1

Serial Number: 47 (KOPRI)

IMEI: 300234063520160

Position: 74° 20.032'S, 120° 31.211'W

Time deployed (UTC): 20180122 0400

Bearing: 320° (Magnetic, from Garmin GPS)

Attenuator/RF: 14dB

Gain/AF: -4 dB

Ice Thickness: 750m (plot_triples)

Triples: 70:15:350, 350:50:600, 600:5:770

100 Burst file: Survey_2018-01-22_034944.dat

Comments: Some uncertainty in the bearing, double checked, but not quadruple checked. Compasses were jumping. Iridium test positive and instrument is transmitting data (25/01/2018). No GPS fix could be obtained. Two reasons: sensitivity of antenna to mount on bracket and Internet Explorer does not display GPS field in browser interface. The instrument clock was set from the handheld GPS. Snow on site dry and loose at surface. Site flat and not crevassed.

Site: GE3

Serial Number: 102 (UIB)

IMEI: 300234065314830

Position: 74° 31.825'S, 119° 48.055'W

Time deployed (UTC): 20180122 0630

Bearing: 120° (Magnetic, from Garmin GPS)

Attenuator/RF: 14dB

Gain/AF: -4 dB

Ice Thickness: 750m (plot_triples)

Triples: 70:15:350, 350:50:600, 600:5:770

100 Burst file: Survey_2018-01-22_061911.dat

Comments: Iridium test positive, but instrument is not transmitting data (25/01/2018). No GPS fix could be obtained. Two reasons: sensitivity of antenna to mount on bracket and Internet Explorer does not display GPS field in browser interface. Snow on site dry, but more wind-packed than GE1. Site flat and not crevassed.

1.6. T-pops Deployments

A total of six T-POP units were deployed at two separate sites on ANA08B. T-POPs are anchored buoys that measure temperature and then pop up to the surface at a given date and time, relaying their data back home via satellite. If trapped under sea ice when surfacing, they fall asleep and then check back for a satellite link at regular intervals, saving batteries until they are eventually out in open water. The T-POPs were developed at the University of Rhode Island. The T-POPs will be logging near-bottom temperatures (2-3 m from bottom) hourly for either one or two years. See Table 1 for deployment details.

In their current iteration the T-POPs do not include a pressure sensor. A good knowledge of the deployment depth is therefore necessary to interpret the temperature time series correctly. We performed short Multibeam surveys before each of the two sets of deployments to determine the exact locations of the target depths (Figure. 1. 21 and 22).

On 27 Jan 2018, four T-POP units (s/n 35-38) were deployed about 50 km north of Dotson Ice Shelf/Bear peninsula, along a depth gradient from 260 to 380 m (Figure 1.21). The aim of this deployment is to investigate the exchange of water across the ridges that separate the deep troughs that channel the CDW towards the ice shelves. The circulation and water mass distribution across these is still poorly known and the T-POP deployment aims to shed light on the time variability of this exchange. CTD station 54 is located at the deployment site of T-POP 38.

Two more units (s/n 39-40) were deployed on 2 Feb 2018 just west of Dean Island at the western Getz Ice Shelf opening, at depths 254 m and 300 m respectively (Figure 1.22). These supplement the S9 mooring that was deployed earlier in the cruise to investigate the outflow of melt water from the western Getz Ice Shelf cavity. CTD station 58 is located at the deployment site of T-POP 40.

Table 1.10. T-POP deployment details

<i>T-POP</i> <i>s/n</i>	<i>CTD statio</i> <i>n</i>	<i>Latitude</i> <i>(DD.ddd)</i>	<i>Longitude</i> <i>(DD.ddd)</i>	<i>Depth</i> <i>(m)</i>	<i>Deployment</i> <i>date</i>	<i>Pop-up date</i>
35	ANA08B54	-73.778	-111.011	260	27-Jan-18	01-Feb-19
36	ANA08B54	-73.761	-111.213	300	27-Jan-18	01-Feb-20
37	ANA08B54	-73.742	-111.412	340	27-Jan-18	01-Feb-19
38	ANA08B54	-73.729	-111.543	380	27-Jan-18	01-Feb-20
39	ANA08B58	-74.2973	-128.1919	254	02-Feb-18	01-Feb-19
40	ANA08B58	-74.2959	-128.1864	300	02-Feb-18	01-Feb-20

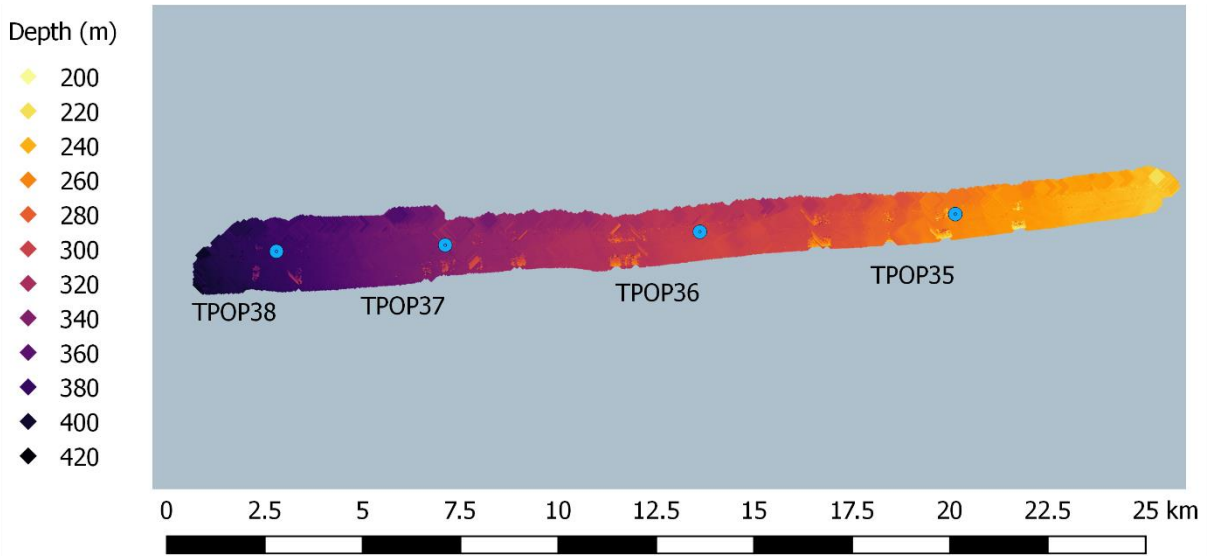


Figure 1.21. Deployment depths for T-POPs 35-38. Bathymetry data acquired with Araon/EM122#107.

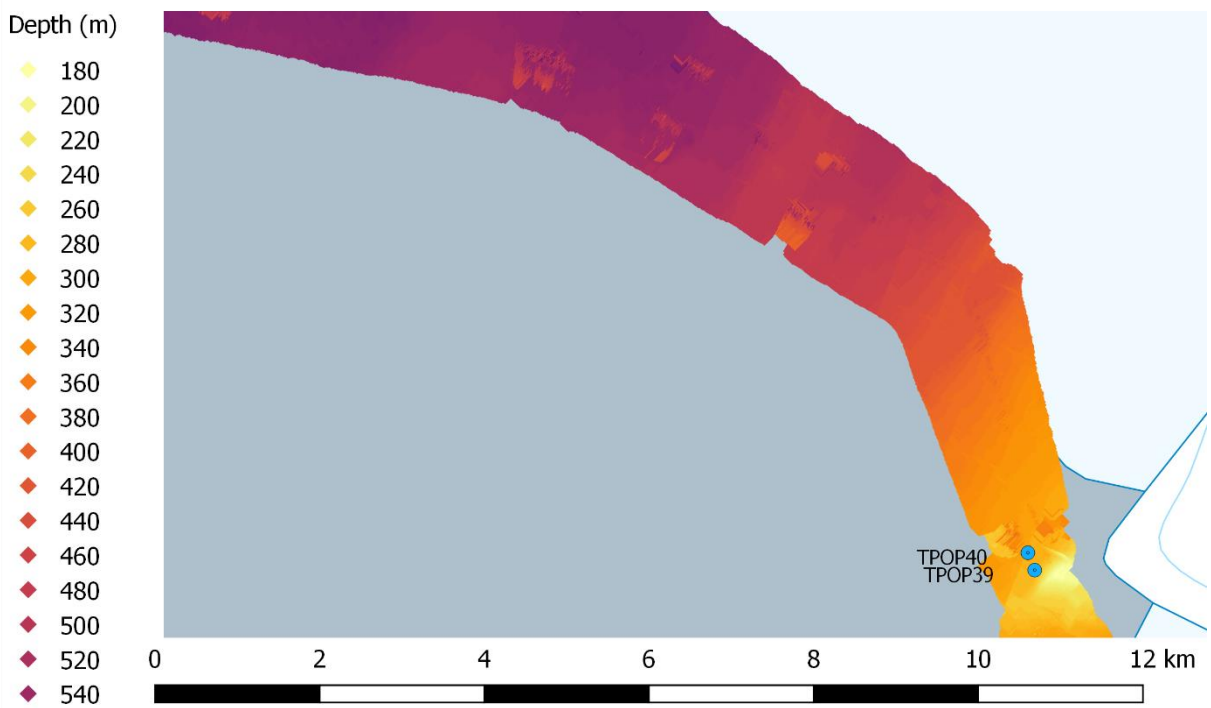


Figure 1.22. Deployment depths for T-POPs 39-40. Bathymetry data acquired with Araon/EM122#107.

1.7. Surface Drifter Deployment

A total of 20 drifters provided by NOAA (Dr. Shaun Dolk) were deployed in transit between Udintsev Fracture Zone and Amundsen Sea. In particular, 7 drifters were deployed in the polynya of Amundsen Sea to investigate the surface circulation in the vicinity of Dotson and Getz Ice Shelf. The details on the drifters deployed during ANA08B were given in Table 1.11

Table 1.11. NOAA drifter deployed during the ANA08B.

No	Model No.	Date (UTC)	Time (UTC)	Latitude (S)	Longitude (W)
1	899830	12/27/2017	12:22	51° 0.03'	143° 49.98'
2	899700	12/28/2017	4:26	52° 0.003'	143° 5.0'
3	898900	12/28/2017	12:22	52° 59.99'	143° 50.00'
4	899730	12/29/2017	12:41	54° 0.006'	143° 50.04'
5	899650	12/30/2017	1:07	54° 54.93'	143° 49.72'
6	823520	12/30/2017	8:51	55° 27.49'	144° 46.38'
7	823550	12/30/2017	19:58	55° 59.79'	145° 42.38'
8	823080	12/31/2017	2:01	56° 30.007'	146° 34.72'
9	823080	12/31/2017	22:27	57° 01.190'	147° 20.388'
10	823200	1/01/2018	8:29	58° 0.02'	147° 30.01'
11	823450	1/27/2018	15:02	74° 12.236'	112° 7.463'
12	823470	1/28/2018	4:10	73° 29.998'	112° 59.991'
13	823500	1/28/2018	20:35	73° 6.810'	114° 14.979'
14	898690	1/29/2018	2:20	72° 46.928'	115° 7.480'
15	898680	1/29/2018	14:56	72° 25.7918'	116° 20.7140'
16	823440	1/30/2018	12:43	70° 59.99'	120° 0.1638'
17	898730	1/30/2018	23:34	72° 0.344'	118° 27.519'
18	823180	2/02/2018	21:03	74° 17.8325'	128° 11.5137'
19	898840	2/05/2018	6:08	70° 0.0062'	162° 13.9587'
20	898830	2/06/2018	0:58	67° 59.995'	170° 17.225'

References

- Dutrieux, P. *et al.* Basal terraces on melting ice shelves. *Geophys. Res. Lett.* **41**, 5506–5513 (2014).
- Dutrieux, P. *et al.* Strong Sensitivity of Pine Island Ice-Shelf Melting to Climatic Variability. *Science* **3**, 468–472 (2014).
- Gohl, K., A. Denk, G. Eagles, and F. Wobbe. 2013. Deciphering tectonic phases of the Amundsen Sea Embayment shelf, West Antarctica, from a magnetic anomaly grid. *Tectonophysics*, 585: 113–123.
- Golynsky, A., M. Chiappini, D. Damaske, F. Ferraccioli, J. Ferris, C. Finn, M. Ghidella, T. Isihara, A. Johnson, H.R. Kim, L. Kovacs, J. LaBrecque, V. Masolov, Y. Nogi, M. Purucker, P. Taylor, and M. Torta. 2001. ADMAP – Magnetic Anomaly Map of the Antarctic, 1:10 000 000 scale map, in Morris, P., and R. von Frese, eds., BAS (Misc.) 10, Cambridge, British Antarctic Survey.
- Jacobs, S. S., Jenkins, A., Giulivi, C. F. & Dutrieux, P. Stronger ocean circulation and increased melting under Pine Island Glacier ice shelf. *Nat. Geosci.* **4**, 519–523 (2011).
- Jenkins, A., P. Dutrieux, S. S. Jacobs, S. D. McPhail, J. R. Perrett, A. T. Webb, and D. White (2010), Observations beneath Pine Island Glacier in West Antarctica and implications for its retreat. *Nature Geosci.* **3**, 468–472.
- Joughin, I. R, B.E. Smith and B. Medley. 2014. Marine Ice Sheet Collapse Potentially Under Way for the Thwaites Glacier Basin, West Antarctica. *Science*, 344(6185): 735–738.
- Kim, C.-S., Kim, T.-W., Cho, K.-H., Ha, H.K., Lee, S., Kim, H.-C, Lee, J.-H. 2016. Variability of the Antarctic Coastal Current in the Amundsen Sea. *Estuarine, Coastal and Shelf Science*. doi:10.1016/j.ecss.2016.08.004
- Mercer, J.H. 1978. West Antarctic ice sheet and CO₂ greenhouse effect- A threat of disaster. *Nature*, 271(5643): 321–325.
- Miles, T. N., Lee, S., Wahlin, A., Ha, K. H., Assmann, K., Schofield, O. 2015. Glider observations of the Dotson Ice Shelf outflow. *Deep Sea Research*. doi:10.1016/j.dsr2.2015.08.008
- Paolo, F. S., H. A. Fricker, and L. Padman. 2015. Volume loss from Antarctic ice shelves is accelerating. *Science*. 348(6232): 327–331.
- Peters, M. E., D.D. Blankenship, S.P Carter, S.D. Kempf, D.A Young, and J.W Holt. 2007. Along-track focusing of airborne radar sounding data from West Antarctica for improving basal reflection analysis and layer detection. *IEEE Transactions on Geoscience and Remote Sensing*, 45(9): 2725–2736.
- Pollard, D., R. M. DeConto, and R. B. Alley. 2015. Potential Antarctic Ice Sheet retreat driven by hydrofracturing and ice cliff failure. *Earth and Planetary Science Letters*, 412: 112–121.
- Pritchard, H.D., S.R.M. Ligtenberg, H.A. Fricker, D.G. Vaughan, M.R. Van den Broeke, and L. Padman. 2012. Antarctic ice-sheet loss driven by basal melting of ice shelves. *Nature*, 484(7395): 502–505.
- Rignot, E. J., J. Mouginot, M. Morlighem, H. Seroussi, and B. Scheuchl. 2014. Widespread, rapid grounding line retreat of Pine Island, Thwaites, Smith and Kohler glaciers, West Antarctica from 1992 to 2011. *Geophysical Research Letters*, 41.

Stanton, T. P. *et al.* Channelized ice melting in the ocean boundary layer beneath Pine Island Glacier, Antarctica. *Science* **341**, 1236–9 (2013).

Schofield, O., Miles, T., Aldercamp A-C, Lee, S, Haskin. C., Roaglsky E., Sipler, R., Sherrell R., Yager, P. 2015. *In situ* phytoplankton distributions in the Amundsen Sea polynya measured by autonomous gliders. *Elementa: Science of the Anthropocene*. doi: 10.12952/journal.elementa.000073

Wåhlin, A. K., X. Yuan, G. Björk, and C. Nohr (2010) Inflow of warm Circumpolar Deep Water in the Central Amundsen Shelf. *J. Phys. Oceanogr.* 40, 1427–1434.

Walker, D. P., M. A. Brandon, A. Jenkins, J. T. Allen, J. A. Dowdeswell, and J. Evans (2007) Oceanic heat transport onto the Amundsen Sea shelf through a submarine glacial trough. *Geophys. Res. Lett.* 34, L02602 (2007).

Acknowledgements

We are very grateful to the captain and crew of IBRV Araon for their professional support with all mooring works in making successful recoveries and deployments. The UGOT part of the project has been funded by the Swedish Research Council and the Swedish Polar Research Secretariats, for which we are grateful.

Appendix 1.1. ANA08B cruise log spreadsheet.

Scientific Cruise Daily Log

Ship: **R/V Araon**

Cruise : **ANA08 . B**

Prepared by Y. KIM (ygkim@kopri.re.kr)

STN No.	Gear	Cast No.	Date	Cast start	Cast end	Latitude	Longitude	Water depth	Cast depth	Wind speed	Wind direction	Ship speed	Heading	Remarks	Device Driver
			UTC time	UTC time	UTC time			(m)	(m)	knot	(°)	knot	(°)		
1	CTD	1	12/27/2017	5:38	8:07	50° 59.99'	143° 49.99'	3694	3683	8.81	245	0.66	253.6	First deep casting	H.W. YANG
	TM	1		8:33	12:04				900					Trace metal	R. Middag
	SDD	1		12:22										Surface drifter deployment	T.W. KIM
2	CTD	1	12/28/2017	1:42	4:17	51° 59.99'	143° 50.00'	3600	3586	6.76	265	0.12	269.4	First deep casting	Y. KIM
	SDD	2		4:26										Surface drifter deployment	T.W. KIM
3	CTD	1	12/28/2017	9:41	12:15	52° 59.99'	143° 49.99'	3760	3738	10.6	290	1.3	224	First deep casting	Y. KIM
	SDD	3		12:22										Surface drifter deployment	T.W. KIM
4	TM	1	12/29/2017	0:11	2:24	54° 00.00'	143° 50.00'		800						R. Middag
	CTD	1		10:20	12:33	53° 59.99'	143° 50.00'	3456	3442	9.87	230	1.04	268.6	First deep casting	Y. KIM
	SDD	4		12:41										Surface drifter deployment	T.W. KIM
5	MR	1	12/29/2017	17:47	21:40	54° 54.96'	143° 49.82'							KIOST mooring recovery	Isabelle Durand
	CTD	1		22:21	1:00	54° 54.9081'	143° 49.6621'	3786	3773	10.18	241	0.21	235.4	First deep casting	H.W. YANG
	SDD	5	12/30/2017	1:07										Surface drifter deployment	T.W. KIM
6	CTD	1	12/30/2017	5:50	8:39	55° 27.48'	144° 46.36'	3972	3959	10.82	164	0.67	175.8	First deep casting	H.W. YANG
	SDD	6		8:51										Surface drifter deployment	T.W. PARK
7	CTD	1	12/30/2017	13:23	15:17	55° 58.85'	145° 41.02'	2731	2711	2.86	161	0.54	278	First deep casting	Y. KIM
	MR	1		15:45	19:36									LOCEAN mooring recovery	Isabelle Durand
	SDD	7		19:58										Surface drifter deployment	T.W. KIM
8	CTD	1	12/30/2017	23:45	1:54	56° 29.99'	146° 34.005'	2967	2952	10.47	304	329	1.35	First deep casting	H.W. YANG
	SDD	8	12/31/2017	2:01										Surface drifter deployment	T.W. PARK
9	CTD	1	12/31/2017	5:29	7:52	56° 58.48'	147° 21.40'	3031	3010	11.16	251	0.62	269	First deep casting	Y. KIM

	MR	1		13:57	22:20	57° 00.08'	147° 22.04'							LOCEAN mooring recovery	Isabelle Durand
	SDD	9		22:27										Surface drifter deployment	T.W. KIM
10	CTD	1	1/1/2018	3:45	5:41	57° 59.99'	147° 30.00'	2706	2688	10.9	266	0.78	288	First deep casting	H.W. YANG
	TM	1		5:50	8:07				950					Trace metal	R. Middag
	SDD	10		8:29										Surface drifter deployment	T.W. PARK
11	CTD	1	1/15/2018	14:06	16:46	66° 27.95'	155° 44.18'	4198	4181	3.77	336	0.82	11.6	First deep casting	Y. KIM
	SD	1		16:49	16:52				19					Secchi disk	H. JOO
	TM	1		17:30	18:13				100					Trace metal, shallow	R. Middag
	PHY	1		18:30	18:46				150					Vertical towing mesh size 20 µm	H. JOO
	BON	1		18:54	19:09				200					Vertical towing mesh size 330 µm, 500 µm	H. NA
	BON	2		19:24	19:37				200					Vertical towing mesh size 330 µm, 500 µm	H. NA
	TM	1		20:00	22:16				1000					Trace metal, deep	R. Middag
	CTD	2		22:41	23:00	66° 27.9550'	155° 44.1981'		130	2.65	266	0.25	299	First shallow casting	H.W. YANG
12	CTD	1	1/18/2018	5:59	6:22	73° 39.51'	127° 24.12'	182	172	9.36	116	0.04	137.3	First deep casting	H.W. YANG
	SD	1		6:24	6:25				7					Secchi disk	H. JOO
	UV	1		6:25	6:30				60					UV meter	H. JOO
	BON	1		6:53	7:03				170					Vertical towing mesh size 330 µm, 500 µm	H. NA
	PHY	1		7:10	7:20				100					Vertical towing mesh size 20 µm	H. JOO
	CTD	2		7:42	7:59	73° 39.5134'	127° 24.1268'		100	7.28	96	0.11	137	First shallow casting	H.W. YANG
13	CTD	1	1/18/2018	9:12	9:56	73° 47.6721'	127° 34.8447'	573	563	5.82	103	0.07	194.6	First deep casting	H.W. YANG
	MR	1		10:07	11:12									UIB4 Mooring recovery	K. Assmann
14	CTD	1	1/18/2018	11:49	12:35	73° 49.91'	127° 46.77'	694	684	4.67	96	0.08	213.5	First deep casting	H.W. YANG
	MR	1		12:44	14:00									UIB1 Mooring recovery	K. Assmann
15	CTD	1	1/18/2018	15:19	16:05	73° 49.62'	127° 16.44'	596	577	10.96	128	0.09	139	First deep casting	Y. KIM
	MR	1		16:15	17:23									S6 Mooring recovery	K. Assmann
16	CTD	1	1/19/2018	0:13	0:45	73° 49.8048'	127° 21.271'	599	586	6.3	198	0.08	205	First deep casting	Y. KIM
	MD	1		1:21	2:40									S7 Mooring deployment	K. Assmann
17	CTD	1	1/19/2018	3:04	3:40	73° 51.5996'	127° 22.2081'	685	674	3.07	159	0.1	172	First deep casting	Y. KIM
	MD	1		3:59	5:15									S8 Mooring deployment	K. Assmann
18	CTD	1	1/19/2018	6:11	7:03	73° 56.7191'	127° 48.4325'	755	745	3.38	194	0.11	213	First deep casting	H.W. YANG
	BON	1		7:15	7:40				200					Vertical towing mesh size 330 µm, 500 µm	H. NA
	PHY	1		7:46	8:03				150					Vertical towing mesh size 20 µm	H. JOO
	CTD	2		8:15	8:30	73° 56.7192'	127° 48.4347'		100	5.04	210	0.02	215	First shallow casting	H.W. YANG
	RTN	1		8:57	9:25									Rectangular net	H. NA
19	CTD	1	1/19/2018	10:19	11:04	74° 2.9813'	127° 55.0004'	710	700	6.45	149	0.02	152.8	First deep casting	Y. KIM
20	CTD	1	1/19/2018	11:51	12:28	74° 8.4702'	128° 12.2437'	568	560	3.75	135	0.1	233	First deep casting	H.W. YANG
	MR	1		12:41	13:37									UIB2 Mooring recovery	K. Assmann
	BC	1		14:11	14:36				568					Box core	S.Y. KIM
21	CTD	1	1/19/2018	16:16	16:51	74° 11.5442'	127° 59.4094'	630	619	11.19	126	0.03	130.2	First deep casting	Y. KIM
	MD	1		17:22	18:50									S9 Mooring deployment	K. Assmann
22	CTD	1	1/19/2018	19:51	20:45	74° 13.6116'	128° 33.4607'	736	725	11.34	119	0.42	120	First deep casting	Y. KIM

	BON	1		20:58	21:11									200	Vertical towing mesh size 330 µm, 500 µm	H. NA	
	PHY	1		21:18	21:30									150	Vertical towing mesh size 20 µm	H. JOO	
	SD	1		21:38	21:39									5	Secchi disk	H. JOO	
	UV	1		21:40	21:42									60	UV meter	H. JOO	
	CTD	2		21:45	22:01	74° 13.6133'	128° 33.4628'							100	12.57 121 0.1 11.6	First shallow casting	Y. KIM
23	CTD	1	1/20/2018	2:35	3:17	73° 21.2537'	128° 3.0934'	615	605	6.82	269	0.02	40.1		First deep casting	Y. KIM	
24	CTD	1	1/20/2018	5:06	5:43	73° 4.7036'	128° 11.5267'	559	549	2.4	261	0.22	43.8		First deep casting	Y. KIM	
25	BC	1	1/20/2018	8:08	8:55			274	274						Box core	S.Y. KIM	
26	CTD	1	1/21/2018	1:19	2:01	73° 40.9101'	123° 34.7119'	587	578	13.11	82	0.09	110		First deep casting	H.W. YANG	
	BC	1		2:20	2:56				580						Box core	S.Y. KIM	
27	MR	1	1/21/2018	12:34	15:24										K4(2016) Mooring recovery	T.W. KIM	
	CTD	1		15:28	16:26	73° 54.2812'	118° 44.8358'	1022	1011	8.79	136	0.16	127		First deep casting	H.W. YANG	
	SD	1		14:28	14:29				9						Secchi disk	H. JOO	
	UV	1		16:30	16:33				60						UV meter	H. JOO	
	BON	1		16:42	16:54				150						Vertical towing mesh size 330 µm, 500 µm	H. NA	
	PHY	1		16:59	17:15				150						Vertical towing mesh size 20 µm	H. JOO	
	CTD	2		17:26	17:53	73° 54.2804'	118° 44.8342'		300	10.89	118	0.33	125.7		First shallow casting	H.W. YANG	
28	AG	1	1/21/2018	21:30	10:10										Aero-geophysics survey	Lucas Beem	
	AP	1		21:30	10:10										ApRES deployment	K.H. CHO	
	CTD	1	1/22/2018	11:50	12:51	74° 1.1518'	117° 58.6874'	1199	1190	6.77	142	0.2	125		First deep casting	H.W. YANG	
	BON	1		13:03	13:16				200						Vertical towing mesh size 330 µm, 500 µm	H. NA	
	PHY	1		13:18	13:36				150						Vertical towing mesh size 20 µm	H. JOO	
	CTD	2		14:07	15:12	74° 1.151'	117° 58.686'	1180	1165	5.45	145	0.15	125		First shallow casting	T.W. PARK	
	RTN	1		15:23	16:12										Rectangular net	H. NA	
29	MR	1	1/22/2018	17:33	20:42										K6(2016) Mooring recovery	T.W. KIM	
	CTD	1		21:02	22:09	73° 53.7740'	117° 17.7433'	1162	1151	1.94	328	0.11	16.9		First deep casting	H.W. YANG	
	SD	1		22:13	22:14				5						Secchi disk	H. JOO	
	UV	1		22:15	22:18				60						UV meter	H. JOO	
	BON	1		22:22	22:34				200						Vertical towing mesh size 330 µm, 500 µm	H. NA	
	PHY	1		22:40	22:53				150						Vertical towing mesh size 20 µm	H. JOO	
	CTD	2		23:06	23:22	73° 53.7739'	117° 17.7428'		120	2.86	54	0.09	17.8		First shallow casting	H.W. YANG	
30	MR	1	1/22/2018	23:25	2:03										K5(2016) Mooring recovery	T.W. KIM	
	CTD	1	1/23/2018	2:46	3:21	73° 56.2641'	117° 16.5186'	655	645	5.98	82	0.08	68.3		First deep casting	H.W. YANG	
	MD	1		3:40	7:30										K4(2018) Mooring deployment	T.W. KIM	
31	CTD	1	1/23/2018	10:21	10:57	73° 30.0032'	116° 30.0082'	373	358	16.79	89	0.77	101.3		First deep casting	H.W. YANG	
	SD	1		11:03	11:04				6						Secchi disk	H. JOO	
	UV	1		11:05	11:06				60						UV meter	H. JOO	
	TM	1		11:25	11:48				100						Trace metal shallow casting (100m)	R. Middag	
	CTD	2		12:02	12:17	73° 30.0018'	116° 30.0030'		100	13.8	90	0.48	91.8		First shallow casting	H.W. YANG	
	BON	1		12:31	12:49				230						Vertical towing mesh size 330 µm, 500 µm	H. NA	
	PHY	1		12:49	13:02				230						Vertical towing mesh size 20 µm	H. JOO	
	TM	1		13:35	14:15				360						Trace metal, deep casting	R. Middag	

	RTN	1		14:43	15:09									Rectangular net	H. NA
32	CTD	1	1/23/2018	17:05	17:52	73° 22.1990'	115° 42.0063'	676	660	13.94	104	0.27	123	First deep casting	Y. KIM
33	MR	1	1/23/2018	19:26	3:50									K2(2016) Mooring recovery	T.W. KIM
	CTD	1	1/24/2018	4:31	5:24	73° 16.773'	114° 56.963'	826	812	10.59	91	0.1	116	First deep casting	T.W. PARK
	SD	1		5:25	5:26				6					Secchi disk	H. JOO
	UV	1		5:26	5:30				60					UV meter	H. JOO
	BON	1		5:37	5:50				200					Vertical towing mesh size 330 µm, 500 µm	H. NA
	PHY	1		5:55	6:10				150					Vertical towing mesh size 20 µm	H. JOO
	CTD	2		6:32	6:47	73° 16.7751'	114° 56.9567'		100	11.3	102	0.1	129.6	First shallow casting	H.W. YANG
	TM	1		7:05	8:40				800					Trace metal, deep casting	R. Middag
	BC	1		9:12	9:50				820					Box core	S.Y. KIM
	MD	1		11:08	13:12									K1(2018) Mooring deployment	T.W. KIM
	RTN	1		13:23	13:57									Rectangular net	H. NA
34	GD		1/24/2018	16:23	17:45	73° 41.2279'	114° 15.4320'							Seaglider deployment	P. Dutriex
	MR	1		15:56	19:17									K3(2016) Mooring recovery	T.W. KIM
	CTD	1		19:43	20:26	73° 42.677'	114° 12.917'	569	558	8.41	114	0.09	132.5	First deep	T.W. PARK
	SD	1		20:30	20:31				7					Secchi disk	H. JOO
	UV	1		20:32	20:33				60					UV meter	H. JOO
	BON	1		20:38	20:52				200					Vertical towing mesh size 330 µm, 500 µm	H. NA
	PHY	1		20:59	21:09				150					Vertical towing mesh size 20 µm	H. JOO
	CTD	2		21:38	21:53	73° 42.6766'	114° 12.9153'		100	8.46	119	0.07	120.6	First shallow casting	H.W. YANG
	TM	1		22:10	23:20				500					Trace metal, deep casting	R. Middag
	RTN	1		23:42	0:16									Rectangular net	H. NA
35	AG	1	1/25/2018	5:58	15:00									Aero geophysics survey	Lucas Beem
	AWS	1		5:58	15:00									AWS installation	S.H. Ham
	CTD	1	1/26/2018	6:20	6:36	74° 9.9675'	113° 23.9667'	262	253	9.03	190	0.08	200	First deep casting	H.W. YANG
36	CTD	1	1/26/2018	7:15	8:03	74° 10.3030'	113° 19.1890'	667	657	6.82	203	0.3	207	First deep casting	H.W. YANG
	BON	1		8:15	8:27				200					Vertical towing mesh size 330 µm, 500 µm	H. NA
	PHY	1		8:31	8:42				150					Vertical towing mesh size 20 µm	H. JOO
	CTD	2		9:09	9:27	74° 10.3048'	113° 19.1743'		175	10.61	204	0.07	210	First shallow casting	H.W. YANG
	TM	2		9:47	11:10				650					Trace metal, deep casting	R. Middag
	MD	1		12:58	14:41									K3(2018) Mooring deployment	T.W. KIM
37	CTD	1	1/26/2018	15:26	16:16	74° 10.3746'	113° 0.0065'	713	704	10.44	166	0.21	186	First deep casting	Y. KIM
38	CTD	1	1/26/2018	17:32	18:29	74° 10.4424'	112° 43.4590'	1058	1047	9.86	137	0.2	170	First deep casting	Y. KIM
	SD	1		18:31	18:33				8					Secchi disk	H. JOO
	UV	1		18:33	18:37				60					UV meter	H. JOO
	BON	1		18:40	19:00				200					Vertical towing mesh size 330 µm, 500 µm	H. NA
	BON	2		19:00	19:07				150					Vertical towing mesh size 330 µm, 500 µm	H. NA
	PHY	1		19:13	19:24				150					Vertical towing mesh size 20 µm	H. JOO
	CTD	2	1/26/2018	19:36	19:55	74° 10.4400'	112° 43.4578'		150	1.22	138	0.08	169	First shallow casting	Y. KIM
		RTN	1		20:12	20:45									Rectangular net
39	BD	1	1/26/2018	22:30	23:42	74° 11.786'	112° 43.106'							Beacon #1 deployment	P. Dutriex

40	CTD	1	1/27/2018	0:29	1:28	74° 10.5075'	112° 25.0014'	958	949	8.73	110	0.21	135	First deep casting	H.W. YANG
41	BD	1	1/27/2018	2:45	3:51	74° 10.506'	112° 25.870'							Beacon #2 deployment	P. Dutrieux
42	CTD	1	1/27/2018	5:52	6:41	74° 10.5779'	112° 8.0782'	768	758	11.47	118	0.23	141.7	First deep casting	H.W. YANG
	SD	1		6:43	6:44				8					Secchi disk	H. JOO
	UV	1		6:45	6:48				60					UV meter	H. JOO
	BON	1		6:50	7:05				200					Vertical towing mesh size 330 µm, 500 µm	H. NA
	PHY	1		7:08	7:20				150					Vertical towing mesh size 20 µm	H. JOO
	CTD	2		7:42	8:03	74° 16.5771'	112° 8.0827'		200	13.08	112	0.14	150	First shallow casting	H.W. YANG
	TM	1		8:23	10:00				760					Trace metal, deep casting	R. Middag
	MD	1		11:40	13:10									K2(2018) Mooring deployment	T.W. KIM
43	BD	1	1/27/2018	13:57	14:56	74° 09.899'	112° 10.506'							Beacon #3 deployment	P. Dutrieux
	SDD	11		15:02										Surface drifter deployment	T.W. KIM
44	EM		1/27/2018	15:43	15:54	74° 07.6308'	112° 08.319'							EM-APEX deployment	P. Dutrieux
54	TPOP	1,2,3,4	1/27/2018	18:05	21:35									T-POP deployment	K. Assmann
	CTD	1		21:51	22:14	73° 43.7347'	111° 32.6176'	378	362	12.96	13.8	0.29	268	First deep casting	Y. KIM
45	CTD	1	1/28/2018	0:46	1:29	73° 30.00'	112° 59.99'	523	518	14.15	130	0.2	134	First deep casting	Y. KIM
	BON	1		1:41	1:52				200					Vertical towing mesh size 330 µm, 500 µm	H. NA
	PHY	1		1:55	2:10				150					Vertical towing mesh size 20 µm	H. JOO
	CTD	2		2:23	2:39	73° 29.98'	112° 59.90'		100	3.88	127	0.33	140.9	First shallow casting	T.W. PARK
	TM	1		2:51	4:00									Trace metal, deep casting	R. Middag
	SDD	12		15:02										Surface drifter deployment	T.W. PARK
46	CTD	1	1/28/2018	7:38	8:16	72° 51.001'	112° 29.973'	450	440	7.81	127	0.09	146	First deep casting	H.W. YANG
	BON	1		8:32	8:44				200					Vertical towing mesh size 330 µm, 500 µm	H. NA
	PHY	1		8:50	8:57				150					Vertical towing mesh size 20 µm	H. JOO
	CTD	2		9:11	9:23	72° 51.001'	112° 29.9737'		80	8.73	113	0.071	149	First shallow casting	H.W. YANG
	TM	1		9:40	10:38				450					Trace metal, deep casting	R. Middag
	RTN	1		10:57	11:38									Rectangular net	H. NA
47	CTD	1	1/28/2018	13:10	13:45	73° 0.0015'	113° 30.0132'	440	430	12.52	152	0.36	164.5	First deep casting	Y. KIM
	SD	1		13:48	13:49				5					Secchi disk	H. JOO
	UV	1		13:49	13:53				60					UV meter	H. JOO
	BON	1		13:55	14:07				200					Vertical towing mesh size 330 µm, 500 µm	H. NA
	PHY	1		14:11	14:26				150					Vertical towing mesh size 20 µm	H. JOO
	CTD	2		14:37	14:48	73° 0.001'	113° 30.013'		60	12.5	150	0.42	164	First shallow casting	Y. KIM
48	CTD	1	1/28/2018	16:31	17:10	73° 6.7809'	114° 14.9931'	615	605	16.6	132	0.42	136	First deep casting	Y. KIM
	PHY	1		17:15	17:30				150					Vertical towing mesh size 20 µm	H. JOO
	BON	1		17:31	17:48				200					Vertical towing mesh size 330 µm, 500 µm	H. NA
	CTD	2		18:35	18:49	73° 6.7802'	114° 14.9962'		100	17.84	127	0.5	133	First shallow casting	Y. KIM
	TM	1		19:10	20:24				600					Trace metal, deep casting	R. Middag
	SDD	13		20:35										Surface drifter deployment	T.W. KIM
49	CTD	1	1/28/2018	22:53	23:32	72° 46.968'	115° 7.4963'	591	577	14.58	139	0.7	136	First deep casting	H.W. YANG
	SD	1		23:36	23:37				9					Secchi disk	H. JOO
	UV	1		23:37	23:41				60					UV meter	H. JOO

	BON	1		23:44	23:55			200					Vertical towing mesh size 330 µm, 500 µm	H. NA	
	PHY	1		23:58	0:11			150					Vertical towing mesh size 20 µm	H. JOO	
	CTD	2	1/29/2018	0:25	0:39	72° 46.918'	115° 7.504'	100	15.87	137	0.84	141.3	First shallow casting	T.W. PARK	
	TM	1		0:57	2:12			600					Trace metal, deep casting	R. Middag	
	SDD	14		2:20									Surface drifter deployment	T.W. PARK	
	RTN	1		2:27	2:50								Rectangular net	H. NA	
50	CTD	1	1/29/2018	10:26	11:05	72° 25.8772'	116° 20.3393'	538	528	11.25	126	0.15	144	First deep casting	H.W. YANG
	BON	1		11:16	11:27			200					Vertical towing mesh size 330 µm, 500 µm	H. NA	
	PHY	1		11:31	11:44			150					Vertical towing mesh size 20 µm	H. JOO	
	CTD	2		11:59	12:12	72° 25.8765'	116° 20.3291'	100	11.41	113	0.03	148	First shallow casting	H.W. YANG	
	TM	1		12:30	13:42			500					Trace metal, deep casting	R. Middag	
	BC	1		14:09	14:34			537					Box core	S.Y. KIM	
	SDD	15		14:56									Surface drifter deployment	T.W. PARK	
	SIS	1											Sea ice sampling	J. JUNG	
	RTN	1		16:35	17:07								Rectangular net	H. NA	
51	CTD	1	1/29/2018	20:43	21:22	72° 13.2763'	117° 35.5433'	522	512	9.74	128	0.1	145	First deep casting	Y. KIM
	BC	1		21:44	22:06			526					Box core	S.Y. KIM	
	BC	2		22:22	22:45			527					Box core	S.Y. KIM	
53	CTD	1	1/30/2018	6:54	8:47	71° 0.005'	120° 0.003'	2380	2371	9.69	160	0.1	91	First deep casting	H.W. YANG
	SD	1		8:49	8:50			11					Secchi disk	H. JOO	
	UV	1		8:51	8:53			60					UV meter	H. JOO	
	BON	1		8:58	9:10			200					Vertical towing mesh size 330 µm, 500 µm	H. NA	
	PHY	1		9:15	9:26			150					Vertical towing mesh size 20 µm	H. JOO	
	CTD	2		9:54	10:09	71° 0.003'	120° 0.010'	100	8.28	142	0.09	100.2	First shallow casting	H.W. YANG	
	TM	1		10:28	12:33			1000					Trace metal, deep casting	R. Middag	
	SDD	16		12:43									Surface drifter deployment	T.W. PARK	
52	CTD	1	1/30/2018	19:22	20:01	71° 59.9968'	118° 25.0040'	496	486	10.62	128	0.31	122	First deep casting	Y. KIM
	TM	1		20:18	20:40			100					Trace metal, Shallow	R. Middag	
	SD	1		20:50	20:51			12					Secchi disk	H. JOO	
	UV	1		20:52	20:58			60					UV meter	H. JOO	
	BON	1		21:00	21:11			200					Vertical towing mesh size 330 µm, 500 µm	H. NA	
	PHY	1		21:17	21:27			150					Vertical towing mesh size 20 µm	H. JOO	
	CTD	1		21:38	21:53	72° 0.1033'	118° 24.9923'	100	9.52	129	0.08	125	First shallow casting	Y. KIM	
	TM	2		22:11	23:15			500					Trace metal, deep casting	R. Middag	
	SDD	17		23:33									Surface drifter deployment	T.W. PARK	
50	MD	1	1/31/2018	7:27	9:08								S1 Mooring deployment	K. Assmann	
26	MR	1	1/31/2018	21:34	22:38	73° 41.1709'	123° 34.4380'						UiB3 Mooring recovery	K. Assmann	
	SIS	1	2/1/2018	4:30	7:48	73° 4.7878'	126° 11.1114'						Sea ice sampling	J. JUNG	
55	CTD	1	2/1/2018	14:12	16:03	72° 49.1091'	128° 3.3117'	2645	2630	7.29	127	0.9	29.5	First deep casting	Y. KIM
	BON	1		16:24	16:37			200					Vertical towing mesh size 330 µm, 500 µm	H. NA	
	PHY	1		16:39	16:52			150					Vertical towing mesh size 20 µm	H. JOO	
	TM	1		17:44	19:58			1000					Trace metal, deep casting	R. Middag	

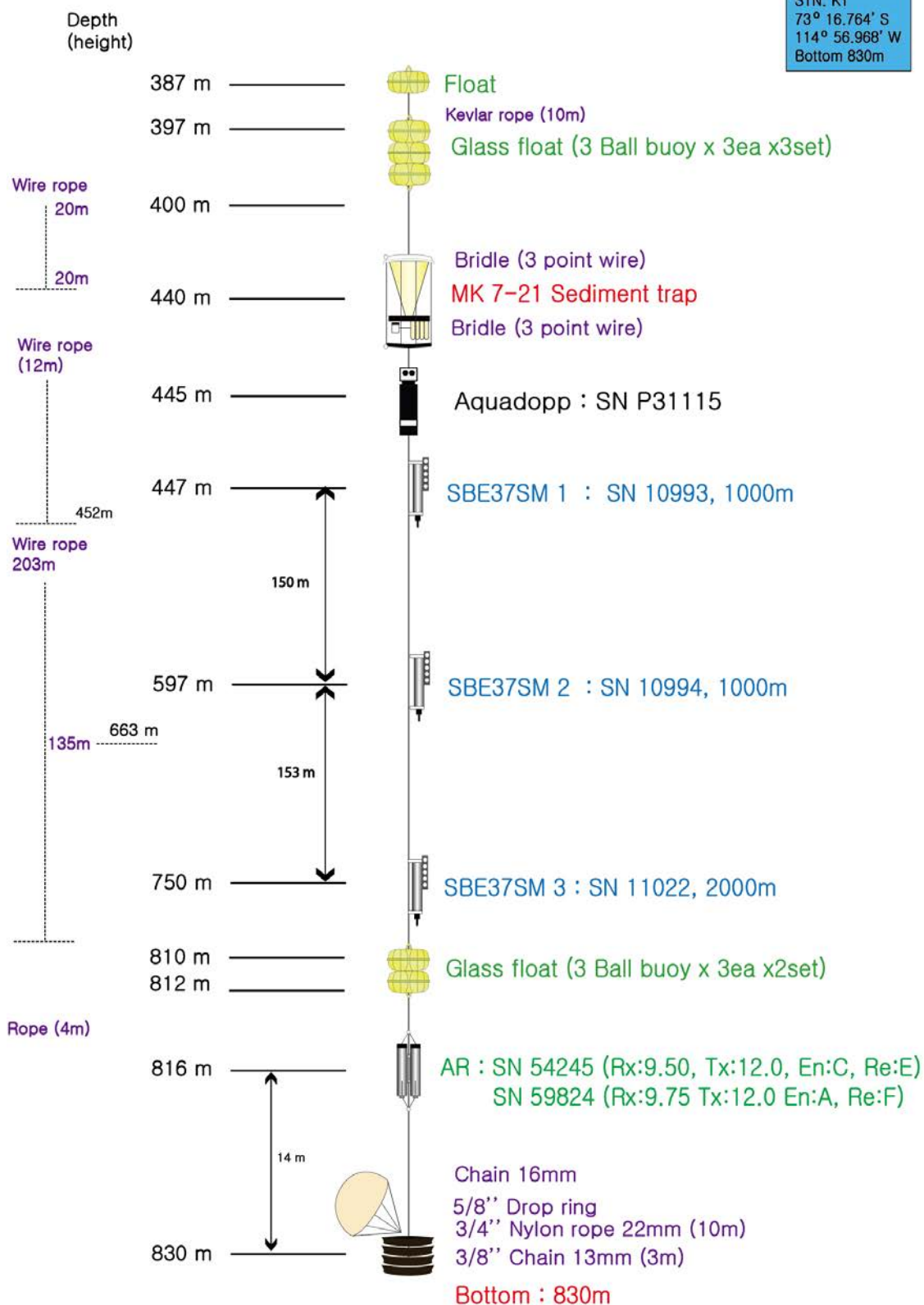
56	CTD	1	2/1/2018	21:06	22:14	72° 56.8536'	128° 7.7586'	1719	1705					First deep casting	Y. KIM
24	CTD	2	2/1/2018	11:30	0:12	73° 4.4592'	128° 8.0155'	571	561	5.16	257	0.07	78.3	Second deep casting	Y. KIM
	BON	1		0:25	0:37				200					Vertical towing mesh size 330 µm, 500 µm	H. NA
	PHY	1		0:40	0:53				150					Vertical towing mesh size 20 µm	H. JOO
	TM	1		1:06	2:20				500					Trace metal, deep casting	R. Middag
23	CTD	2	2/2/2018	7:20	8:07	73° 21.2582'	128° 3.0813'	618	608	2.3	168	0.02	9.5	Second deep casting	H.W. YANG
	SD	1		8:10	8:12				5					Secchi disk	H. JOO
	UV	1		8:13	8:19				60					UV meter	H. JOO
	BON	1		8:20	8:35				200					Vertical towing mesh size 330 µm, 500 µm	H. NA
	BON	2		8:38	8:44				50					Vertical towing mesh size 330 µm, 500 µm	H. NA
	PHY	1		8:48	8:57				150					Vertical towing mesh size 20 µm	H. JOO
	CTD	3		9:08	9:20	73° 21.2600'	128° 3.0471'		100	4.07	206	0.04	20	Second shallow casting	H.W. YANG
57	CTD	1	2/2/2018	11:41	12:30	73° 45.8170'	128° 18.1748'	713	704	2.71	196	0.11	179.3	First deep casting	H.W. YANG
	BON	1		12:37	12:56				200					Vertical towing mesh size 330 µm, 500 µm	H. NA
	PHY	1		12:56	13:11				150					Vertical towing mesh size 20 µm	H. JOO
	TM	1		13:31	15:05				700					Trace metal, deep casting	R. Middag
	BC	1		15:27	16:13				650					Box core	S.Y. KIM
	BC	2		16:13	16:44				650					Box core	S.Y. KIM
58	TPOP	5,6	2/2/2018	19:35	21:14	72° 0.1033'	118° 24.9923'							T-POP deployment	K. Assmann
	CTD	1		21:25	21:40	74° 17.7564'	128° 11.1588'	298	288	6.57	88	0.19	68.1	First deep casting	Y. KIM
	SDD	18		21:03										Surface drifter deployment	T.W. KIM
	SDD	19	2/5/2018	6:08		70° 0.000'	162° 13.9530'							Surface drifter deployment	T.W. KIM
59	SDD	20	2/6/2018	0:58		67° 59.995'	170° 17.225'							Surface drifter deployment	T.W. KIM

Appendix 1.2. All design diagrams of moorings

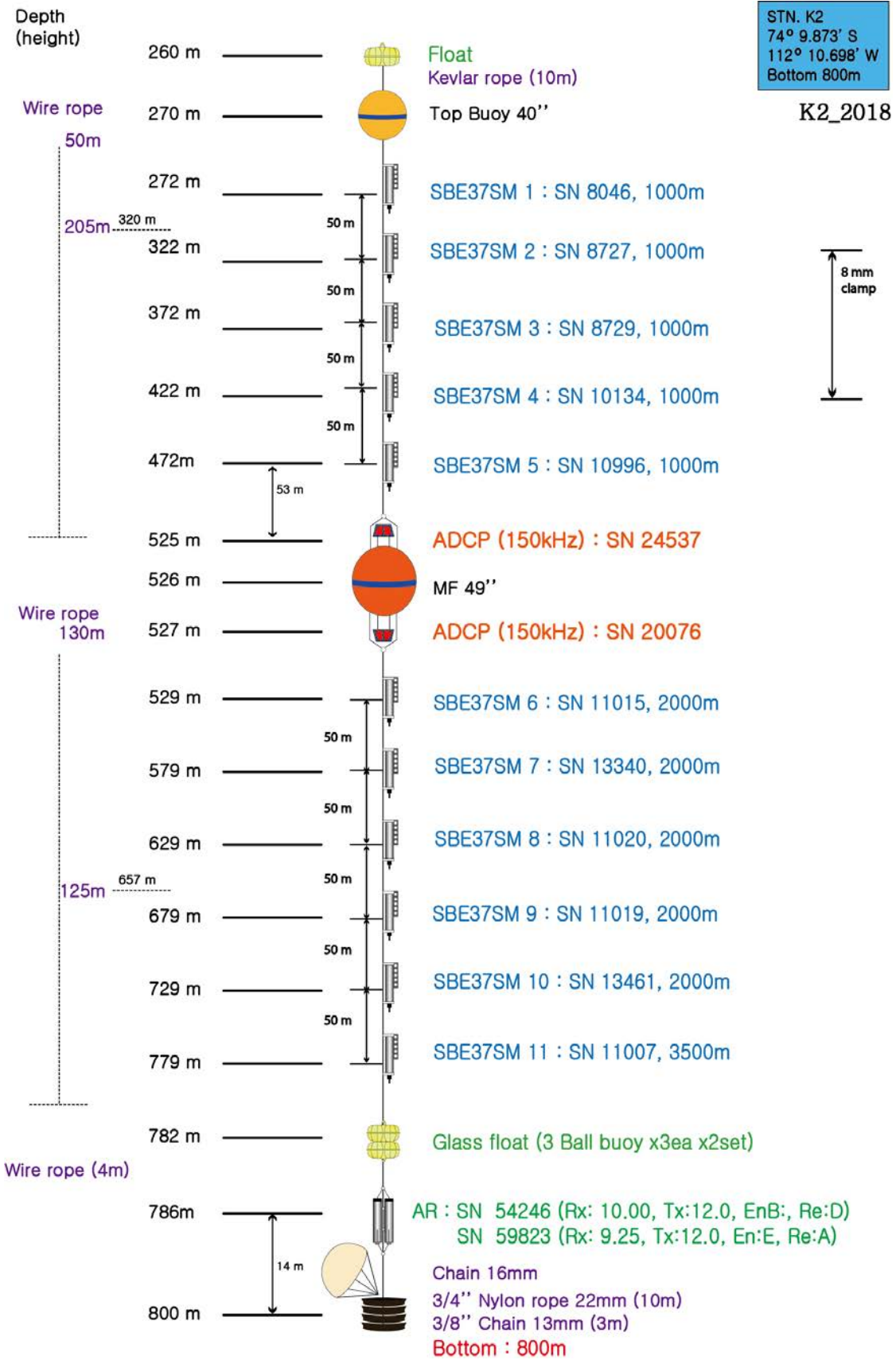
AP2 1 mooring design K1

K1_2018

STN. K1
 73° 16.764' S
 114° 56.968' W
 Bottom 830m



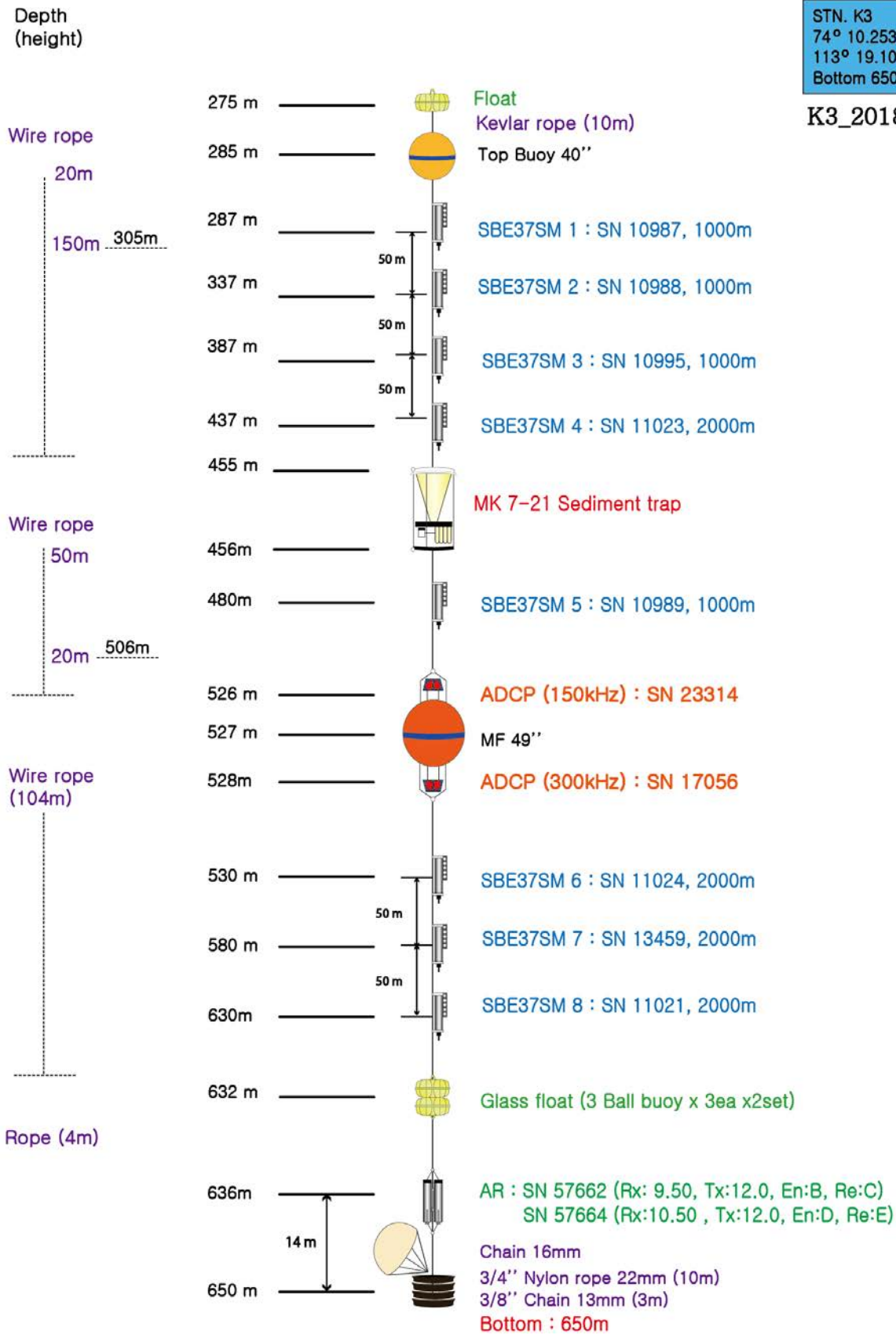
AP2 2 mooring design K2



AP2 3 mooring design K3

STN. K3
 74° 10.253' S
 113° 19.107' W
 Bottom 650m

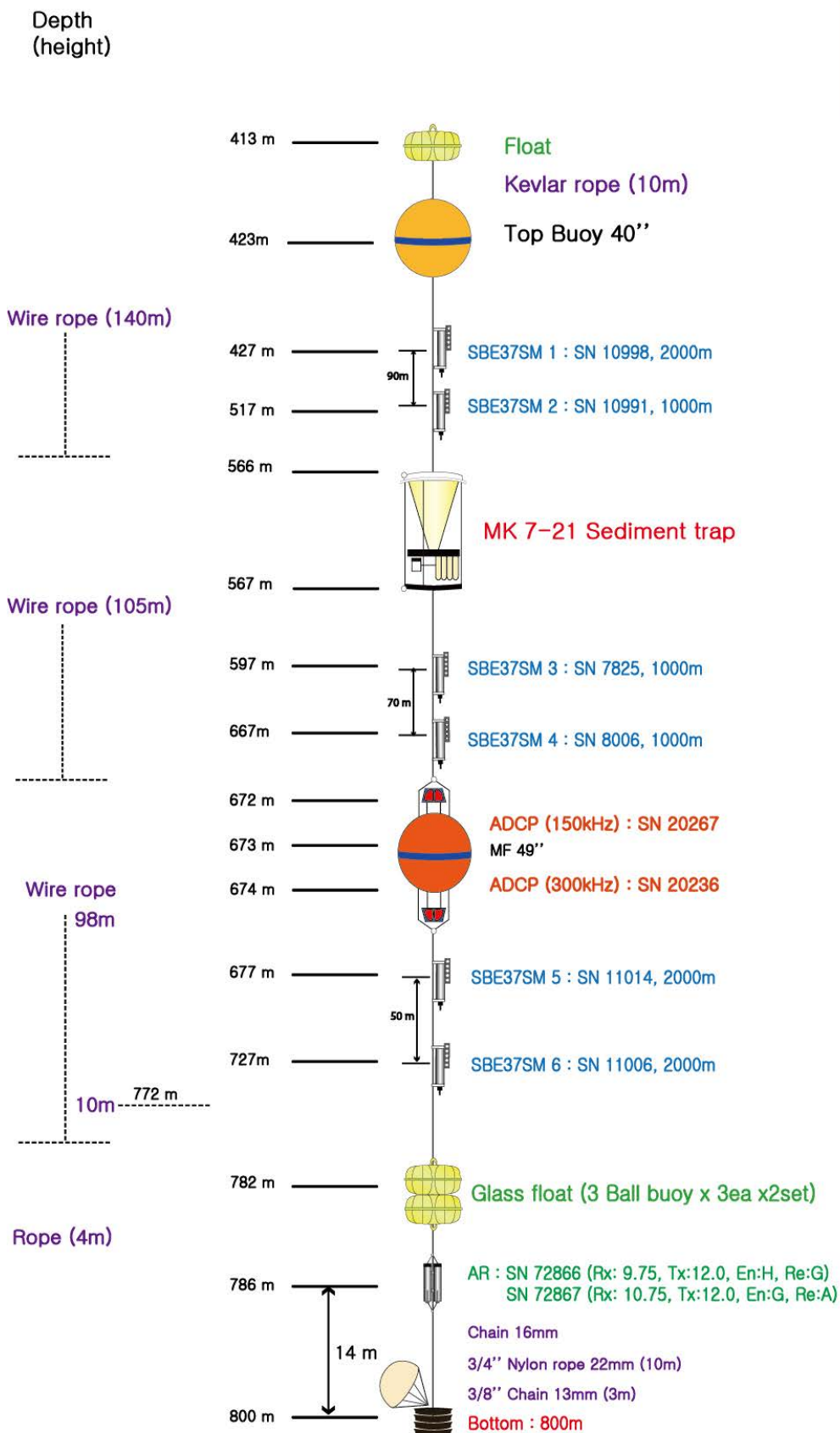
K3_2018



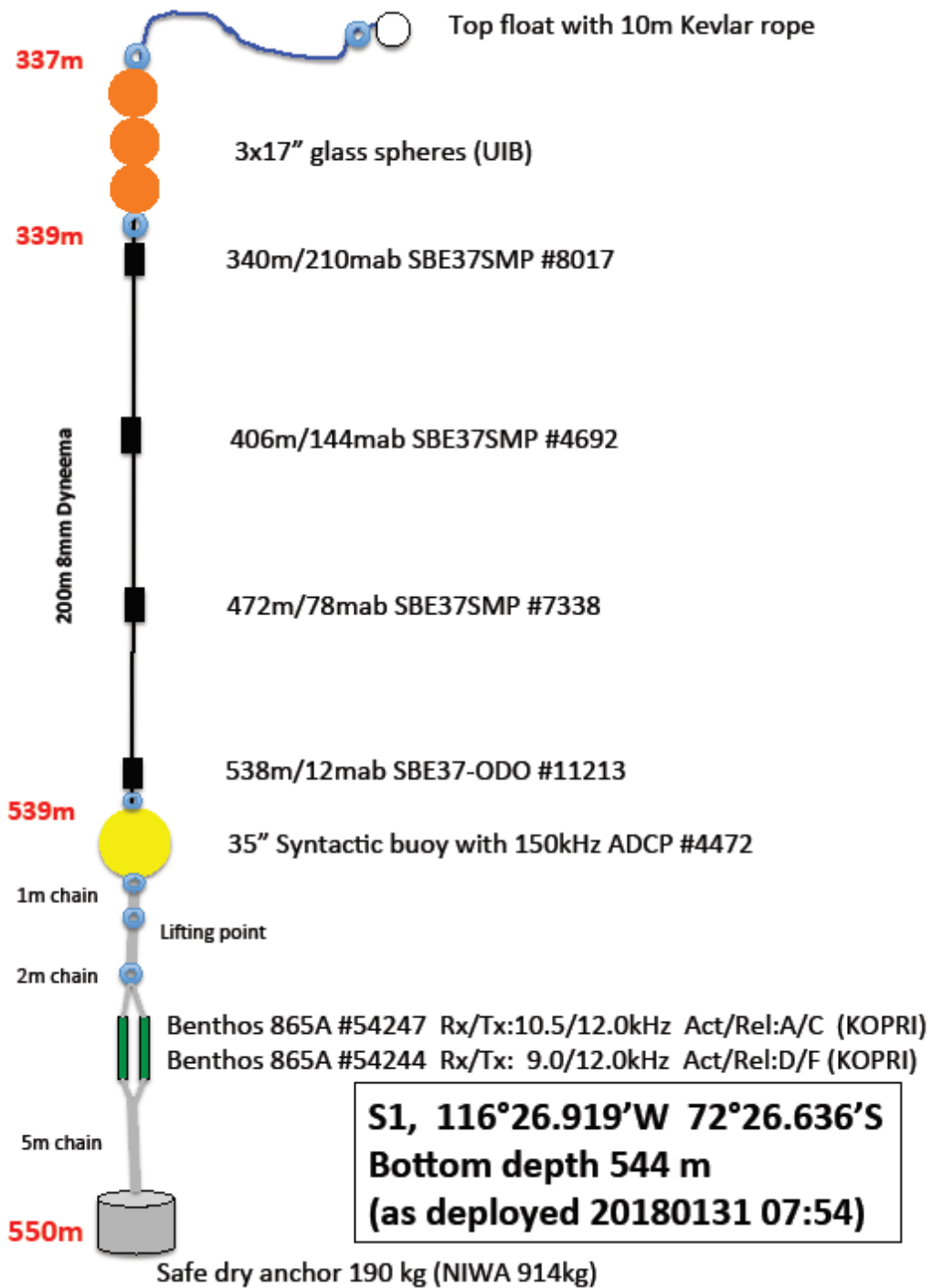
AP2 4 mooring design K4

STN. K4
 73 ° 55.315' S
 117 ° 17.485' W
 Bottom 800m

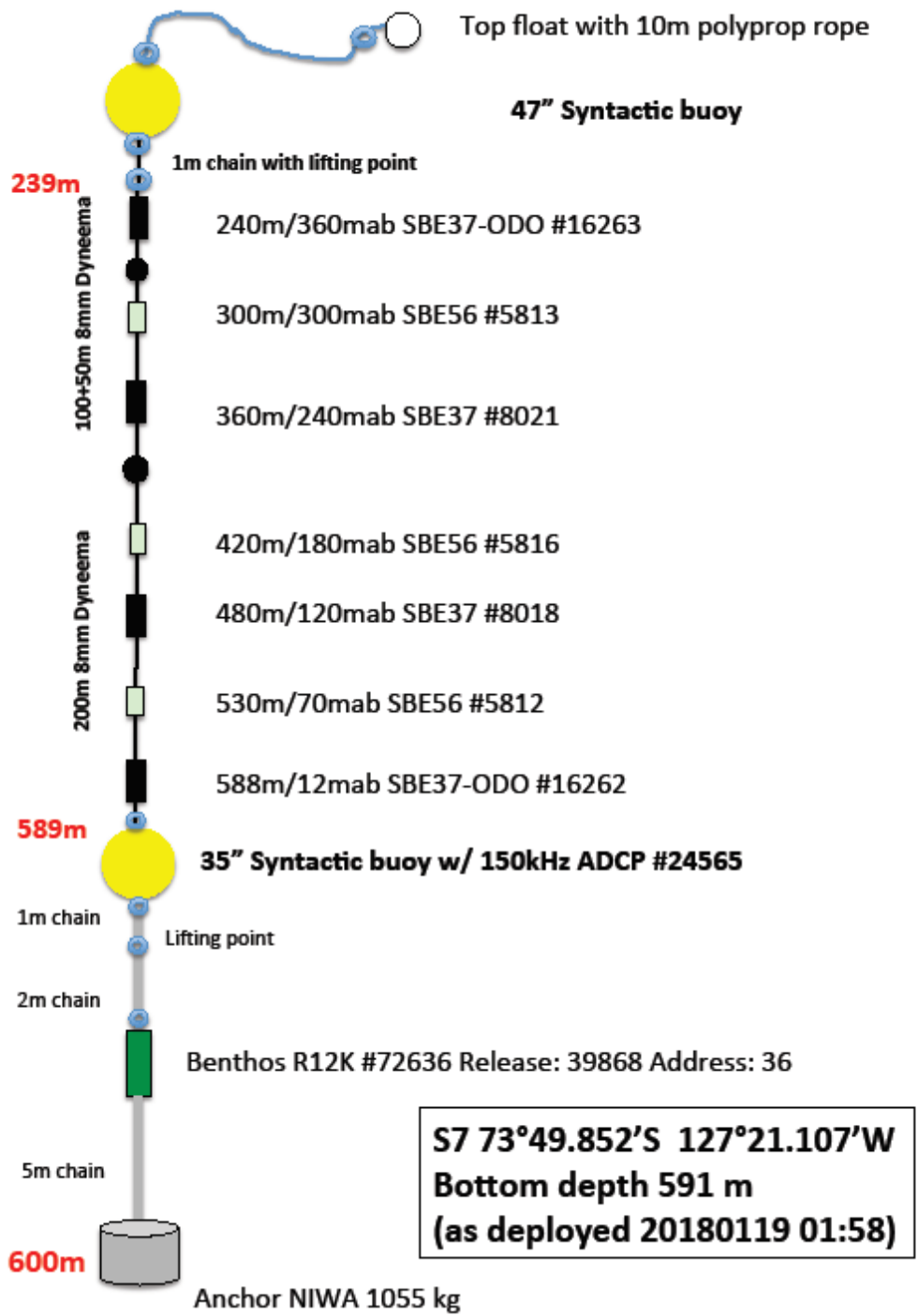
K4_2018



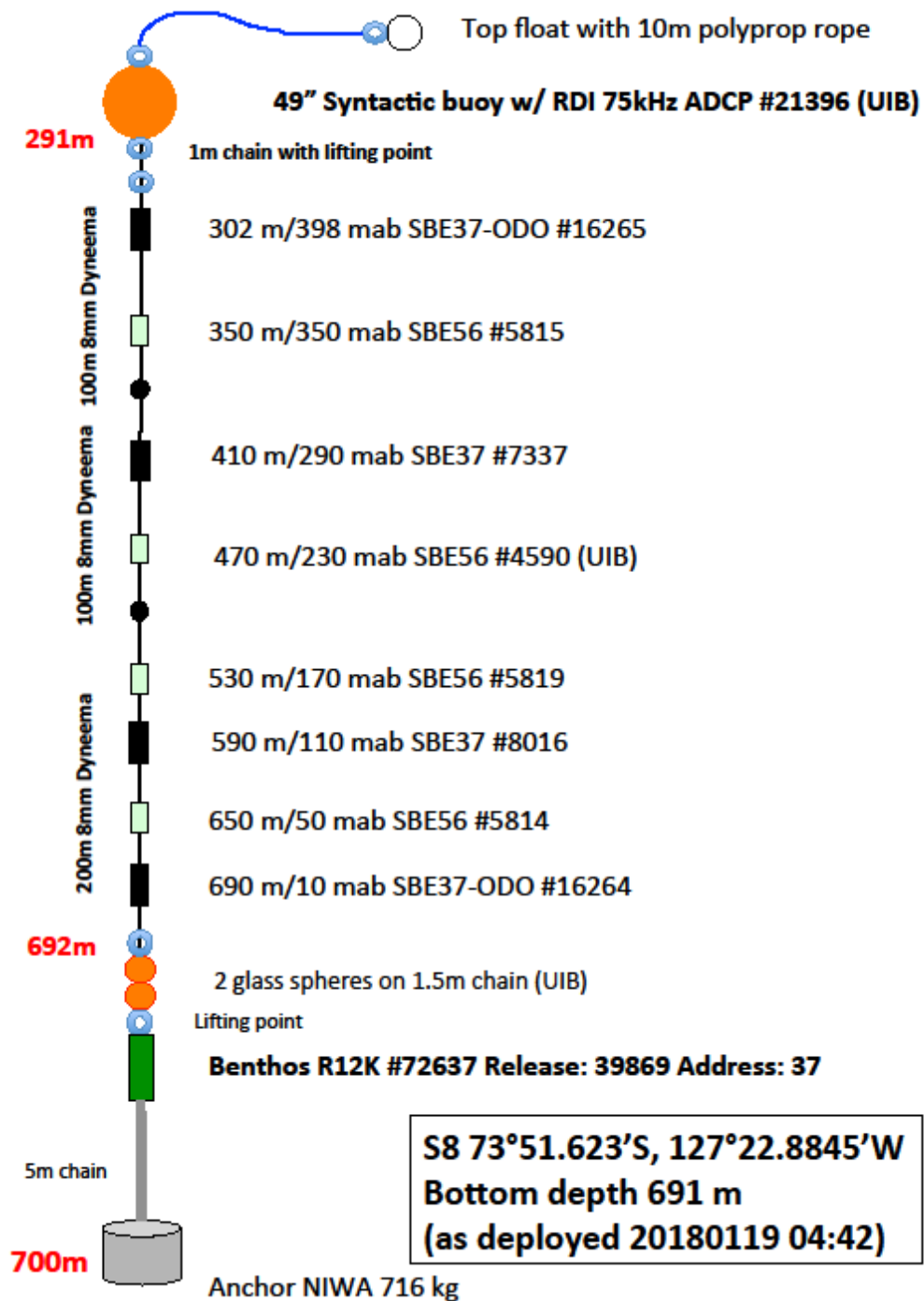
AP2 5 mooring design S1



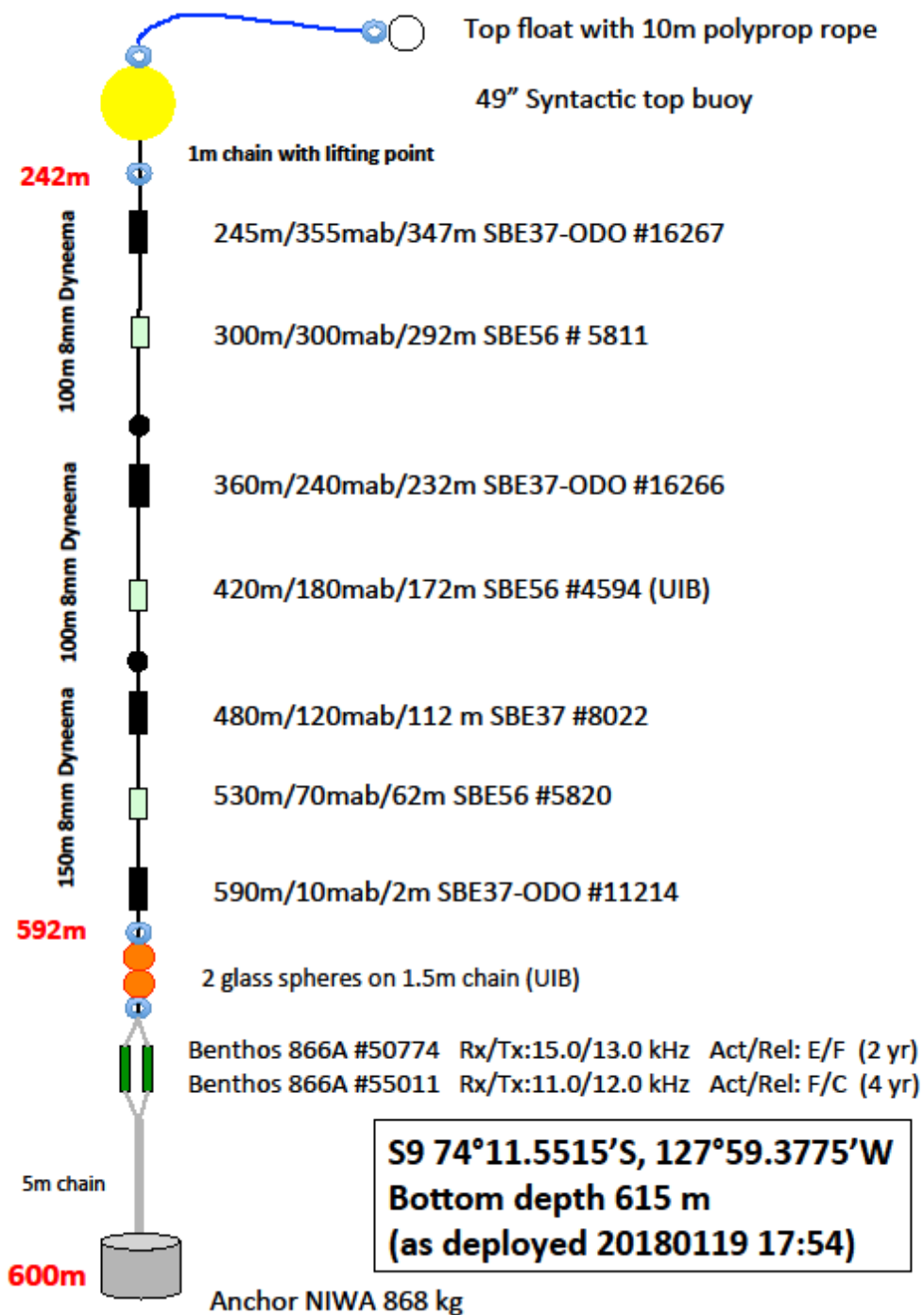
AP2 6 mooring design S7



AP2 7 mooring design S8

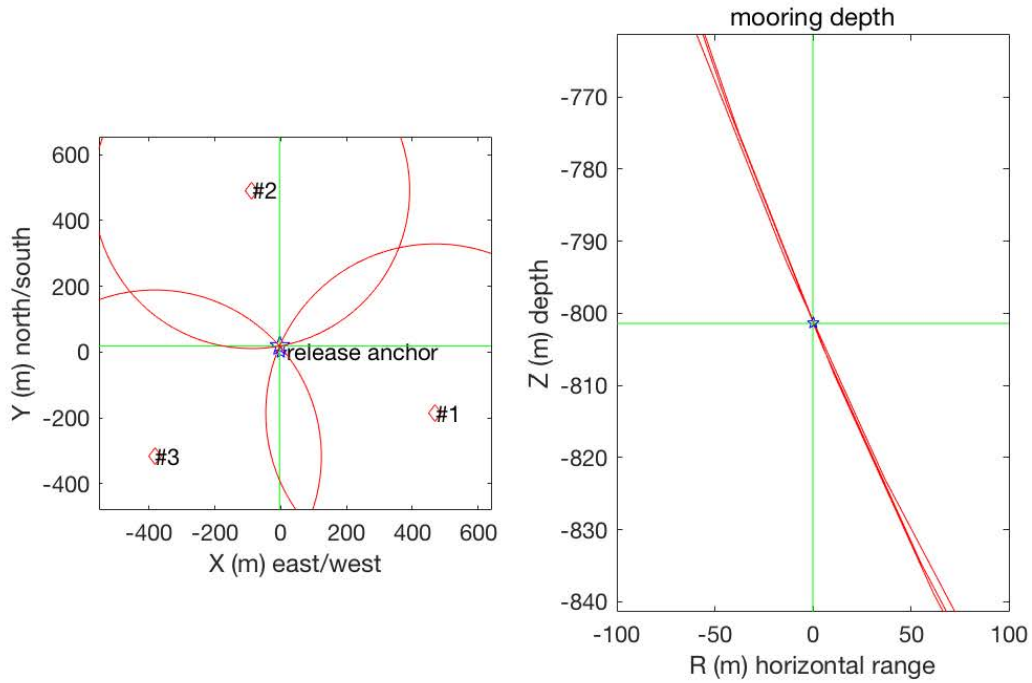


AP2 8 mooring design S9



Appendix 1.3. Triangulation results

AP3 1 K1 range



anchor release position: 73°S 16.773' 114°W 56.961'; depth: 830 m

3D mooring position: 73°S 16.763' 114°W 56.968'

drift: 18 m; direction: 350°

mooring depth: 801 m; slant error: 0 m

2D mooring position: 73°S 16.764' 114°W 56.968'

drift: 16 m; direction: 348°

horizontal error: 24 m

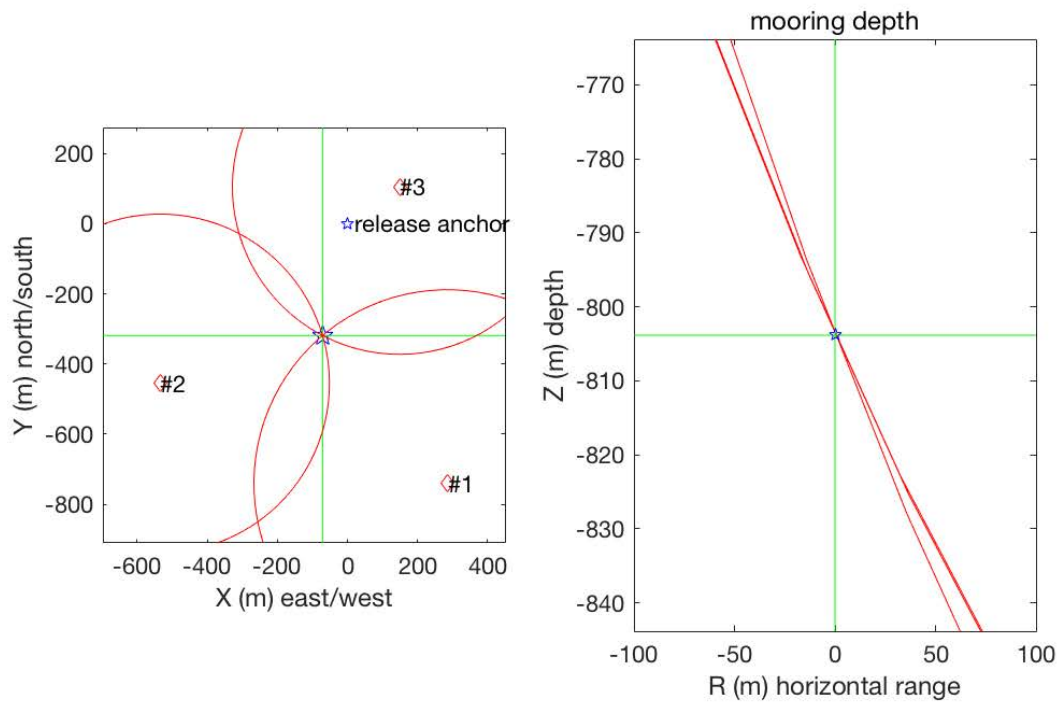
sound speed at site: 1445 m/s

#1 pos: 73°S 16.873' 114°W 56.080' range: 933 m range soundspeed 1500

#2 pos: 73°S 16.507' 114°W 57.128' range: 914 m range soundspeed 1500

#3 pos: 73°S 16.944' 114°W 57.679' range: 928 m range soundspeed 1500

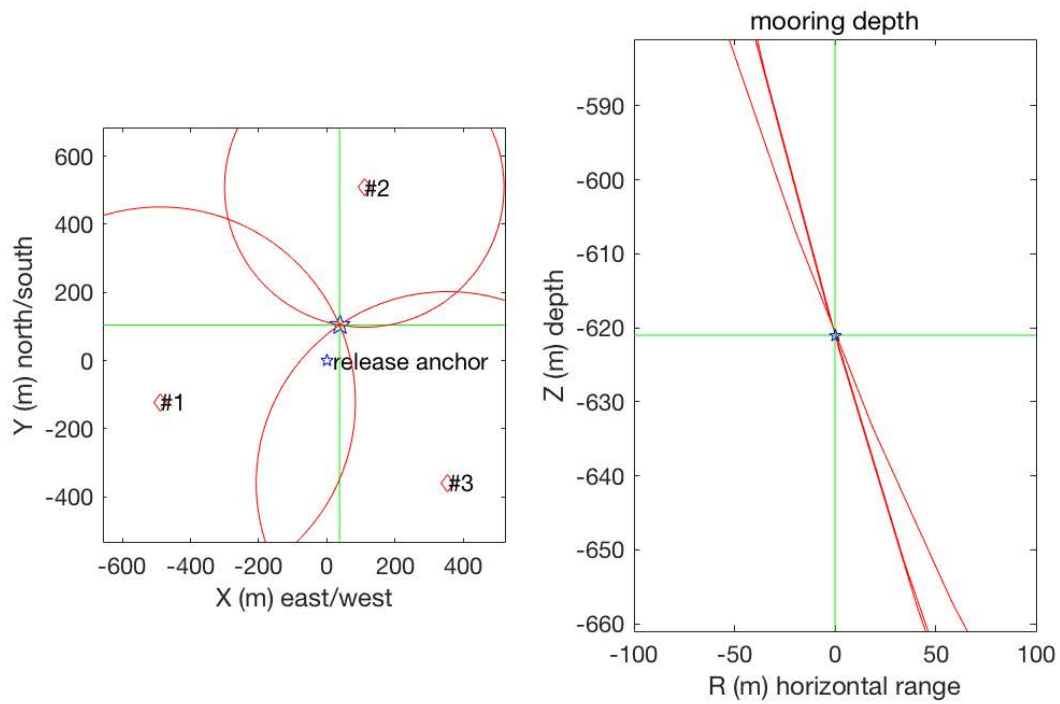
AP3 2 K2 range



anchor release position: 74°S 9.702' 112°W 10.556'; depth: 800 m
 3D mooring position: 74°S 9.874' 112°W 10.697'
 drift: 326 m; direction: 193°
 mooring depth: 804 m; slant error: 0 m
 2D mooring position: 74°S 9.873' 112°W 10.698'
 drift: 326 m; direction: 193°
 horizontal error: 3 m
 sound speed at site: 1445 m/s

#1 pos: 74°S 10.102' 112°W 9.991' range: 956 m range soundspeed 1500
 #2 pos: 74°S 9.948' 112°W 11.613' range: 917 m range soundspeed 1500
 #3 pos: 74°S 9.645' 112°W 10.262' range: 914 m range soundspeed 1500

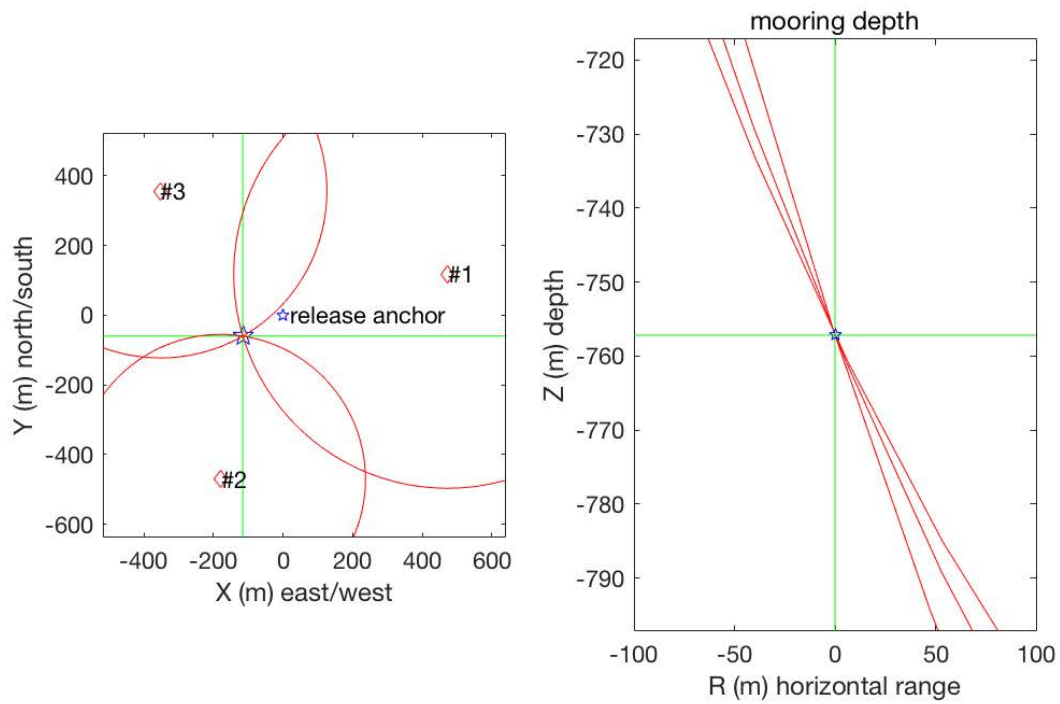
AP3 3 K3 range



anchor release position: 74°S 10.306' 113°W 19.172'; depth: 650 m
 3D mooring position: 74°S 10.250' 113°W 19.098'
 drift: 111 m; direction: 20°
 mooring depth: 621 m; slant error: 0 m
 2D mooring position: 74°S 10.253' 113°W 19.107'
 drift: 104 m; direction: 18°
 horizontal error: 21 m
 sound speed at site: 1445 m/s

#1 pos: 74°S 10.372' 113°W 20.140' range: 828 m range soundspeed 1500
 #2 pos: 74°S 10.032' 113°W 18.954' range: 724 m range soundspeed 1500
 #3 pos: 74°S 10.500' 113°W 18.470' range: 820 m range soundspeed 1500

AP3 4 K4 range



anchor release position: 73°S 55.287' 117°W 17.287'; depth: 800 m

3D mooring position: 73°S 55.319' 117°W 17.513'

drift: 130 m; direction: 243°

mooring depth: 757 m; slant error: 0 m

2D mooring position: 73°S 55.315' 117°W 17.485'

drift: 114 m; direction: 243°

horizontal error: 34 m

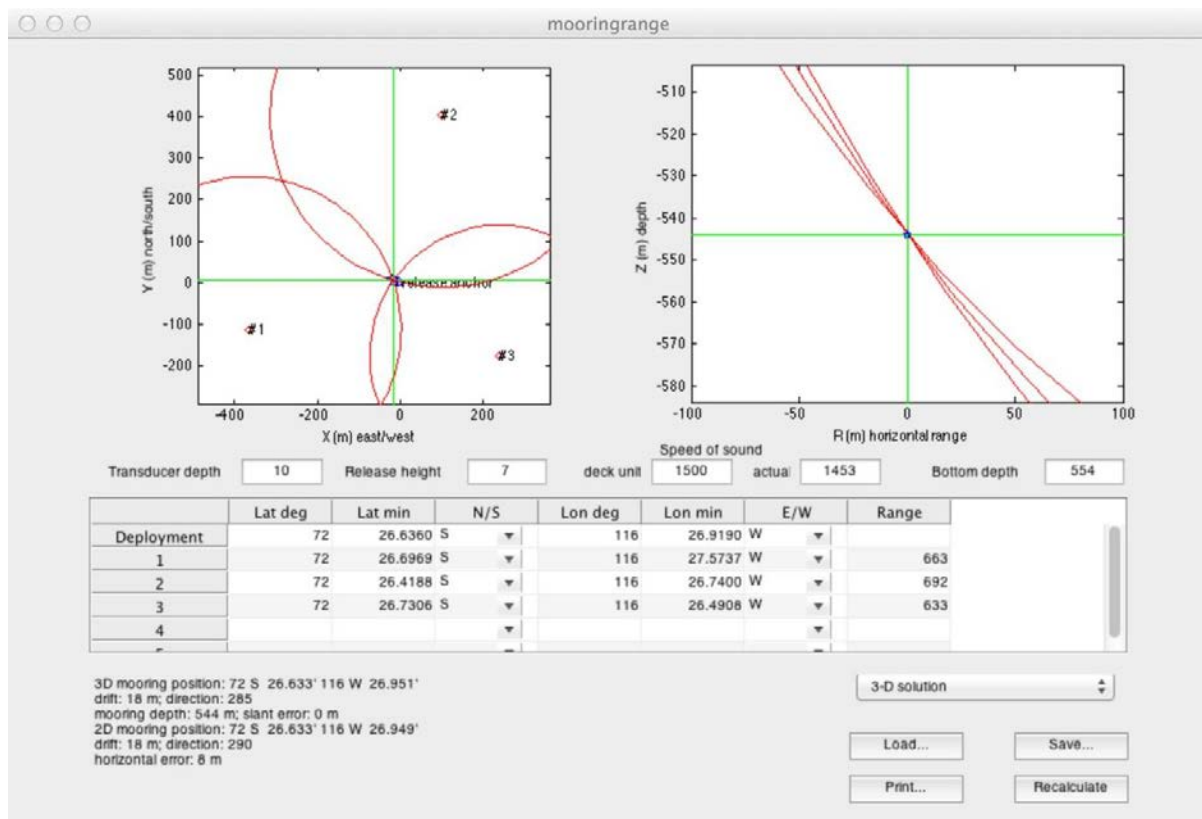
sound speed at site: 1445 m/s

#1 pos: 73°S 55.223' 117°W 16.366' range: 957 m range soundspeed 1500

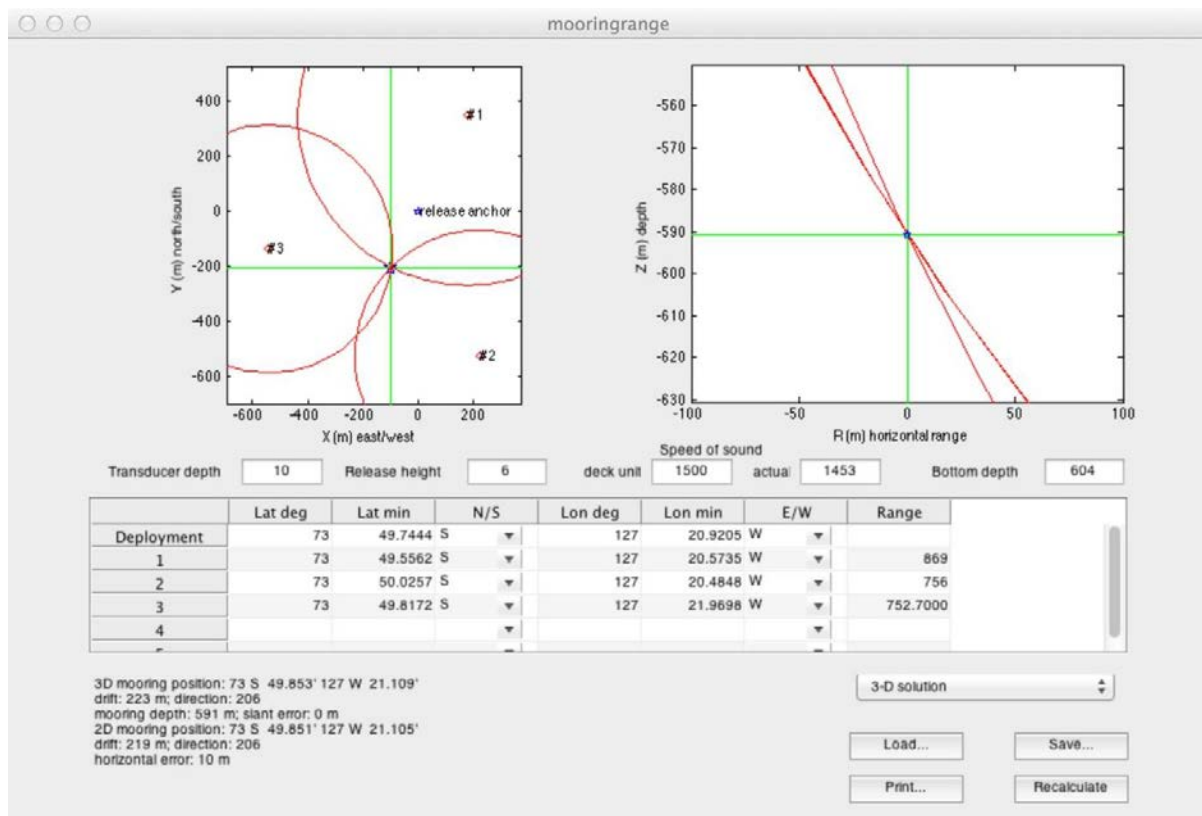
#2 pos: 73°S 55.541' 117°W 17.636' range: 843 m range soundspeed 1500

#3 pos: 73°S 55.094' 117°W 17.975' range: 876 m range soundspeed 1500

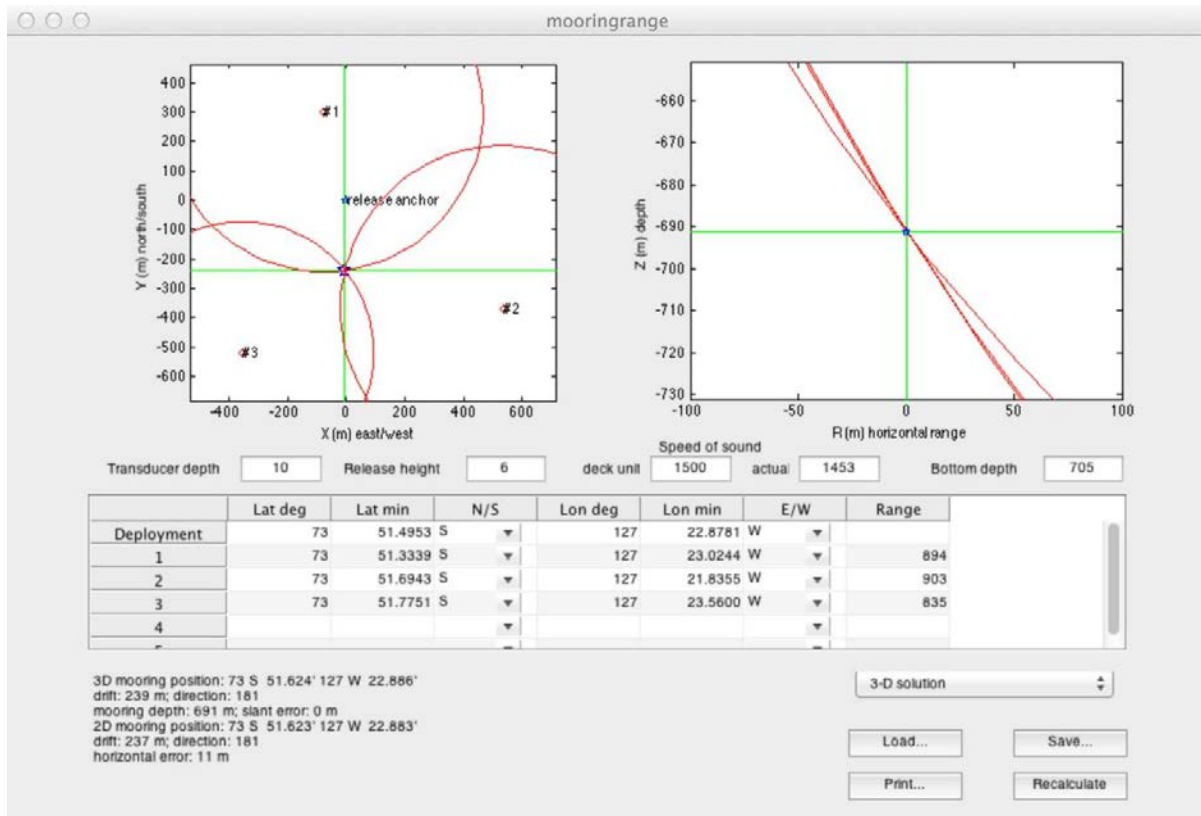
AP3 5 S1 range



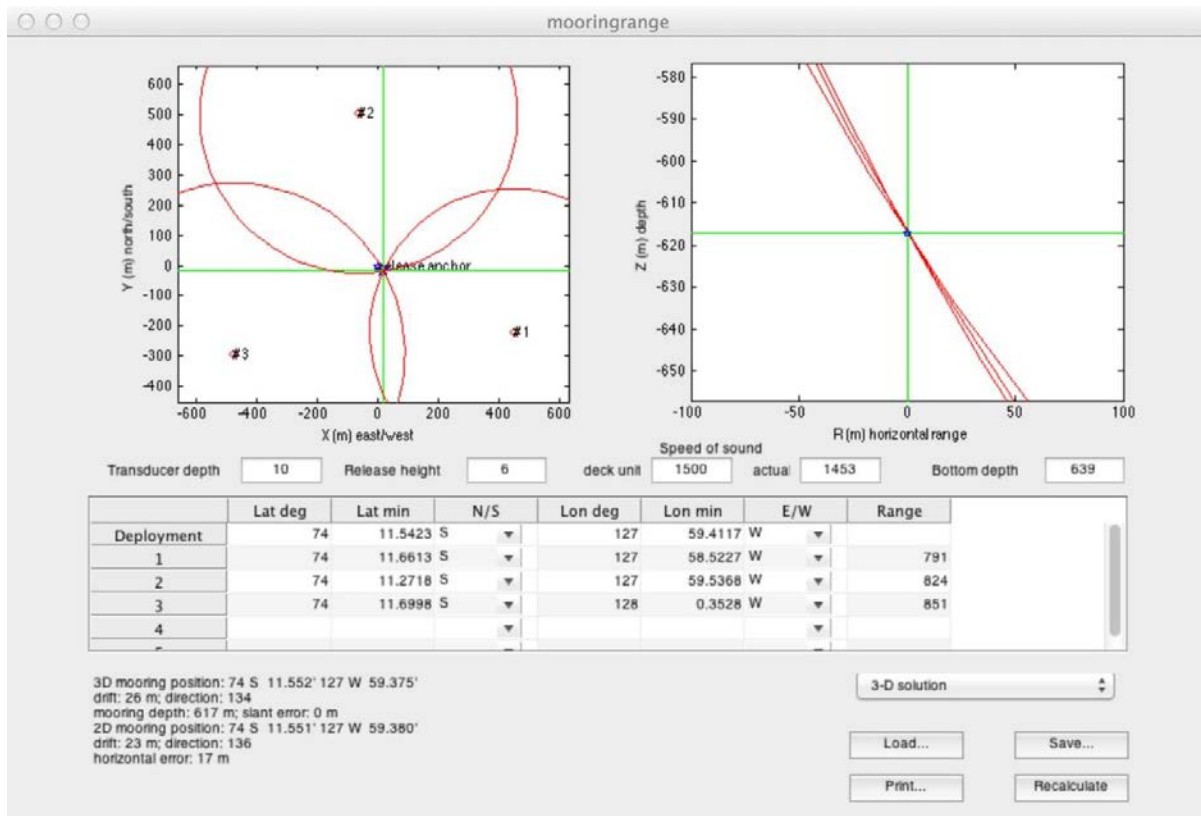
AP3 6 S7 range



AP3 7 S8 range



AP3 8 S9 range



Appendix 1.4. ADCP deployment files

AP4 1 ADCP setup S1 150kHz

```
CR1
CF11101
EA0
EB0
ED5700
ES35
EX11111
EZ1111101
WA50
WB1
WD111100000
WF352
WN44
WP30
WS800
WV175
TE00:30:00.00
TF18/01/30 23:30:00
TP00:03.00
CK
CS
;
;Consequences generated by PlanADCP version 2.06:
;First cell range = 12.21 m
;Last cell range = 356.21 m
;Max range = 345.39 m
;Standard deviation = 1.30 cm/s
;Ensemble size = 1034 bytes
;Storage required = 37.87 MB (39705600 bytes)
;Power usage = 1171.08 Wh
;Battery usage = 2.6
;
; WARNINGS AND CAUTIONS:
; Advanced settings have been changed.
```

AP4 2 ADCP setup S7 150kHz

CR1

CF11101

EA0

EB0

ED5900

ES35

EX11111

EZ1111101

WA50

WB1

WD111100000

WF352

WN44

WP30

WS800

WV175

TE00:30:00.00

TF18/01/17 12:00:00

TP00:03.00

CK

CS

;

;Consequences generated by PlanADCP version 2.06:

;First cell range = 12.21 m

;Last cell range = 356.21 m

;Max range = 352.96 m

;Standard deviation = 1.30 cm/s

;Ensemble size = 1034 bytes

;Storage required = 37.87 MB (39705600 bytes)

;Power usage = 1172.81 Wh

;Battery usage = 2.6

;

; WARNINGS AND CAUTIONS:

; Advanced settings have been changed.

AP4 3 ADCP setup S8 75kHz

CR1
CQ255
CF11101
EA0
EB0
ED3000
ES35
EX11111
EZ1111101
WA50
WB0
WD111100000
WF704
WN25
WP15
WS1600
WV175
TE02:00:00.00
TF18/01/19 00:00:00
TP00:05.00
CK
CS

;

;Consequences generated by PlanADCP version 2.06:

;First cell range = 24.69 m

;Last cell range = 408.69 m

;Max range = 570.56 m

;Standard deviation = 1.02 cm/s

;Ensemble size = 654 bytes

;Storage required = 5.99 MB (6278400 bytes)

;Power usage = 1269.26 Wh

;Battery usage = 2.8

;

; WARNINGS AND CAUTIONS:

; Advanced settings have been changed.

Chapter 2

Chemical Oceanography

2.1. Nutrient measurements

¹Jinyoung Jung and ¹Jin-Eui Son

¹Korea Polar Research Institute, Incheon 21990, South Korea

요약문

아문젠 폴리냐는 남극에서 확인된 폴리냐 중 생물생산력이 가장 높은 폴리냐로 알려져 있으며, 동시에 남극순환류 (Circumpolar Deep Water)의 유입으로 인해 빙봉이 빠르게 녹고 있는 지역이다. 아문젠 폴리냐가 높은 생물생산력을 보이는 이유로는 겨울철에서 봄철로 접어들면서 증가한 태양광의 양, 남극순환류의 유입에 따른 퇴적물 및 해빙, 빙봉에서 유입되는 철 성분에 의한 것으로 알려져 있다. 본 항해에서는 아문젠 폴리냐에서의 생물생산의 중요 요소 중 하나인 영양염 성분을 분석하여 높은 생물생산 및 생물 종조성에 따른 영양염 분포 변화양상을 조사하기 위해 아문젠해 탐사기간 동안 36개의 정점에서 영양염(아질산염+질산염, 인산염, 암모늄, 규산염)시료를 채취하여 선상에서 분석하였다. 영양염의 농도는 외양에서 높았고, 아문젠 폴리냐에서 급격히 감소하는 경향을 보여 폴리냐 내의 활발한 해양생물활동으로 인해 영양염의 소비가 증가하는 것이 확인되었다.

2.1.1. Introduction

The Amundsen Sea Polynya (ASP) is s the most productive polynya (per unit area) among 37 identified coastal polynya systems in the Antarctic (Arrigo and van Dijken, 2003) due to the combined effects of the enhanced light condition, supply of Fe from melting sea ice and/or glaciers and continental shelf sediments resulted from the intrusion of relatively warm, salty, and nutrient-rich Circumpolar Deep Water (CDW) onto the continental shelf down deep troughs. (Arrigo et al., 2012). To improve our understanding of roles of nutrients in biological processes such as variations of N/P ratio in water column and N and P uptake ratio by different phytoplankton species, we investigated spatial and temporal variations of nutrients (PO_4^{3-} , $\text{NO}_3^- + \text{NO}_2^-$, NH_4^+ , and SiO_2) in seawater collected in the Amundsen Sea. The results for nutrients would be valuable for filling the data gap, and useful to understand biogeochemical cycles of C, N, and P as well as carbon sequestration by biological carbon pump in the Amundsen Sea.

2.1.2. Methodology and preliminary results

Seawater sampling for nutrients was carried out at 37 stations (35 stations + 2 revisit stations) in the Amundsen Sea using a CTD/rosette sampler holding 24-10L Niskin bottles (SeaBird Electronics, SBE 911 plus) during Korea research Ice Breaker R/V Araon cruise (ANA08B, January 18, 2018–February 2, 2018) (Fig. 2.1). Samples for nutrients were collected from the Niskin rosette into 50 ml conical tubes and immediately stored in a refrigerator at 4°C prior to chemical analyses. All nutrients samples were analyzed within 3 days. Concentrations of nutrients were measured using standard colorimetric methods adapted for use on a 4-channel continuous Auto-Analyzer (QuAatro, Seal Analytical). The channel configurations and reagents were prepared according to the ‘QuAatro Applications’. Standard curves were run with each batch of samples using freshly

prepared standards that spanned the range of concentrations in the samples. The r^2 values of all the standard curves were greater than or equal to 0.99. Surface $\text{NO}_2^- + \text{NO}_3^-$ and PO_4^{3-} concentrations in the open ocean stations were higher than those observed in the polynya owing to low biological activity in these two stations. The surface $\text{NO}_2^- + \text{NO}_3^-$ and PO_4^{3-} concentrations gradually decreased with increasing fluorescence, indicating that $\text{NO}_2^- + \text{NO}_3^-$ and PO_4^{3-} were utilized by phytoplankton.

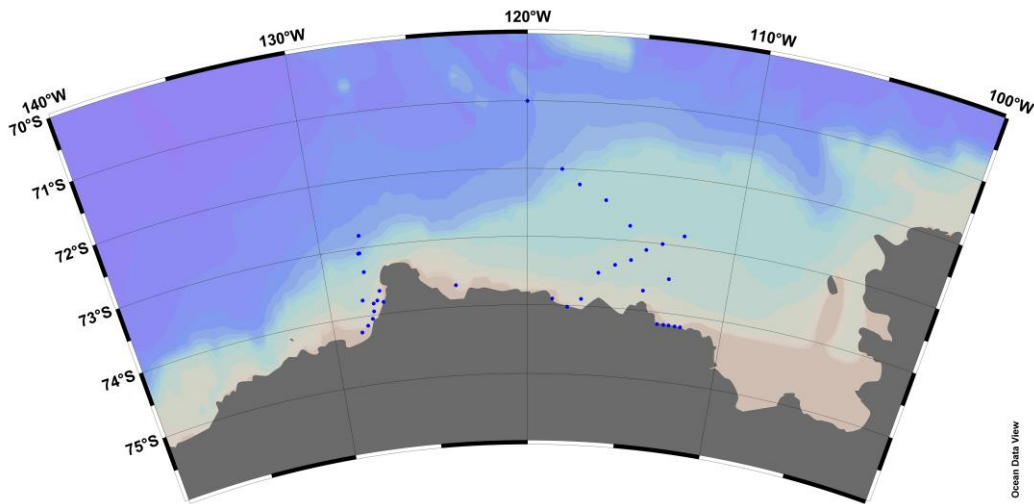


Figure 2.1. Map of study area. Blue dots show the CTD stations during the expedition.

References

- Arrigo, K. R., van Dijken, G. L., (2003) Phytoplankton dynamics within 37 Antarctic coastal polynya systems. *Journal of Geophysical Research*, 108(C8), 3271, doi:10.1029/2002JC001739.
- Arrigo, K. R., Lowry, K. E., van Dijken, G. L., (2012) Annual changes in sea ice and phytoplankton in polynyas of the Amundsen Sea, Antarctica, *Deep-Sea Research Part II*, 71-76(c), 5–15, doi:10.1016/j.dsr2.2012.03.006.

2.2. Observations of dissolved and particulate matters

¹Jinyoung Jung, and ¹Jin-Eui Son

¹Korea Polar Research Institute, Incheon 21990, South Korea

요약문

유기탄소의 해양 심층으로의 저장은 해양생태계에서의 탄소균형을 조절하는 중요한 생지화학적 과정이며 해양에서 존재하는 용존 및 입자상 유기탄소화합물은 생물학적 펌프를 결정하는 주요 화합물로 알려져 있다. 아문젠 해역의 주요 식물플랑크톤 종인 *Phaeocystis antarctica*는 colony를 형성하고, *diatom*은 상대적으로 크기가 크기 때문에 탄소저장에 있어서 다른 거동을 보인다고 알려져 있다. 본 연구에서는 아문젠해에서의 식물 종 조성에 따른 입자상, 용존 유기물질의 생지화학적 특성을 이해하고자 한다.

2.2.1. Introduction

Export of organic matter is an important biogeochemical process contributing to the carbon balance in marine ecosystem (Ducklow et al., 2015). In the ocean, export is defined as the transport, by sinking, advection or migration, of dissolved and particulate organic carbon (DOC and POC). Together the processes of export and its consumption in the upper 1000 m determine the amount of carbon ultimately stored in the deeper ocean, isolated from exchange with the atmosphere over time scales of centuries to millennia. The processes governing the export and the efficiency of its transfer to deep sea are poorly understood, especially in the Amundsen Sea, an important ocean carbon dioxide (CO₂) sink. In the Amundsen Sea, *Phaeocystis antarctica* and *diatom* are the dominant phytoplankton taxa. Because of the different behaviors of *Phaeocystis antarctica* and *diatom* in terms of sinking particles, potential shift in plankton community composition can influence the biological pump efficiency in the Amundsen Sea. Until now, few studies have been carried out to investigate the distribution and dynamics of dissolved and particulate organic matter in the Amundsen Sea. Our objective of this study therefore is to examine the biogeochemical characteristics of dissolved organic matter (DOM) and particulate organic matter (POM) and their C:N ratios during the expedition.

2.2.2. Methodology

Seawater sampling for dissolved organic matter was carried out at 37 stations (35 stations + 2 revisit stations) in the Amundsen Sea using a CTD/rosette sampler holding 24-10L Niskin bottles. For dissolved organic matter measurements, a pre-cleaned (soaked in 10% HCl and rinsed with ultrapure water) Teflon tube was used to connect between spigot and pre-cleaned 47 mm filtration holder made of PP (PP-47, ADVANTEC) (Fig. 2.2 (a)). About 200 ml of seawater was filtered through a pre-combusted (at 550°C for 6 hours) Whatman GF/F filter (47 mm in diameter) under gravity. The filtered samples were collected directly into pre-cleaned glass bottles. The filtrate was distributed into two pre-combusted 20 ml glass ampoules with a sterilized serological pipette. Each ampoule was sealed with a torch, quick-frozen, and preserved at approximately -24°C until the analysis in our land laboratory. Simultaneous dissolved organic carbon/total dissolved nitrogen analyses will be basically made with an HTCO system consisting of a commercial unit, the Shimadzu TOC-L system (Shimadzu Co.), fitted with a chemiluminescence (CLS) detector that was incorporated into the total nitrogen micro analyzer. The concentration of dissolved organic nitrogen (DON) will be obtained by the difference between total dissolved nitrogen and dissolved inorganic nitrogen (i.e., NO₂⁻+NO₃⁻ and NH₄⁺) concentrations.

A 1 L of seawater for analysis of POC was drained from the Niskin bottles into a pre-cleaned amber polyethylene bottle, as was the particulate organic nitrogen (PON) sample. POC and PON samples were filtered with pre-combusted (at 550°C for 6 hours) GF/F filters (47 mm in diameter) using a filtering system under gentle vacuum at 0.1 MPa (Fig. 2.2 (b)). The GF/F filters for POC and PON measurements were stored at -24°C in hinged-lid and airtight PP containers. Prior to analysis of POC sample, particulate inorganic carbon should be removed using acid. The filters for POC and PON measurements will be analyzed using a CHN analyzer in our land laboratory.

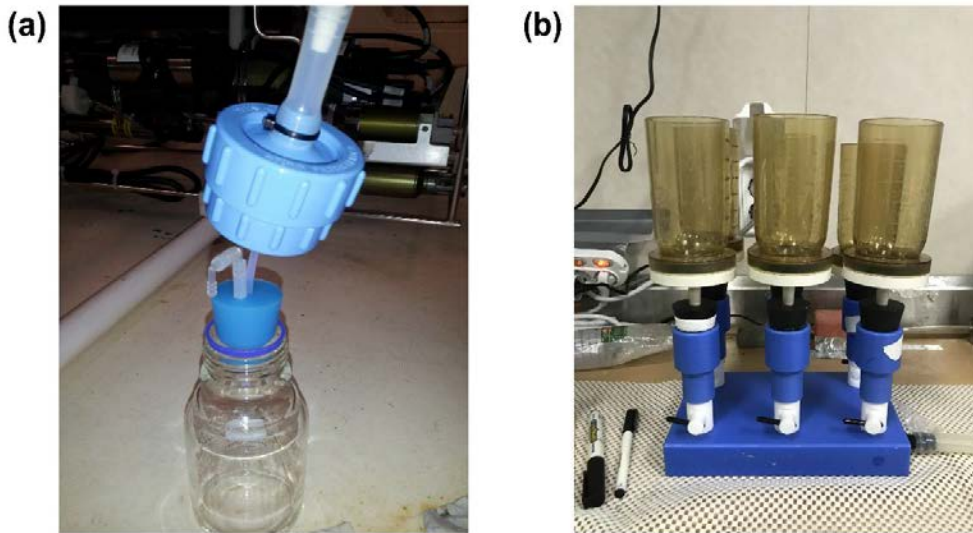


Figure 2.2. Instruments for sampling of dissolved (a) and particulate (b) organic matters.

References

Ducklow, H.W., Wilson, S.E., Post, A.F., Stammerjohn, S.E., Erickson, M., Lee, S., Lowry, K.E., Sherrell, R.M., Yager, P.L., (2015) Particle flux on the continental shelf in the Amundsen Sea Polynya and Western Antarctic Peninsula. *Elementa: Science of the Anthropocene*, 3, 1–20.

2.3. Observations of sulfur species in marine aerosols

¹Jinyoung Jung

¹Korea Polar Research Institute, Incheon 21990, South Korea

요약문

해양에서 가장 주요한 황화합물은 dimethylsulfide (DMS)이며, 이는 식물플랑크톤의 물질대사작용에 의해 생성된다. 대부분의 DMS는 해양에서 박테이아에 의해 분해되지만 일부는 대기 중으로 배출된다. 대기중으로 배출된 DMS는 산화되며 입자상 물질인 비해염성 황산염 (nss-SO_4^{2-})과 메탄술폰산 (MSA)으로 존재하게 된다. 이들 황화합물은 구름의 응결핵으로 작용하여 구름을 형성, 태양복사광 균형에 영향을 미쳐 지구냉각 효과를 일으킨다고 알려져 있다. 아문젠 폴리냐는 남극에서 생물학적 생산이 가장 높고 인위적 오염발생원이 극히 적은 지역이므로 DMS기원의 비해염성 황산염과 메탄술폰산의 연구에 적합한 장소이다. 뿐만 아니라 아문젠해에서의 주요 식물플랑크톤 종인 *Phaeocystis antarctica*는 많은 양의 DMS를 생산한다고 알려져 있다. 본 연구에서는 아문젠해역에서의 대기 중 황화합물의 생지화학적 순환을 이해하고자 한다.

2.3.1. Introduction

The biogeochemical cycle of sulfur between the marine atmosphere and the ocean has received considerable attention in the last two decades due to its potential for climate regulation. Dimethylsulfide (DMS), the most dominant sulfur species throughout the ocean, is a metabolic byproduct of the production of dimethylsulfoniopropionate (DMSP), which is produced primarily by phytoplankton. Although most DMS is consumed by bacteria, sea surface layers are always supersaturated with it, which implies a net flux of DMS to the atmosphere. As a result, about 1% of the DMSP produced in seawater is transported to the atmosphere in the form of DMS through sea-to-air flux. Atmospheric non-sea-salt sulfate (nss-SO_4^{2-}) and methanesulfonic acid (MSA) derived from DMS oxidation could affect the Earth's radiation balance through the formation of cloud condensation nuclei and, thereby, exert a cooling effect by increasing planetary albedo (Quinn and Bates, 2011). Phytoplankton taxonomic abundances in the Amundsen Sea are dominated by colonial haptophyte *Phaeocystis antarctica*, which produces large amounts of DMS in Antarctic waters (Schoemann et al., 2005). Although considerable effort has been devoted to estimating the contribution of biogenic source through the investigation of spatial and temporal characteristics of nss-SO_4^{2-} and MSA in aerosols collected over various regions and during different periods, few data has been reported for the Amundsen Sea. The results for sulfur compounds obtained from the expedition would be valuable for filling the data gap, and useful to understand biogeochemical cycles of sulfur in the Amundsen Sea.

2.3.2. Methodology

Two high-volume (1000 LPM) air samplers (Sibata Co., Ltd.) were used to collect fine ($D < 2.5 \mu\text{m}$) and coarse ($D > 2.5 \mu\text{m}$) marine aerosols on a quartz filter (8X10 inch, Sibata), respectively. The aerosol samplers were put on the front of the compass deck of the ship (Fig. 2.3). A wind-sector controller was used to avoid contamination from ship's exhaust during the cruise. The wind-sector controller was set to collect marine aerosol samples only when the relative wind directions were within plus or minus 100° relative to the ship's bow and the relative wind speeds were over 1 m s^{-1} during the cruise. The total aerosol sampling intervals varied between 2–3 days. After sampling, the filter was stored frozen at -24°C prior to chemical analysis in our land laboratory. A total of 21 samples were collected during the cruises. In the land laboratory, aerosol samples will be ultrasonically extracted using 50 ml of

Milli-Q water. The extraction solution was then filtered through a 13-mm diameter, 0.45-mm pore-size membrane filter (PTFE syringe filter, Millipore Co.). The filtrates were analyzed by ion chromatography (IC; Dionex-320, Thermo Scientific Dionex) for anions including SO_4^{2-} and MSA and for cations including Na^+ . The concentrations of nss-SO_4^{2-} were calculated as total SO_4^{2-} minus the Na^+ concentration times 0.2516, the $\text{SO}_4^{2-}/\text{Na}^+$ mass ratio in bulk seawater.



Figure 2.3. The high volume air samplers and the wind-sector controller set in the compass deck.

References

- Quinn, P.K., Bates, T.S., (2011) The case against climate regulation via oceanic phytoplankton sulfur emissions. *Nature*, 480, 51–56.
- Schoemann, V., Becquevort, S., Stefels, J., Rousseau, V. and Lancelot, C., (2005) *Phaeocystis* blooms in the global ocean and their controlling mechanisms: a review. *Journal of Sea Research*, 53(1-2), 43–66, doi:10.1016/j.seares.2004.01.008.

2.4. Noble gases as tracers of glacial meltwaters: sample collection and onboard measurements in the Amundsen Sea

¹ Dong-young Shin and ¹Doshik Hahm

¹Department of Oceanography, Pusan National University, Busan 46241, Republic of Korea

2.4.1. Objectives

The noble gases, especially helium isotopes (^3He and ^4He) in conjunction with tritium (^3H), have been widely used to trace water mass movement by exploiting their conservative behavior and to give time constraints (i.e., ^3H – ^3He age) on physical and biological processes in the ocean. In addition, noble gases have been proven to be excellent tracers of ice-related processes in polar oceans. This application is based on the fact that different noble gases have different partitioning characteristics in water, sea-ice and glacier. For example, the dissolution of air bubbles trapped in glacial ice results in an approximately tenfold super-saturation of He and Ne (Schlosser, 1986). The hydrography of the Amundsen Sea is in substantial change partly due to rapid melting of glacial ice shelves. Given the high resolving power of noble gases for ice-related processes, they will provide invaluable information on the influence of glacial melting on the changes of hydrography and, in turn, biological processes in the Amundsen Sea.

2.4.2. Sample collection in copper tubes

Water samples for noble gases were collected at 26 stations, including 2 in the Udintsev Fracture Zone, among over 50 CTD stations covered in the cruise (Figure 2.4). The sampling locations were selected to constitute sections of (1) along the Amundsen Trough, (2) across the trough, (3) along the Dotson ice shelf and (4) along the the Getz between Siple and Dean islands (the station with red circles in Figure 2.4).

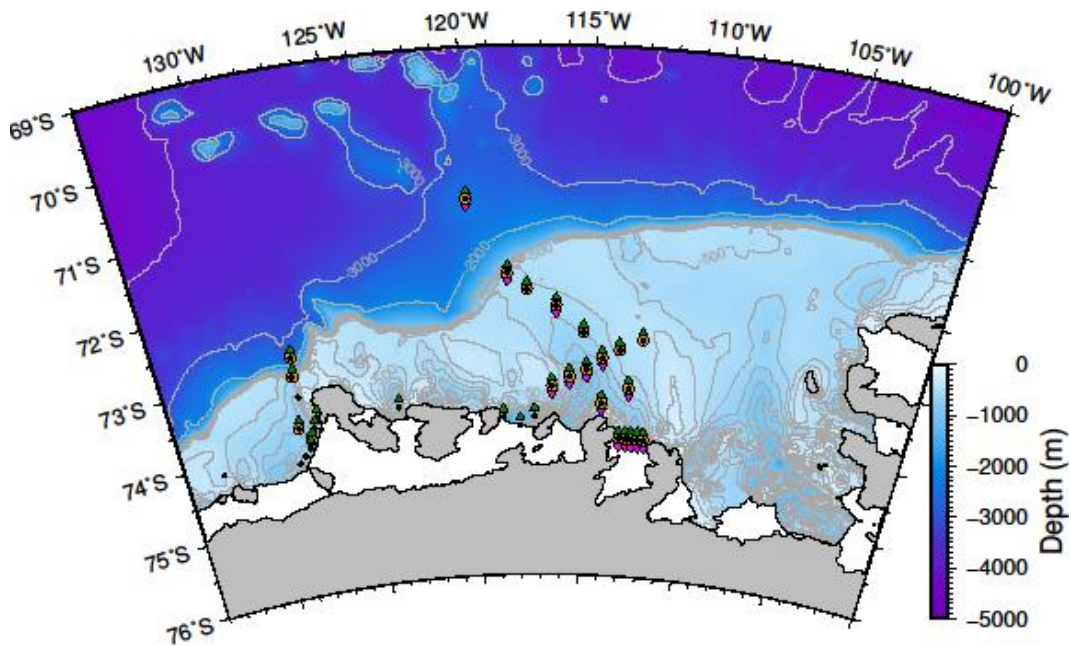


Figure 2.4. Bathymetric map of the Amundsen Sea. Black circles and green triangles stand for the stations where samples were analyzed on-board for noble gases and DMS/ ΔO_2 /Ar, respectively. Orange circles and purple triangles stand for the stations where samples were collected for noble gases in Cu-tubes and for FDOM, respectively.

2.4.3. On-board measurements using a membrane inlet mass spectrometer

The conventional method to determine noble gases involves (1) sample collection in copper tubes, (2) gas extraction in a shore-based laboratory, (3) large sample preparation and mass spectrometric systems. The method is time-consuming and very expensive. During the cruise, we measured 4 noble gases (He, Ne, Ar, and Kr) in seawater using a membrane inlet mass spectrometer, which can perform a sample measurement in 5 minutes. This method is a modification of Visser et al. (2013), which was originally developed for measurements of groundwater samples. Figure 2.5 shows the schematic of the sample preparation system. We removed water and CO₂ traps present in Visser et al. (2013) for an easy maintenance at sea and rely on two St2002 getters for the removal of reactive gases. One was kept hot at 300°C and the other was at room temperature.

A triple filter quadrupole mass spectrometer was used for the detection of noble gases (Hiden HAL 3F RC201). Source and detector settings used for the measurements were similar to those of Manning et al. (2016); ²²Ne were measured at an electron energy of 35 V to prevent the formation of doubly-charged CO₂. Figure 2.6 shows a typical cycle of the measurements. Filtered seawater equilibrated with air at 10°C were used for standard solution. The standard was measured repeatedly after 3 - 4 measurements of samples. Blank was determined by stopping the peristaltic pump used to carry water through the membrane for 30 minutes and by averaging the last 3 minutes of the measurements.

Total 380 samples collected at 41 stations were analyzed onboard (Figure 2.4). The samples collected in glass vials were immersed in water and kept in a refrigerator until analyses. All the samples were measured within 3 hours after sampling to minimize contamination. Some of aforementioned Cu-tube samples will be used to make precise measurements of noble gases and He isotopic ratios at the laboratory. The results will be compared with the on-board measurements to check if any bias is present.

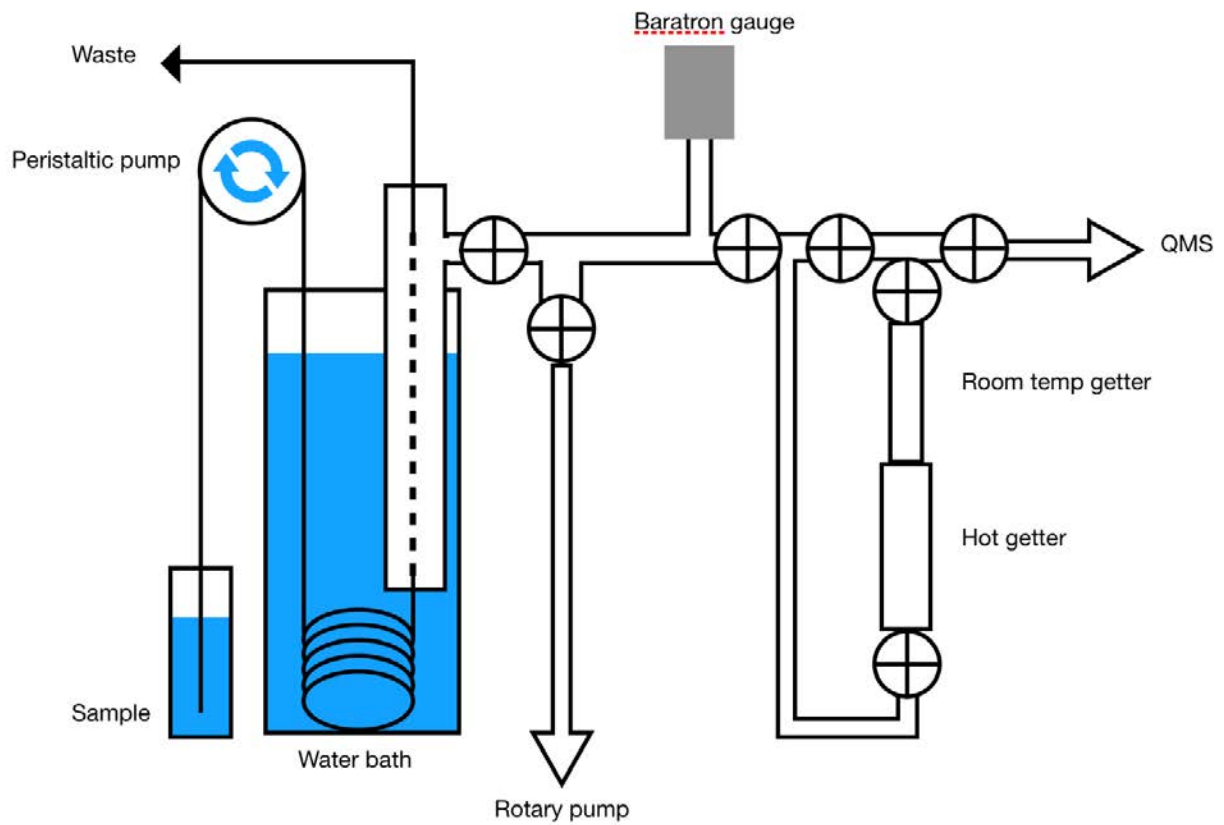


Figure 2.5. The schematic of the membrane inlet mass spectrometer used for on-board noble gas measurements.

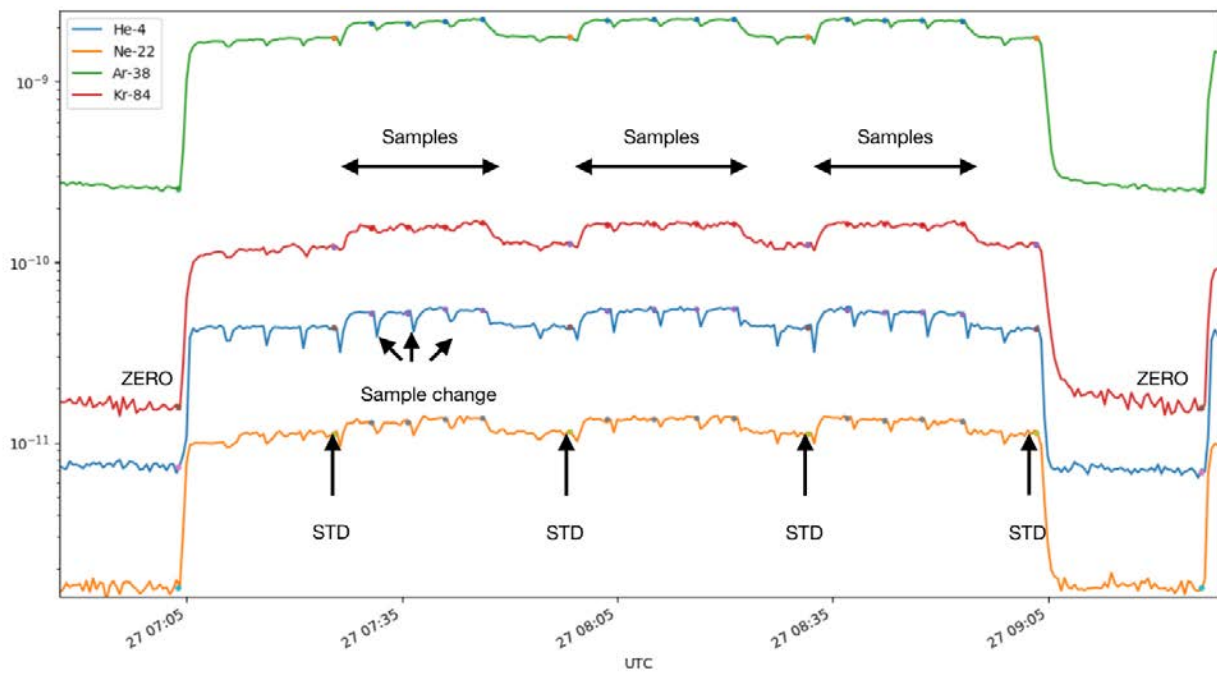


Figure 2.6. A typical cycle of noble gas measurements using MIMS. Sample, standard, and zero measurements are marked with arrows.

2.3.4 Preliminary results

Data processing of the measured samples is still in its early stage. In this report we only present exemplary vertical profiles of ΔHe ($=([\text{He}]_{\text{sample}}/[\text{He}]_{\text{sat}} - 1) * 100$) from the centers of Getz and Dotson ice shelves. While the profile from Getz (between Siple and Dean islands) showed the ΔHe close to the previously observed background values (Hohmann et al., 2002), those from near Dotson ice shelf displayed large excess He attributable to glacier meltwater (GMW), consistent with our earlier observation (Kim et al., 2016). Kim et al. (2016) used He and Ne only to trace the GMW. Because two additional nobles gases (Ar and Kr) will be available from the measurements, we will apply optimum multi-parameter analysis (OMP) to trace the origins of GMW in the Amundsen Sea.

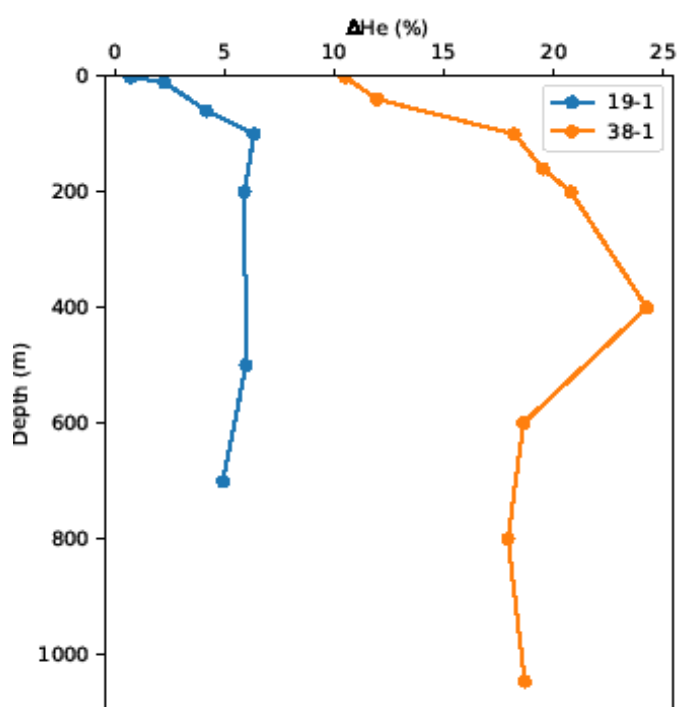


Figure 2.7. Exemplary vertical profiles of ΔHe from near the Getz (Siple-Dean) and Dotson ice shelves.

References

- Hohmann, R., Schlosser, P., Jacobs, S., Ludin, A., Weppernig, R., 2002. Excess helium and neon in the southeast Pacific: Tracers for glacial meltwater. *Journal of Geophysical Research-Oceans*, 107, doi:10.1029/2000JC000378.
- Kim, I., Hahm, D., Rhee, T. S., Kim, T. W., Kim, C.-S., & Lee, S. (2016). The distribution of glacial meltwater in the Amundsen Sea, Antarctica, revealed by dissolved helium and neon. *Journal of Geophysical Research*,

- Manning, C. C., Stanley, R. H. R., & Lott, D. E. (2016). Continuous Measurements of Dissolved Ne, Ar, Kr, and Xe Ratios with a Field-Deployable Gas Equilibration Mass Spectrometer. *Anal. Chem.*, 88(6), 3040–3048.
- Schlosser, P. (1986). Helium: a new tracer in Antarctic oceanography. *Nature*, 321, 233–235.
- Visser, A., Singleton, M. J., Hillegonds, D. J., Velsko, C. A., Moran, J. E., & Esser, B. K. (2013). A membrane inlet mass spectrometry system for noble gases at natural abundances in gas and water samples. *Rapid Communications in Mass Spectrometry*, 27(21), 2472–2482.

2.5. Underway measurements of net community production and dimethylsulfide in the Amundsen Sea

¹Changjin Lee and ²Doshik Hahm

¹Division of Polar Ocean Sciences, Korea Polar Research Institute, Incheon 21990, Republic of Korea

²Department of Oceanography, Pusan National University, Busan 46241, Republic of Korea

2.5.1. Objectives

The coastal polynyas in the Amundsen Sea are known for high primary production in austral summer (Arrigo et al., 2012). Rapid environmental changes in the Amundsen Sea poses questions such as how the biological and chemical systems respond to the environmental changes. During the cruise, we measured net community production (NCP), defined as the difference between autotrophic photosynthesis and (autotrophic and heterotrophic) respiration, as a measure of biological pump. By measuring chemically and biologically inert Ar together with O₂, it is possible to remove O₂ variation by physical processes (e.g., air temperature and pressure change and mixing of water masses) and deduce O₂ variation by biological processes (Craig and Hayward, 1987). Due to the high primary production and high abundance of efficient dimethylsulfide (DMS) producers, *Phaeocystis antarctica*, the Southern Ocean is responsible for ~62% of the global DMS flux (Lana et al, 2011). In order to investigate the spatial and temporal variations of NCP and DMS in the surface waters of the polynyas and the proposed correlation between them, we observed the horizontal and vertical (upper 100 m) distributions of DMS and $\Delta\text{O}_2/\text{Ar}$, a proxy of NCP, in the Amundsen Sea using a membrane inlet mass spectrometer (MIMS) (Figure 2.8; Tortell, 2005). Water temperature, salinity, oxygen and fluorescence were also obtained to help the interpretation of temporal and spatial variation of O₂/Ar and DMS.

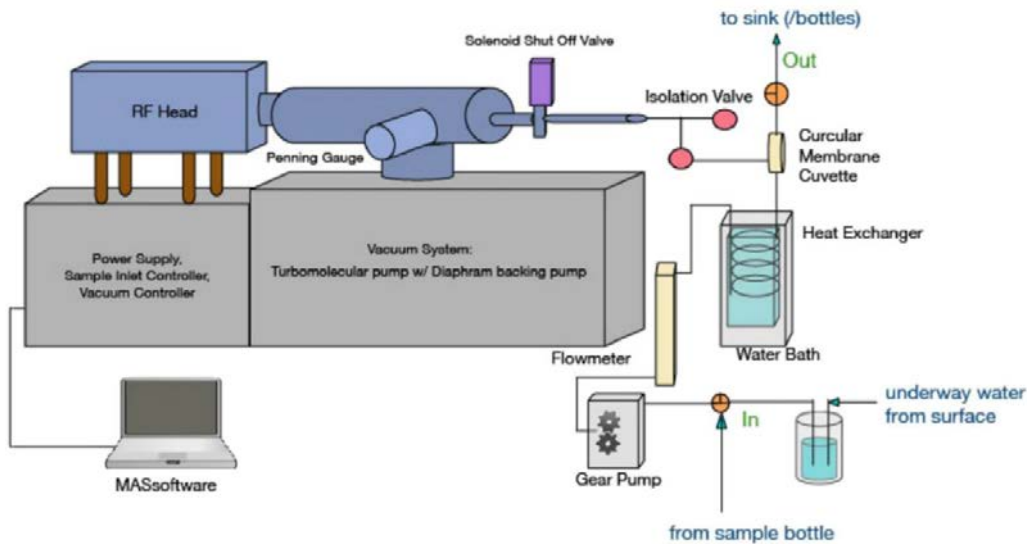


Figure 2.8. Schematic of the MIMS used for the underway measurements of $\Delta O_2/Ar$ and DMS (Kim et al., 2017).

2.5.2. Preliminary results

The preliminary results were summarized in Figure 2.9, 2.10 and 2.11. It was noted that Wrigley Gulf (WG) near Siple and Dean islands slightly warmer than the Amundsen Sea Polynya (ASP). This is partly because many of the stations in the ASP were either close to the ice shelves or in high concentrations of sea ice. $\Delta O_2/Ar$ ($= [(O_2/Ar)_{sample}/(O_2/Ar)_{air} - 1] * 100$) and DMS values also appeared to be slightly higher in the WG than in the ASP; Some of the highest values ($\Delta O_2/Ar > 30\%$ and DMS > 100 nM) appeared in the WG. Many high productive areas in 2011 - 2014 had high sea surface temperature and salinity (Hahm et al., 2014). This correlation was not evident in this year's observations. Overall, the $\Delta O_2/Ar$ values within the polynya were in a range similar to those January of 2016.

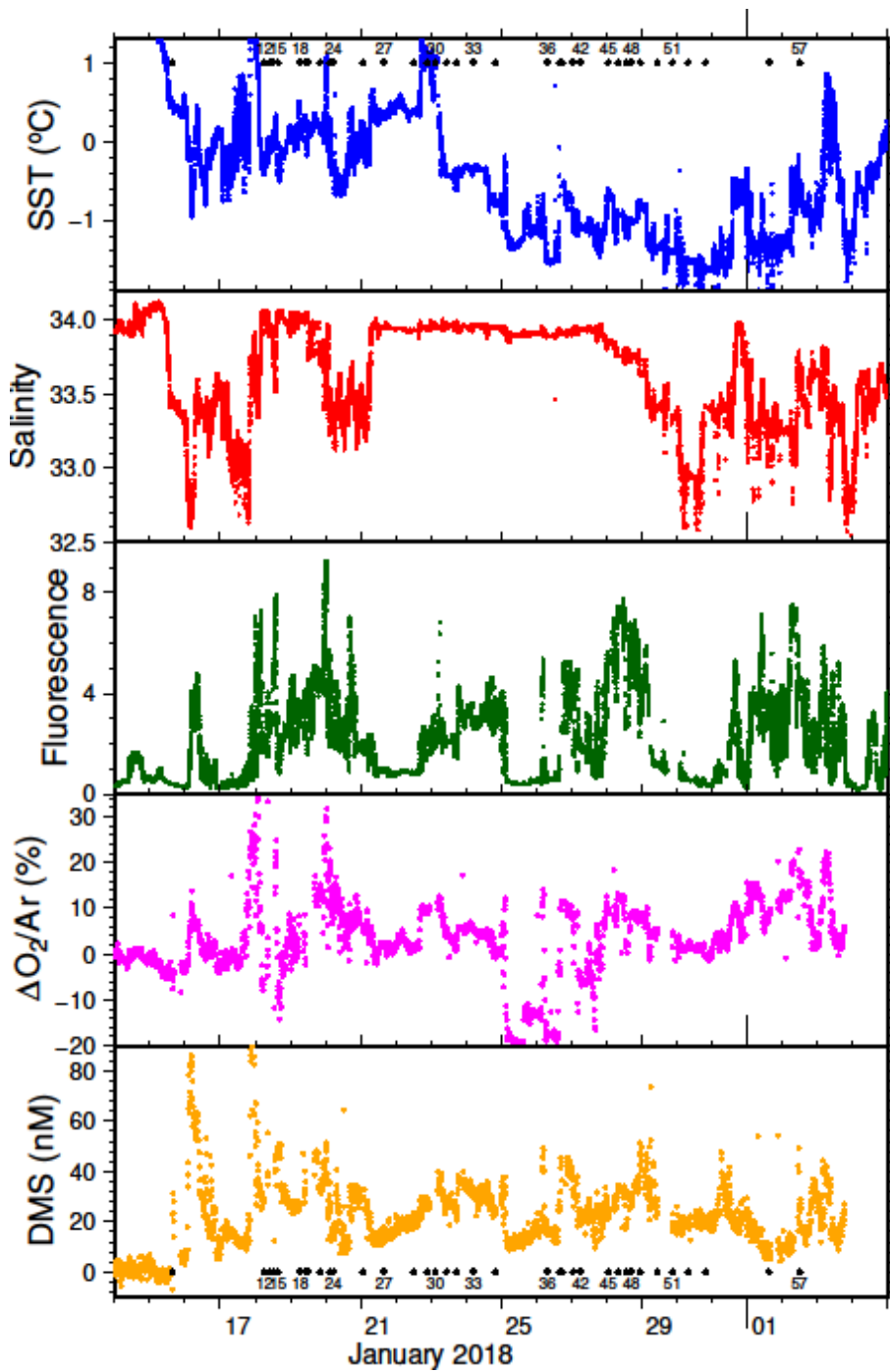


Figure 2.9. Time-series of the underway measurements of SST, SSS, fluorescence, $\Delta O_2/Ar$, and DMS. The fluorescence values have not been calibrated yet.

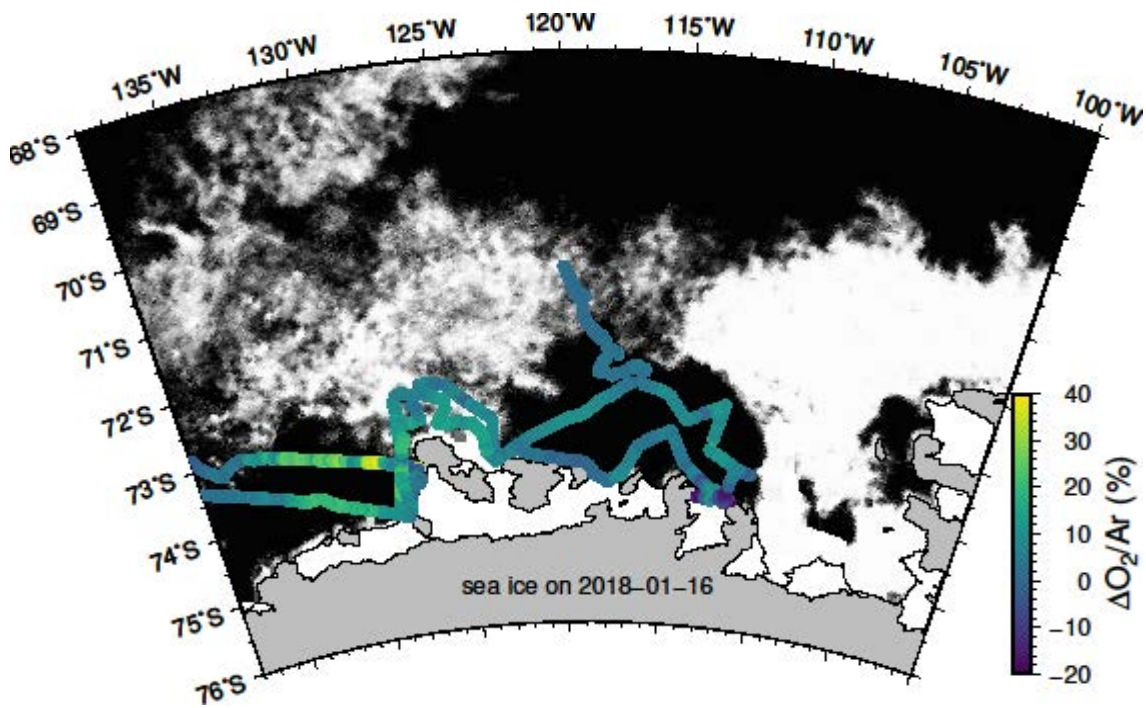


Figure 2.10. Spatial distribution of $\Delta O_2/Ar$ in the Amundsen Sea superimposed on AMSR2 sea-ice image on 16 January 2018.

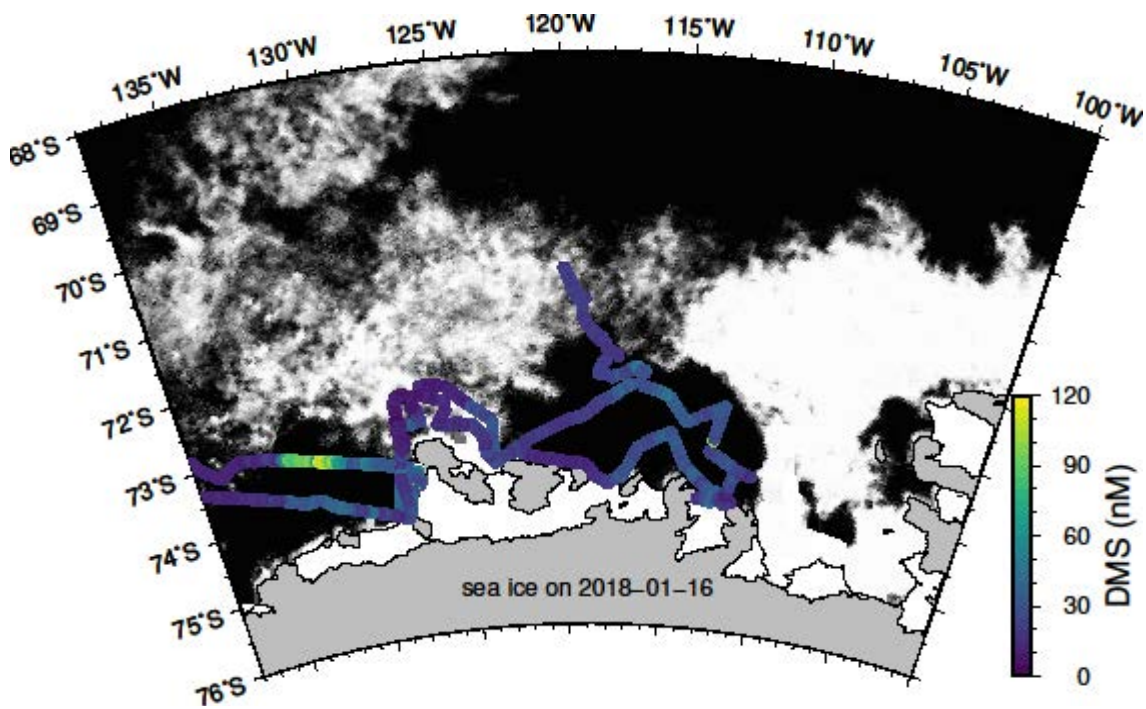


Figure 2.11. Spatial distribution of DMS in the Amundsen Sea superimposed on AMSR2 sea-ice image on 16 January 2018.

References

- Arrigo, K. R., Lowry, K. E., & van Dijken, G. L. (2012). Annual changes in sea ice and phytoplankton in polynyas of the Amundsen Sea, Antarctica. *Deep-Sea Research Part II*, 71-76, 5–15.
- Craig, H., & Hayward, T. (1987). Oxygen supersaturation in the ocean: Biological versus physical contributions. *Science*, 235(4785), 199–202.
- Hahm, D., Rhee, T. S., Kim, H.-C., Park, J., Kim, Y. N., Shin, H. C., & Lee, S. (2014). Spatial and temporal variation of net community production and its regulating factors in the Amundsen Sea, Antarctica. *Journal of Geophysical Research*, 119(5), 2815–2826.
- Kim, I., Hahm, D., Park, K., Lee, Y., Choi, J.-O., Zhang, M., et al. (2017). Characteristics of the horizontal and vertical distributions of dimethyl sulfide throughout the Amundsen Sea Polynya. *Science of the Total Environment*, 584-585, 154–163.
- Lana, A. et al. (2011), An updated climatology of surface dimethylsulfide concentrations and emission fluxes in the global ocean, *Global Biogeochemical Cycles*, 25(1), doi: 10.1029/2010GB003850.
- Tortell, P. D. (2005), Dissolved gas measurements in oceanic waters made by membrane inlet mass spectrometry, *Limnology and Oceanography - Methods*, 3, 24–37.

2.6. Inorganic Carbon System

¹Yewon Kim

¹Korea Institute of Ocean Science & Technology, Busan, Korea

요약문

아문젠해에서 수층의 무기탄소 시스템을 분석하였다. 총용존무기탄소 (Dissolved Inorganic Carbon; DIC), 총알칼리도 (Total Alkalinity; TA) 농도를 36개 정점 (2정점 재방문)에서 채수한 400여개 시료를 KIOST에서 분석할 예정이다. DIC는 인산을 이용하여 모두 이산화 탄소로 산화시킨 후 이들 이산화탄소를 적정하는 쿨로메트릭 방법을 이용하며 TA는 알고 있는 농도의 염산을 해수에 적정하여 적정점을 찾아 농도를 계산한다. 이들 자료를 이용하여 아문젠해 폴리냐와 해빙역, 외양의 무탄소 시스템의 차이를 알아보려고 한다.

2.6.1. Objectives

The Amundsen Sea in the west Antarctic has been experiencing rapid ocean warming (Meredith and King, 2005) and pronounced declines in sea ice cover (Stammerjohn et al., 2012). The Upper Circumpolar Deep Water (UCDW) upwelled to the continental shelf drives melting of the glaciers, which will influence ecosystem in the Amundsen Sea with changing carbon storage compartments. To understand the impact of glacier melt to the carbon flux in the water column of the Amundsen Sea, we investigated inorganic carbon system in the polynyas of Dotson and Getz Island Glaciers, sea-ice zone, and the offshore.

2.6.2. Work at sea

Hydrographic survey was conducted in the Amundsen Sea from the Niskin attached in CTD/Rosette at 36 stations, and among them 2 stations were replicated to investigate short-term variation of ecosystem parameters (Table 2.1).

Inorganic carbonate system in the water column compose of ionic form of carbonate (CO_3^{2-}), bicarbonate (HCO_3^-), hydrogen ion (hydronium, H^+) and neutral form of carbonic acid and dissolved CO_2 . These carbonate species exist in equilibrium in seawater depending on alkalinity of the seawater. These species, however, cannot be analyzed directly using analytical instruments except CO_2 and hydronium. Thus, to determine the carbonate system in the water column, we measure total dissolved inorganic carbon (DIC) and total alkalinity (TA) by which one can derive ionic and neutral form of carbonate system. DIC and TA are defined as follows:

$$\text{DIC} = [\text{HCO}_3^-] + [\text{CO}_3^{2-}] + [\text{CO}_2] + [\text{H}_2\text{CO}_3]$$

$$\text{TA} = [\text{HCO}_3^-] + 2[\text{CO}_3^{2-}] + \Sigma[\text{anions}] - \Sigma[\text{cations}]$$

The sample bottles were flushed 3 times before starting collection in 250 mL borosilicate bottle (Figure 2.12). Making small headspace, to prevent the seawater samples from being altered due to biological activities in the seawater, HgCl_2 solution were injected upon injecting seawater. Then the sample bottles were tightened with rubber band or black electric tape and stored in a dark place before analysis. The 36 experiment samples will be analyzed with VINDTA system in KIOST after this cruise.



Figure 2.12. Bottled water samples for DIC and TA analysis

Table 2.1. Number of samples collected at the station for analyses of DIC and TA

Station	Sampling Date	DIC/TA	Station	Sampling Date	DIC/TA
11	2018.01.16	12	34	2018.01.25	11
12	2018.01.18	9	36	2018.01.26	11
13	2018.01.18	11	38	2018.01.28	12
14	2018.01.19	12	40	2018.01.28	12
15	2018.01.19	10	42	2018.01.28	12
18	2018.01.19	10	45	2018.01.28	12
19	2018.01.19	10	46	2018.01.28	11
20	2018.01.20	9	47	2018.01.29	11
22	2018.01.20	11	48	2018.01.29	11
23	2018.01.20	10	49	2018.01.29	11
24	2018.01.20	9	50	2018.01.29	11
26	2018.01.21	12	51	2018.01.30	10
27	2018.01.22	11	53	2018.01.30	12
28	2018.01.23	9	52	2018.01.31	11
29	2018.01.23	11	55	2018.02.02	12
31	2018.01.23	11	24 (Revist)	2018.02.02	11
32	2018.01.24	11	23 (Revist)	2018.02.02	12
33	2018.01.24	11	57	2018.02.03	12

References

- Meredith MP, King JC. 2005. Rapid climate change in the ocean west of the Antarctic Peninsula during the second half of the 20th century. *Geophys Res Lett* 32: doi:10.1029/2005GL024042.
- Stammerjohn S, Massom RA, Rind D, Martinson D. 2012. Regions of rapid sea ice change: An inter-hemispheric seasonal comparison. *Geophys Res Lett* 39: doi:10.1029/2012GL050874.

Chapter 3

Biological Oceanography

3.1. Biodiversity of phytoplankton community

¹Hyoungh Min Joo

¹Korea Polar Research Institute, Incheon 406-840, Korea (hmjoo77@kopri.re.kr)

요약문

여름철 규조류와 편모조류인 *Phaeocystis antarctica* (군집형) 가 우점하는 것으로 보고되고 있는 남극 아문젠 해역에서 식물플랑크톤 군집의 종다양성을 파악하기 위해 2017년 12월 27일부터 2018년 2월 2일까지 총 43개 정점에서 선상조사를 실시하였다. 현장에서 CTD자료를 기반으로 각 정점에서 유광층 내 5-6개의 수심을 정한 뒤 니스킨 채수기로 채수하여 HPMA 슬라이드를 제작하였다. 제작된 슬라이드는 실험실로 운반하여 식물플랑크톤의 정량분석을 실시할 예정이며 정성적 종조성 분석 및 생체량 (biovolume)을 측정하기 위해 망목크기 20um 그물로 식물플랑크톤 채집을 실시하여 고정액으로 고정된 시료를 실험실로 운반하여 광학/형광현미경 및 주사전자현미경 (SEM)으로 관찰할 예정이다. 해당 연구를 통하여 아문젠 해역에서의 대표 우점종 및 종 수준의 군집구조, 일차생산을 주도하는 군집군을 파악할 수 있을 것으로 기대된다.

3.1.1. Introduction

High-latitude marine ecosystems are particularly sensitive to climate change. In part, this is because small temperature changes can have large effects on the extent and thickness of sea ice (Holland et al., 2006), According to Baar et al. (1995), The Southern Ocean plays an important role in the export of anthropogenic CO₂ (around 25% of total anthropogenic carbon emission), in part via primary production by phytoplankton.

The Amundsen Sea occurs along Marie Byrd Land between 100 and 135°W. It has historically been known as a region of persistent summer sea ice that made it one of the most remote and least known continental shelf regions of the Southern Ocean (Jones, 1982). The Amundsen has received more attention in recent years because of the observation of rapid sea ice retreat (Jacobs and Comiso, 1997) and the melting of the Pine Island Glacier (PIG) (Jenkins et al., 1997, 2010). The PIG has experienced a melt rate exceeding 40 m y⁻¹ near its grounding line (Rignot and Jacobs, 2002), likely due to the warm CDW that moves through the deep troughs (such as the one at 114°W that is more than 1000m deep) of the continental shelf to the ice shelf, causing basal ablation. The southern boundary of the ACC reaches the continental margin and brings the CDW near the shelf-break, inducing intrusions of CDW across the continental shelf (Dinniman et al., 2010). Numerical models suggest that these intrusions occur ca. 8 times per month and may persist for weeks as discrete features (Dinniman et al., 2010). There is the possibility that Fe may be derived from the basal melt waters and augmented by the surface glacial melt water in this region.

So far, there have been many results about phytoplankton communities in the Amundsen Sea by pigments. However, it is rare that species level studies have been carried out in coastal areas. Therefore, our main objective of this research was to investigate in phytoplankton distribution and communities under microscope and SEM in the Amundsen Sea during austral summer 2017-2018.

3.1.2. Material and methods

Data collection

The data were collected in the Amundsen Sea from December 27, 2017 to February 2, 2018 (Table 3.1). A total of 43 stations were visited (Figure 3.1) include revisit stations. Water samples were collected at 5-6 depths (Surface, 10m, 20m, 30m, 50m, 75m, 100m, and subsurface chlorophyll a maximum depth) with a rosette sampler equipped with 20 L Niskin-type bottles, an in situ fluorometer, and a high-precision Sea-Bird plus CTD probe. The subsurface chlorophyll maximum layer depths were estimated by CTD profiles.

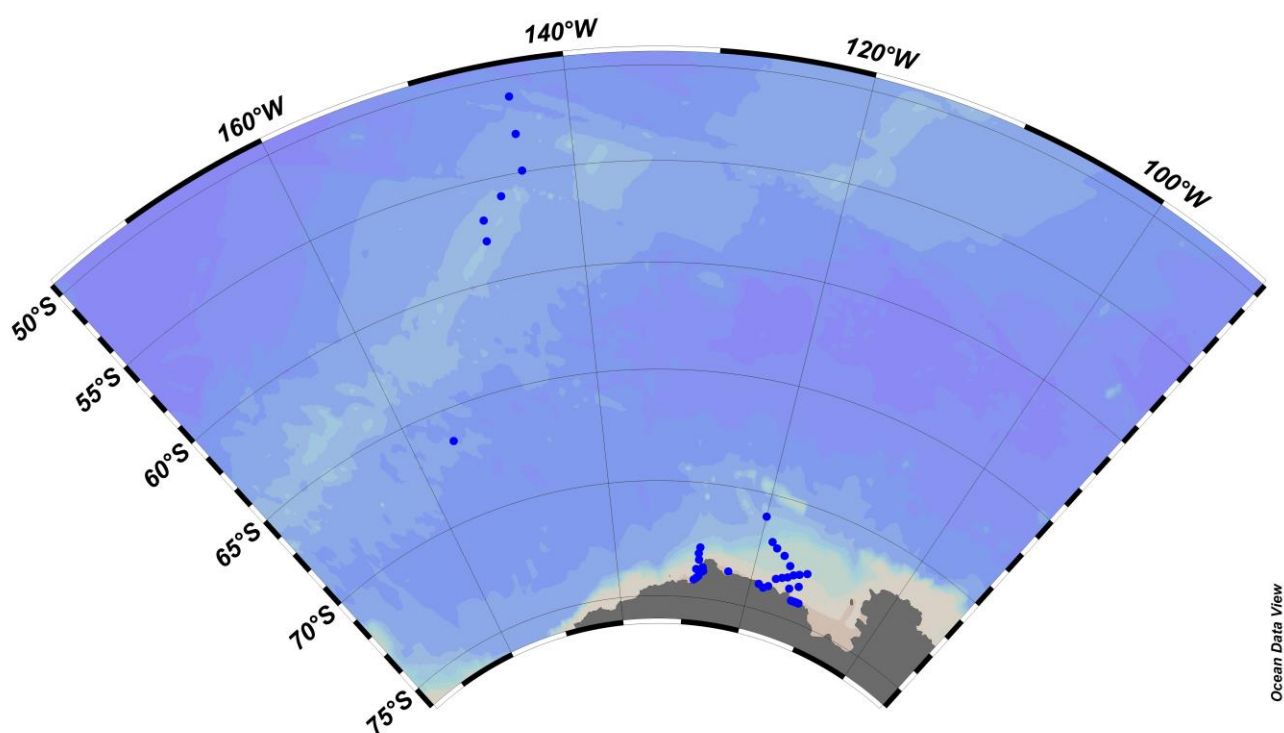


Figure 3.1. Locations of the austral summer season phytoplankton sampling stations in 2017-2018.

Table 3.1. Sampling locations of phytoplankton species compositions during the ANA08B cruise.

No.	Cruise	Leg	Station	Bottom Depth (m)	Latitude		Longitude		Sampling date (UTC)	Sampling time (UTC)
					Degree	Minute	Degree	Minute		
1	ANA08	B	ANA08B01	3764	50	59.99	143	50	2017-12-27	5:40
2	ANA08	B	ANA08B03	3730	52	60	143	50	2017-12-28	9:40
3	ANA08	B	ANA08B05	3750	54	54.9	143	49.66	2017-12-29	22:20
4	ANA08	B	ANA08B07	2740	55	58.86	145	41.01	2017-12-30	13:22
5	ANA08	B	ANA08B09	3000	56	58.48	147	21.41	2017-12-31	5:28
6	ANA08	B	ANA08B10	2600	57	60	147	30	2018-01-01	3:45
7	ANA08	B	ANA08B11	4200	66	27.95	155	44.2	2018-01-15	22:40
8	ANA08	B	ANA08B12	180	73	39.51	127	24.13	2018-01-18	7:45
9	ANA08	B	ANA08B13	578	73	47.67	127	34.85	2018-01-18	9:10
10	ANA08	B	ANA08B14	700	73	49.91	127	46.77	2018-01-18	11:48
11	ANA08	B	ANA08B15	596	73	49.62	127	16.44	2018-01-18	15:10
12	ANA08	B	ANA08B18	752	73	56.72	127	48.43	2018-01-19	6:10
13	ANA08	B	ANA08B19	709	74	2.98	127	55.6	2018-01-19	10:20
14	ANA08	B	ANA08B20	571	74	8.47	128	12.24	2018-01-19	11:50
15	ANA08	B	ANA08B22	736	74	13.61	128	33.46	2018-01-19	21:45
16	ANA08	B	ANA08B23	616	73	21.25	128	3.09	2018-01-20	2:35
17	ANA08	B	ANA08B24	557	73	4.7	128	11.53	2018-01-20	5:08
18	ANA08	B	ANA08B26	590	73	40.91	123	34.71	2018-01-21	1:20
19	ANA08	B	ANA08B27	1020	73	54.28	118	44.83	2018-01-21	17:25
20	ANA08	B	ANA08B28	1180	74	1.15	117	58.69	2018-01-22	14:04
21	ANA08	B	ANA08B29	1151	73	53.77	117	17.74	2018-01-22	23:05
22	ANA08	B	ANA08B31	372	73	30	116	30	2018-01-23	12:00
23	ANA08	B	ANA08B32	666	73	22.2	115	42	2018-01-23	17:03
24	ANA08	B	ANA08B33	826	73	16.78	114	56.96	2018-01-24	6:30
25	ANA08	B	ANA08B34	566	73	42.68	114	12.92	2018-01-24	21:35
26	ANA08	B	ANA08B36	650	74	10.3	113	19.17	2018-01-26	9:10
27	ANA08	B	ANA08B37	700	74	10.37	112	60	2018-01-26	15:25
28	ANA08	B	ANA08B38	1031	74	10.44	112	43.46	2018-01-26	19:35
29	ANA08	B	ANA08B39	949	74	10.51	112	25	2018-01-27	0:25
30	ANA08	B	ANA08B42	742	74	10.58	112	8.03	2018-01-27	7:40
31	ANA08	B	ANA08B45	521	73	30	112	60	2018-01-28	2:24
32	ANA08	B	ANA08B46	450	72	51	112	29.97	2018-01-28	9:11
33	ANA08	B	ANA08B47	534	73	0	113	30	2018-01-08	14:37
34	ANA08	B	ANA08B48	609	73	6.78	114	14.99	2018-01-28	18:33
35	ANA08	B	ANA08B49	587	72	46.92	115	7.5	2018-01-29	0:25
36	ANA08	B	ANA08B50	538	72	25.88	116	20.33	2018-01-29	12:00
37	ANA08	B	ANA08B51	522	72	13.28	117	35.54	2018-01-29	20:45
38	ANA08	B	ANA08B53	2380	71	0	120	0	2018-01-30	9:55
39	ANA08	B	ANA08B52	490	72	0.1	118	25	2018-01-30	21:39
40	ANA08	B	ANA08B55	2645	72	49.11	128	3.31	2018-02-01	14:12
41	ANA08	B	ANA08Bre24	569	73	4.46	128	8.22	2018-02-01	23:30
42	ANA08	B	ANA08Bre23	567	73	21.26	128	3.05	2018-02-02	9:10
43	ANA08	B	ANA08B57	712	73	45.82	128	18.17	2018-02-02	11:40

Sample collection: HPMA slides

Water samples were obtained with a CTD/rosette unit in 20L PVC Niskin bottles during the 'up' casts. Aliquots of 125 mL were preserved with glutaraldehyde (final concentration 1 %). Sample volumes of 50 to 100 mL were filtered through Gelman GN-6 Metrical filters (0.45 μm pore size, 25 mm diameter; Gelman Sciences, Inc., NY, USA). The filters were mounted on microscopic slides in a water-soluble embedding medium (HPMA, 2-hydroxypropyl methacrylate) on board (Figure 3.2). The HPMA slides were used for identification and estimation of cell concentration and biovolume. The HPMA-mounting technique, first described by Crumpton (1987), has some advantages over the classical Utermöhl sedimentation method (Kang et al., 1993b). Samples were also collected via phytoplankton net tows (20 μm mesh) and preserved with glutaraldehyde (final concentration 2 %); these samples were used only for identification of small species in the phytoplankton assemblage (Figure 3.3). Since the results from this can be biased towards larger specimens, these data were not used for statistical analysis, but only for morphological and systematic analysis.

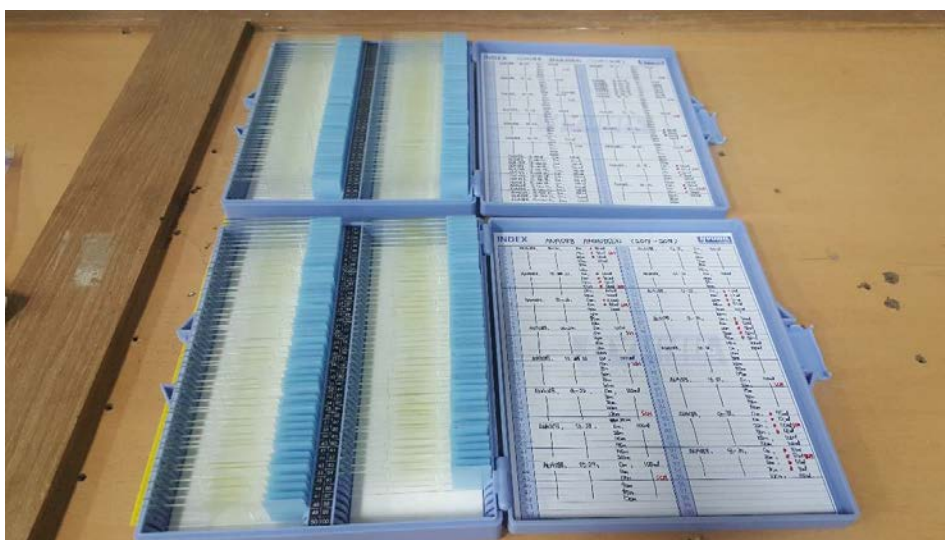


Figure 3.2. HPMA slide for Phytoplankton quantities analysis

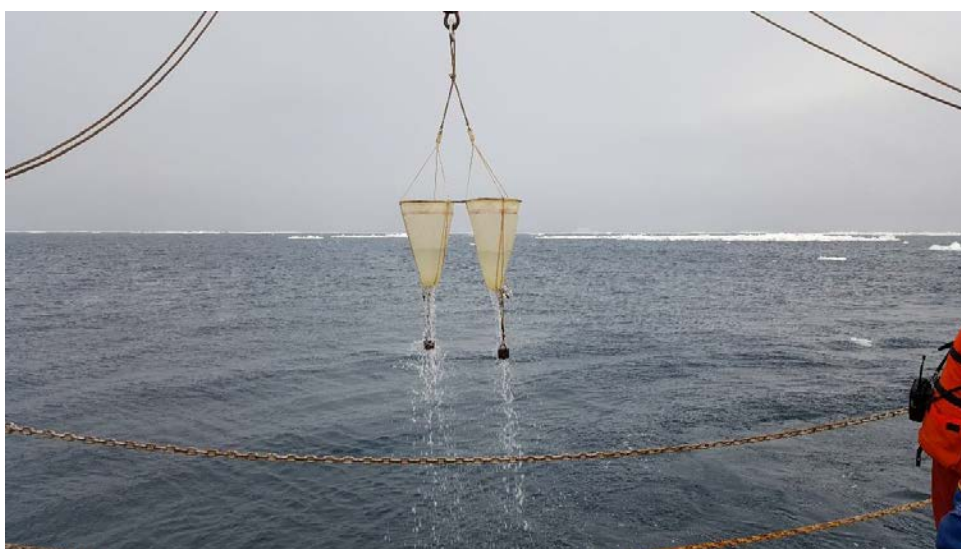


Figure 3.3. Sampling by 20um meshed Phytoplankton Net

Identification, counts, and biovolume of phytoplankton

Identification by light microscopy is time-consuming and requires a high level of taxonomic skills, but it is still the most reliable method of microalgal identification (Tomas, 1997; Bérard-Therriault et al., 1999). Therefore, at least 300 cells were identified from each sample using a microscope (BX51, Olympus, Inc., Tokyo, Japan), with a combination of light and epifluorescence microscopy at 400x for microplankton, and at 1000x for autotrophic pico- and nanoplankton (Booth 1993). For species that could not be identified with light microscopy, a JEOL JSM-5600LV scanning electron microscope (JEOL, Inc., Tokyo, Japan) was used. Autotrophic pico- and nanoflagellates were filtered, dehydrated, and dried according to methods described by Jung et al. (2009). Whole mounts coated with graphite and gold were used for SEM analysis. Cell counts were converted to cell concentrations as described by Kang and Fryxell (1991) and Kang et al. (1993a). Cell dimensions of dominant phytoplankton species were measured to the nearest 1 µm for subsequent estimations of biovolume using appropriate geometric shapes (Sun and Liu, 2003; Strathmann, 1967). Linear dimensions were measured by light microscopy (BX51, Olympus) and SEM (JSM-5600LV, JEOL). Twenty or more individual cells were measured to avoid biasing results. The information on taxa and linear dimensions were then transferred to a Microsoft Excel worksheet and biovolume was calculated according to Sun and Liu (2003 – see also Menden-Deuer and Lessard, 2000).

References

- Bérard-Therriault, L., Poulin, M., Bossé, L., 1999. Guide d'identification du phytoplancton marin de l'estuaire et du golfe du Saint-Laurent incluant également certains protozoaires. Conseil national de recherches du Canada, Ottawa.
- Booth, B.C., 1993. Estimating cell concentration and biomass of autotrophic plankton using microscopy. In: Kemp, P.F., Sherr, B.F., Sherr E.B., Cole, J.J. (Eds.), Handbook of methods in aquatic microbial ecology. Lewis Publishers, Boca Raton, pp. 199-205.
- Crumpton, W.G., 1987. A simple and reliable method for making permanent mounts of phytoplankton for light and fluorescence microscopy. *Limnology and Oceanography* 32, 1154-1159.
- De Baar, H.J.W., de Jong, J.T.M., Bakker, D.C.E., Loscher, B.M., Veth, C., Bathmann, U., Smetacek, 1995.
- Dinniman, M.S., Klinck, J.M., Smith Jr., W.O., 2010. A model study of Circumpolar Deep Water on the West Antarctic Peninsula and Ross Sea continental shelves. *Deep Sea Res. II* 58, 1508–1523.
- Holland, M.M., Bitz, C.M., Hunke, E.C., Lipscomb, W.H., Schramm, J.L., 2006. Influence of the Sea Ice Thickness Distribution on Polar Climate in CCSM3. *J. Climate* 19, 2398–2414.
- Importance of iron for plankton blooms and carbon dioxide draw down in the Southern Ocean. *Nature* 373 (6513), 412–415.
- Jacobs, S.S., Comiso, J.C., 1997. Climate variability in the Amundsen and Bellingshausen Seas. *J. Clim.* 10, 697–709.
- Jenkins, A., Vaughan, D.G., Jacobs, S.S., Hellmer, H.H., Keys, J.R., 1997. Glaciological and oceanographic evidence of high melt rates beneath Pine Island glacier, West Antarctica. *J. Glaciol.* 43, 114–121.
- Jenkins, A., Dutrieux, P., Jacobs, S.S., McPhail, S.D., Perrett, J.R., Webb, A.T., White, D., 2010. Observations beneath Pine Island Glacier in West Antarctica and implications for its retreat. *Nat. Geosci.* 3, 468–472.
- Jones, A.G.E., 1982. Antarctica Observed. Caedmon of Whitby, Yorkshire, UK. 118 pp.
- Jung, S.W., Joo, H.M., Park, J.S., Lee, J.H., 2009. Development of a rapid and effective method for preparing delicate dinoflagellates for scanning electron microscopy. *Journal of Applied Phycology* 22, 313-317.
- Kang, S.H., Fryxell, G.A., 1991. Most abundant diatom species in water column assemblages from five ODP

Leg 119 drill sites in Prydz Bay, Antarctica: distributional patterns. In: Barron, J., Larsen, B. (Eds.), Proceedings of the ODP scientific results, 119 (Ocean Drilling Program). College Station, TX. pp. 645-666.

Kang, S.H., Fryxell, G.A., Roelke, D.I., 1993a. *Fragilariopsis cylindrus* compared with other species of the diatom family Bacillariaceae in Antarctic marginal ice-edge zones. *Nova Hedwigia*, Beiheft 106, 335-352.

Kang, S.H., Suk, M.S., Chung, C.S., Nam, S.Y., Kang, C.Y., 1993b. Phytoplankton populations in the western Bransfield Strait and the southern Drake Passage, Antarctica. *Korean Journal of Polar Research* 4, 29-43.

Menden-Deuer, S., Lessard, E.J., 2000. Carbon to volume relationships for dinoflagellates, diatoms, and other protist plankton. *Limnology and Oceanography* 45, 569-579.

Rignot, E., Jacobs, S.S., 2002. Rapid bottom melting widespread near Antarctic ice sheet grounding lines. *Science* 296, 2020-2023.

Strathmann, R.R., 1967. Estimating the organic carbon content of phytoplankton from cell volume, cell area or plasma volume. *Limnology and Oceanography* 12, 411-418.

Sun, J., Liu, D., 2003. Geometric models for calculating cell biovolume and surface area for phytoplankton. *Journal of Plankton Research* 25, 1331-1346.

Tomas, C.R., 1997. Identifying marine phytoplankton. Academic Press, San Diego, CA.

3.2. Phytoplankton ecology in the Amundsen Sea

¹Youngju Lee and Jung Kuk Moon

¹Korea Polar Research Institute, Incheon, 21990, Korea (yjlee@kopri.re.kr)

요약문

아문젠해 연안 해역에서 식물플랑크톤 군집의 분포와 이를 조절하는 주요 환경요인을 파악하기 위하여 현장 조사가 수행되었다. 2017년 12월 27일부터 2018년 2월 3일까지 25개 정점 (revisit 포함)에서 수심에 따른 엽록소-a, 크기별 엽록소-a 농도가 측정되었으며 광합성색소 기반의 군집연구 및 초미소식물플랑크톤 현존량 분석을 위한 시료를 확보하여 추후 실험실에서 분석될 예정이다. 광조건 변화에 따른 식물플랑크톤 성장반응을 살펴보기 위하여 현장해수를 이용한 배양실험을 수행하였으며 식물플랑크톤 종조성, 광합성 색소, 초미소식물 플랑크톤 현존량 등을 모니터링 하였다.

3.2.1. Phytoplankton distribution

The Southern Ocean is a net sink for atmospheric CO₂ on annual timescales, accounting for 20% of global ocean (Takahashi et al., 2009) due to high primary productivity (Arrigo et al., 2008). Phytoplankton bloom appeared in austral summer in the coastal Polynya which is local areas of reduced ice cover that generally form due to offshore katabatic winds and seasonal ice melt (Tremblay and Smith, 2007). In the growing season, higher insolation and thinner sea ice allow sufficient irradiance to penetrate and drive photosynthesis in this continental shelf area. Seasonal variation of phytoplankton biomass and primary production in the Antarctic shelf waters plays an important role in the biogeochemical cycle in the Southern Ocean.

Several researches have been intensively studied the dynamics of phytoplankton in the Antarctic coastal waters and revealed that diatoms and prymnesiophyte *Phaeocystis antarctica* formed massive bloom in different season and area in the coastal waters (Arrigo et al., 1999). However, variations occur among years not only in the dominant rate of these two major groups, but also in the controlling mechanisms, and it is hard to predict their distribution (Smith Jr et al., 2006). Moreover, most studies were mainly concerned with regions in the Ross Sea, Weddell Sea, and eastern Antarctica (Arrigo et al., 1999; Lancelot et al., 1993; Wright et al., 2010).

Amundsen Sea Polynya (ASP) is the most productive area per unit area of the 37 identified coastal polynya systems in the Antarctic (Arrigo and van Dijken, 2003). It is also well known that Amundsen Sea is the highest melting area in the Antarctica by the global warming (Rignot et al., 2013). Modified Circumpolar Deep Water (mCDW) intruded onto the continental shelf and accelerate the basal melting of ice shelves in the ASP (Rignot et al., 2013). The changes in water column stratification, water circulation, coastal upwelling and Fe supply could also be caused by mCDW extending in the ASP (Gerringa et al., 2012). Therefore, the distribution and response of whole phytoplankton groups in the rapidly melted Amundsen Sea need to be understood for prediction of phytoplankton response under climate change.

3.2.2. The influence of reduced light on the phytoplankton growth and community structure

It is well known the difference of spatial and temporal distributions between *P. antarctica* and diatoms in the Antarctic coastal waters (Arrigo et al., 1999). Several studies on the autecology of these key species have been documented and important environmental factors such as light, MLD, seeding from sea ice, Fe, sinking, grazing were suggested to control the phytoplankton distribution in the Ross Sea (Lancelot et al., 1993). Compared to the Ross Sea, few studies reported in the Amundsen Sea and it is suggested that light, Fe, seeding from sea ice as important environmental factors influenced on the phytoplankton community based on photosynthetic pigments analysis (Alderkamp et al., 2012). However, more study is required to verify and understand their response to environmental change. In this study, incubation experiments were performed to understand the response of phytoplankton community to light level in the Amundsen Sea.

3.2.3. Materials and methods

Field survey

Field survey was conducted onboard the Korean Research IBRV Araon in the ASP and the seas around ASP during austral summer from 27 December 2017 to 3 February 2018 (Figure 3.4). Water samples for chlorophyll a (Chl a) concentration, picophytoplankton, and pigments were collected from 4~12 depths in the whole water column using a 10-L PVC Niskin water sampler attached to a CTD rosette system.

Size-fractionated Chl-a concentration

Subsamples from the Niskin bottles were filtered through a cascade connection of 20- μm nylon mesh, Nuclepore filter (Whatman International) with pore size of 3 μm , and a Whatman GF/F filter to determine size-fractionated Chl-a (Sieburth 1978). Thus, micro-Chl-a (>20 μm), nano-Chl a (3-20 μm), and pico-Chl-a (<3 μm) could be measured directly. Subsamples for total Chl-a were filtered onto 47 mm GF/F Whatman filters. Each filter was extracted in 90% acetone, and Chl-a concentrations were measured with a fluorometer (model Trilogy, Turner Designs, USA; method: Parson et al., 1984).

Heterotrophic bacteria and picophytoplankton abundance

Water samples for flow cytometry analysis were fixed for 15 min with paraformaldehyde (final concentration: 1%) and stored at -80 °C. Since fixation with added chemical reagents may result in loss of cells, natural samples were also analyzed on a Accuri C6 flow cytometer (Becton Dickinson) equipped with an air-cooled argon laser (488 nm, 15 mW), placed on-board so that after sample collection the analyses could immediately be performed. Picophytoplankton groups were identified and their abundance enumerated using the characteristics of 90°-

angle light scatter, orange fluorescence from phycoerythrin, and red fluorescence from chlorophyll (Marie et al., 1997). For the enumeration of heterotrophic bacteria, seawater samples were stained with SYBR green I (Molecular Probes), and incubated in the dark at room temperature for 15 min before analysis. Bacteria were identified for their side light scatter and green fluorescence signals. Raw data from the flow cytometer will be processed using the FlowJo program (Tree Star, www.flowjo.com).

Photosynthetic pigments

The CHEMTAX program based on photosynthetic pigments data has potential benefits for the estimation of phytoplankton composition, including small and fragile forms. For photosynthetic pigments analysis, 0.5~1 L subsamples from the Niskin bottles were filtered onto 25 mm GF/F Whatman filters and stored at -80 °C. The pigments will be analyzed with high performance liquid chromatography (HPLC) in the laboratory.

Phytoplankton species abundance

To estimate the phytoplankton abundance, water samples from incubation experiments were collected in 200-mL high density polyethylene bottles, preserved with glutaraldehyde (final concentration 1%), and stored at 4 °C until analysis. Sample volumes of 50 - 150 mL were filtered through nuclepore filters (0.8 µm pore size, black, 25 mm diameter). During filtration, the samples were drawn down until 5 mL remained in the filtration tower. Concentrated DAPI (50 µg mL⁻¹ final concentration) was then added and allowed to sit briefly (5 seconds) before filtering the remaining sample until dry (Taylor et al., 2011).

Light experiment

For the incubation experiment, 20 L water was collected from the mixed layer (20m depth) at station 31 using the NIOZ sampler. Water samples were collected into the 2-L polycarbonate bottles and they were incubated in two light controlled deck-board incubators (Figure 3.5). Two incubators were screened to 90% and 99% of incident light, respectively, using sunscreen filters and those were kept at sea surface temperature. Bottles were incubated for twelve days, after which two different treatments were applied to triplicate bottles and subsampled daily at noon. Samples for picophytoplankton abundance, heterotrophic bacteria abundance, Fv/Fm and nutrients were taken once in two days. Samples were taken at time zero, on day 4, day 7 and the final day for photosynthetic pigments and phytoplankton species abundance.

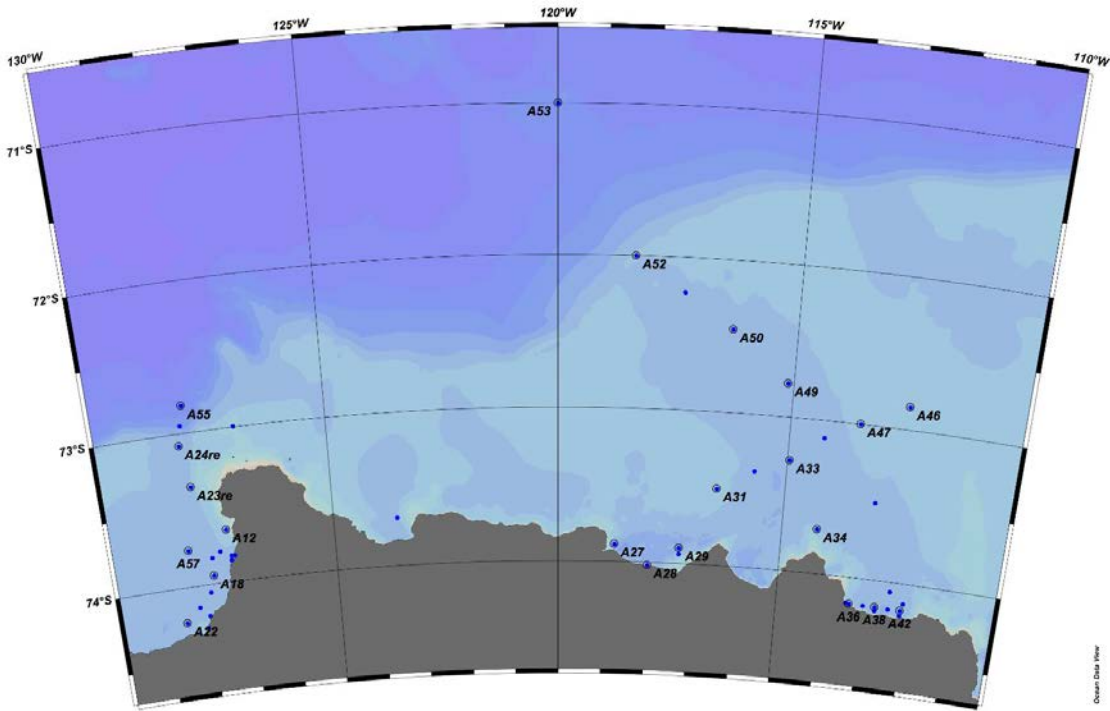


Figure 3.4. Sampling stations of phytoplankton community in the Amundsen Sea during the Amundsen 2017-2018 cruise.

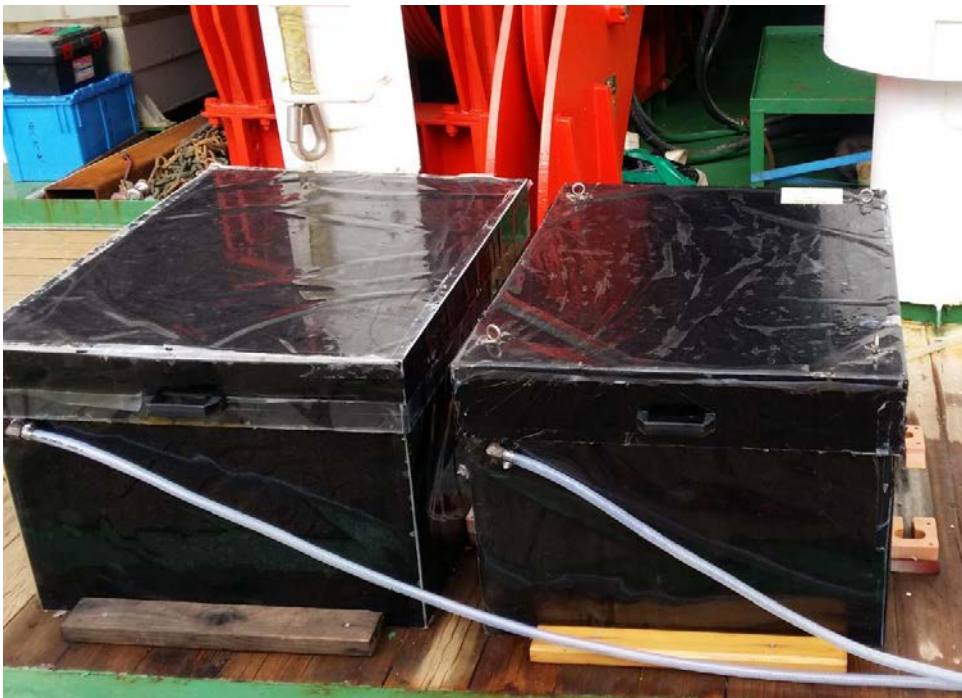


Figure 3.5. The incubators for physiological experiment on deck. Bottles were incubated in 1% and 10% of incident light.

References

- Alderkamp, A.-C., Mills, M.M., van Dijken, et al., 2012. Iron from melting glaciers fuels phytoplankton blooms in the Amundsen Sea (Southern Ocean): phytoplankton characteristics and productivity. *Deep-Sea Res. II* 71–76, 32–48.
- Arrigo, K.R., Robinson, D.H., Worthen, D.L., Dunbar, R.B., DiTullio, G.R., VanWoert, M., Lizotte, M.P., 1999. Phytoplankton community structure and the drawdown of nutrients and CO₂ in the Southern Ocean. *Science* 283 (5400), 365-367.
- Arrigo, K.R., van Dijken, G., Long, M., 2008. Coastal Southern Ocean: A strong anthropogenic CO₂ sink. *Geophysical Research Letters* 35 (21).
- Arrigo, K.R., van Dijken, G.L., 2003. Phytoplankton dynamics within 37 Antarctic coastal polynya systems. *Journal of Geophysical Research: Oceans* (1978–2012) 108 (C8).
- Gerringa, L.J.A., Alderkamp, A.C., Laan, P., Thuróczy, C.E., De Baar, H.J.W., Mills, M.M., van Dijken, G.L., Haren, H.V., Arrigo, K.R., 2012. Iron from melting glaciers fuels the phytoplankton blooms in Amundsen Sea (Southern Ocean): Iron biogeochemistry. *Deep-Sea Research Part II: Topical Studies in Oceanography* 71-76, 16-31.
- Lancelot, C., Mathot, S., Veth, C., de Baar, H., 1993. Factors controlling phytoplankton ice-edge blooms in the marginal ice-zone of the northwestern Weddell Sea during sea ice retreat 1988: field observations and mathematical modelling. *Polar Biology* 13 (6), 377-387.
- Marie, D., Partensky, F., Jacquet, S., Vaulot, D., 1997. Enumeration and cell cycle analysis of natural populations of marine picoplankton by flow cytometry using the nucleic acid stain SYBR Green I. *Appl. Environ. Microbiol.* 63 (1), 186-193.
- Rignot, E., Jacobs, S., Mouginot, J., Scheuchl, B., 2013. Ice-shelf melting around Antarctica. *Science* 341 (6143), 266-270.
- Sieburth, J.McN., 1978. Pelagic ecosystem structure: Heterotrophic compartments of the plankton and their relationship to plankton size fractions. *Limnology and Oceanography*, 23: 1256-1263.
- Smith Jr, W.O., Shields, A.R., Peloquin, J.A., Catalano, G., Tozzi, S., Dinniman, M.S., Asper, V.A., 2006. Interannual variations in nutrients, net community production, and biogeochemical cycles in the Ross Sea. *Deep-Sea Research Part II: Topical Studies in Oceanography* 53 (8-10), 815-833.
- Takahashi, T., Sutherland, S.C., Wanninkhof, R., Sweeney, C., Feely, R.A., Chipman, D.W., Hales, B., Friederich, G., Chavez, F., Sabine, C., 2009. Climatological mean and decadal change in surface ocean pCO₂, and net sea–air CO₂ flux over the global oceans. *Deep Sea Research Part II: Topical Studies in Oceanography* 56 (8), 554-577.
- Taylor, A.G., Landry, M.R., Selph, K.E., Yang, E.J., 2011. Biomass, size structure and depth distributions of the microbial community in the eastern equatorial Pacific. *Deep Sea Research Part II: Topical Studies in Oceanography* 58 (3), 342-357.
- Tremblay, J.-É., Smith, W., 2007. Primary production and nutrient dynamics in polynyas. *Elsevier Oceanography Series* 74, 239-269.
- Wright, S.W., van den Enden, R.L., Pearce, I., Davidson, A.T., Scott, F.J., Westwood, K.J., 2010. Phytoplankton community structure and stocks in the Southern Ocean (30-80°E) determined by CHEMTAX analysis of HPLC pigment signatures. *Deep-Sea Research Part II: Topical Studies in Oceanography* 57 (9-10), 758-778.

3.3. Phytoplankton physiology (photochemistry)

¹Eunho Ko

¹Korea Polar Research Institute, Incheon 21990, Korea (ehko@kopri.re.kr)

요약문

본 연구항해에서 식물플랑크톤이 광에너지를 흡광하여 광화학과 형광으로 전환하는 양자수율을 측정하기 위해서 Miniaturized Fluorescence Induction and Relaxation (mini-FIRe)과 Picosecond Lifetime Fluorometer (PicoLiF)을 사용하였다. 또한 표층과 엽록소 최대층에서 채수한 해수를 25mm GF/F 여과지에 걸러 식물플랑크톤 흡광계수를 측정하였다. 총 45개 정점 중 아문젠 해역이 36개 정점 (2정점 재방문), Udintsev fracture zone (UFZ) 해역 9개 정점에서 관측을 수행하였다. 식물플랑크톤의 광화학 반응의 양자수율은 모든 정점(수직적으로 6개 수층), 식물플랑크톤 흡광계수는 16개 정점 (2개 수층)에서 채수한 해수를 활용하여 분석하였다. 동시에 연구항차 중 선저 펌프로부터 공급되는 표층해수를 이용하여 광화학, 형광 양자수율의 표층 연속관측도 실시하였다.

3.3.1. Introduction/Objectives

To investigate the impact of physico-chemical conditions on photosynthesis in the Amundsen Sea, we measured photosynthetic characteristics of phytoplankton at total 45 stations (including two revisit stations) using Miniaturized Fluorescence Induction and Relaxation (mini-FIRe) and Picosecond Lifetime Fluorometer (PicoLiF) System (Figure 3.6). Active (and fast) fluorometry is a non-destructive and rapid method, and it has been used to monitor variations in the photochemistry (Kolber and Falkowski, 1993; Falkowski and Kolber, 1995). Especially, variable fluorescence is the most sensitive signal recorded in the upper ocean that reflects phytoplankton photophysiology. These measurements provide an express diagnostics of the effects of environmental factors on photosynthetic processes such as iron limitation, nitrogen limitation and photoacclimation effects.

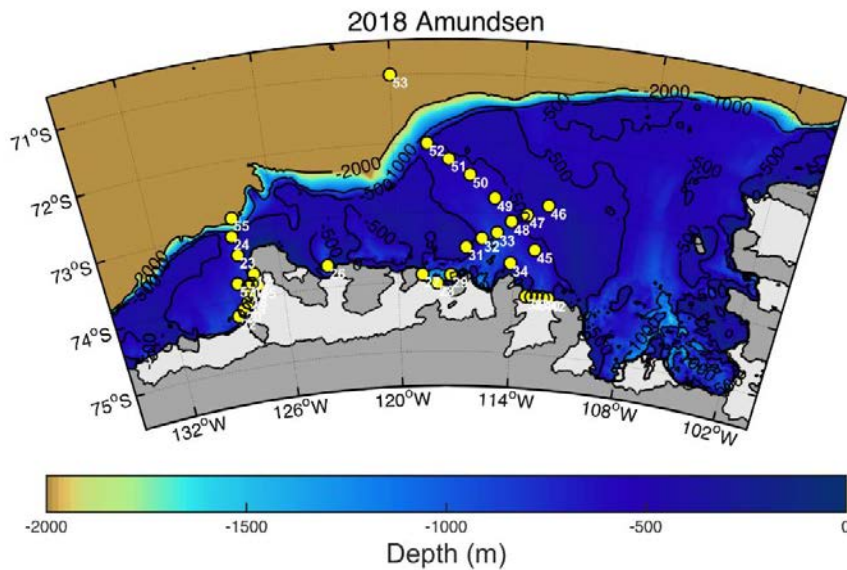


Figure 3.6. Station map in 2018 Amundsen cruise for phytoplankton physiological study.

3.3.2. Work at sea

During this cruise, we observed phytoplankton physiological (photochemistry) parameters using mini-FIRE and PicoLiF (Figure 3.7). After collection of seawater from Niskin bottles at five to six depths in upper layer (0 – 200m), samples were kept under *in situ* temperature in light bottles. These samples were measured after 30 minutes low light adaptation. Photosystem II (PSII) parameters such as the minimal fluorescence yield (F_0 ; when all reaction centers are open), the maximal fluorescence yield (F_m ; all reaction centers are closed), the quantum efficiency of PSII (F_v/F_m), the functional (or effective) absorption cross-section of PSII (σ_{PSII}) were measured as describe in Kolber *et al.* (1998). Quantum efficiency of photochemistry in PSII (F_v/F_m) was calculated as a ratio of variable fluorescence ($F_v = F_m - F_0$) to the maximum one (F_m). The fluorescence measurements were corrected for the blank signal recorded from filtered seawater (by 0.2 μ m syringe filter set) because of background fluorescence (Dissolved organic matter and dissolved degradation products in water). In addition, we measured fluorescence excited by radiation from five spectrums (450, 470, 500, 530, 590nm). To estimate phytoplankton absorption coefficient, water samples (200 ~ 2000 mL) were filtered by 25mm GF/F from surface and subsurface chlorophyll maximum at total 16 stations. When the ship was moving (from New Zealand to Amundsen Sea), underway pumped on the seawater near surface (ca. 7 m depth) and the fluorescence was measured continuously on real time. Moreover, we also observed photosynthetic parameters using pumped seawater through a flow-through cuvette in a fluorometer on deck laboratory of a ship during this Amundsen cruise and ARAON transit from New Zealand to Amundsen Sea.

Iron enrichment experiments were set up as follow. Seawater samples were collected from Titan, which was clean technique sampler from Royal Netherlands Institute for Sea Research (NIOZ). Seawater samples were kept in 500 ml bottle (control, +Fe (20 nM), +all nutrient (N: 20 μ M, P: 2 μ M, Si: 50 μ M, Fe: 20 nM, respectively), and incubated on the deck (ambient water temperature were controlled) during 6 - 8 days. Here, the changes of photosynthetic parameters (P-E curve) were monitored at every day.



Figure 3.7. A custom built-Miniaturized Fluorescence Induction and Relaxation (mini-FIRE) and Picosecond Lifetime Fluorometer (PicoLiF) System onboard Araon.

References

- Falkowski, P. G. and Z. Kolber (1995) "Variations in chlorophyll fluorescence yields in phytoplankton in the world oceans." *Aust. J. Plant Physiol.* 22(2): 341-355.
- Kolber, Z. and P. G. Falkowski (1993) "Use of active fluorescence to estimate phytoplankton photosynthesis in situ." *Limnol. Oceanogr.* 38(8): 1646-1665.
- Kolber, Z. S., O. Prasil, et al. (1998) "Measurements of variable chlorophyll fluorescence using fast repetition rate techniques: defining methodology and experimental protocols. " *Biochimica et Biophysica Acta-Bioenergetics* 1367(1-3):88-106.

3.4. Primary production and macromolecular composition of phytoplankton

¹Yu Jeong Lim and Sang H. Lee

¹Pusan National University, Korea

요약문

아문젠해의 16개 정점(revisit 1정점 포함)에서 식물플랑크톤의 탄소와 질소 섭취율을 알아보기 위하여 ¹³C-¹⁵N dual stable isotope tracer technique을 이용해 6개의 light depths(표층 광도의 100, 50, 30, 12, 5, 1 %)에서 채수된 해수 시료를 자연광 아래에서 5-8시간 배양하였다. 배양이 끝난 후, 실험실로 옮겨와 25 mm GF/F 필터에 여과하였고, 이에 대한 작은 식물플랑크톤의 기여도를 알아보기 위하여 47 mm Membrane 필터(pore size; 5 µm)에 여과한 후 25mm GF/F 필터에 여과한 뒤 냉동보관하였다. 현장조사가 끝난 후, 시료의 탄소와 질소 안정동위원소 결과값은 미국 알래스카 대학교의 안정동위원소 실험실의 Finnigan Delta+XL mass spectrometer를 이용하여 측정될 예정이다.

3.4.1. Introduction

The Southern Ocean is known as the high-nutrient and low-chlorophyll (HNLC) region (Minas et al., 1986), whereas this region plays an important role as the efficient biological pump in the world's ocean (Siegenthaler and Sarmiento, 1993). The Amundsen Sea is located in the West Antarctic between the Ross Sea and the Bellingshausen Sea. Recently, the West Antarctic was issued because the region was covered by West Antarctic Ice sheet (WAIS), which has been declining in extent and thinning unlike the East Antarctic (Rignot et al., 2008). The primary production has been estimated by satellite observations in the Amundsen Sea (Arrigo et al., 2008; Arrigo et al., 2012) but *in-situ* data are scarce due to a difficult accessibility caused by sea ice cover (Lee et al., 2012). *In-situ* studies revealed that the Amundsen Sea polynya has the high primary productivity (Arrigo and van Dijken, 2003; Lee et al., 2012) and large seasonal variations (Kim et al., 2015). The warming ocean is expected to increase the importance of small phytoplankton (Moran et al., 2010) but little information has been reported in the Amundsen Sea (Lee et al., 2017). Moreover, the contribution of small phytoplankton to the total

primary production was known to have a negative correlation with the total primary production (Lee et al., 2013; Lee et al., 2017). Therefore, in this study we measured *in-situ* carbon and nitrogen uptake rates to investigate seasonal variations in primary and new productions and the proportion of small phytoplankton to the overall phytoplankton productions in the Amundsen Sea.

3.4.2. Methods and Materials

To estimate the carbon and nitrogen uptake rate of phytoplankton in the Amundsen Sea, productivity experiments were executed by incubating phytoplankton in the incubators on the deck for 5-8 hours (Figure 3.8) after stable isotopes (^{13}C , $^{15}\text{NO}_3$, and $^{15}\text{NH}_4$) as tracers were inoculated into each bottle. Total 16 productivity experiments were completed at water column (revisit : 1) station during this cruise (Figure 3.9 and Table 3.2), respectively. At primary production stations, the seawater samples were collected by CTD rosette water samplers at 6 different light depths (100, 50, 30, 12, 5, and 1%). After the incubation, all sample waters for the total phytoplankton production were filtered on GF/F ($\phi = 25$ mm) filters and those for small phytoplankton production were filtered sequentially 5 μm pore size Membrane filters ($\phi = 47$ mm) and GF/F ($\phi = 25$ mm) filters for laboratory isotope analysis at University of Alaska Fairbanks after this cruise. For the background data of the productivity stations, water samples were collected for alkalinity, total and size-fractionated chlorophyll-*a* concentrations. In addition, water samples for macromolecular composition of total and small phytoplankton obtained from 3 light depths (100, 30, and 1%) to study the physiological status and nutritional conditions of phytoplankton at selected 17 stations (revisit : 1) in the Amundsen Sea (Figure 3.9 and Table 3.2).



Figure 3.8. *In-situ* incubation on deck for 5-8 hours

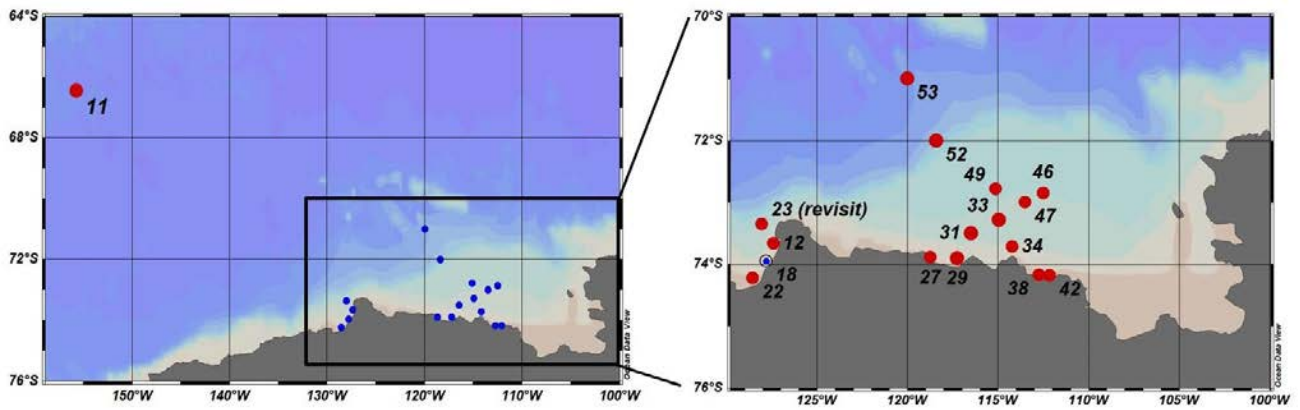


Figure 3.9. Stations for primary production (red circles) and macromolecular composition (blue circles with line) during the 2017/18 Antarctic cruise

Table 3.2. Sampling station for primary production and macromolecular composition of total and small (< 5 μm) phytoplankton during the 2017/18 Antarctic cruise

Station	Primary production		Macromolecular composition	
	total	small	total	small
11	O	O	O	O
12	O	O	O	O
18	X	X	O	O
22	O	O	O	O
27	O	O	O	O
29	O	O	O	O
31	O	O	O	O
33	O	O	O	O
34	O	O	O	O
38	O	O	O	O
42	O	O	O	O
46	O	O	O	O
47	O	O	O	O
49	O	O	O	O
52	O	O	O	O
53	O	O	O	O
23 (revisit)	O	O	O	O

References

- Arrigo, K.R., Lowry, K.E., and van Dijken, G.L. (2012) Annual changes in sea ice and phytoplankton in polynyas of the Amundsen Sea, Antarctica. *Deep Sea Res., Part II*, 5: 71-76.
- Arrigo, K.R., van Dijken, G.L. (2003) Phytoplankton dynamics within 37 Antarctic coastal polynya systems. *J. Geophys. Res.* 108.doi:10.1029/2002JC001739.
- Arrigo, K. R., van Dijken, G. L., and Bushinsky, S. (2008) Primary production in the Southern Ocean, 1997–2006. *J. Geophys., Res.*, 113: DOI: 10.1029/2007JC004551.
- Arrigo, K. R., Worthen, D. L. and Robinson, D. H. (2003) A coupled ocean -ecosystem model of the Ross Sea: 2. Iron regulation of phytoplankton taxonomic variability and primary production. *J. Geophys. Res.*, 108 (C7): 3231, doi:10.1029/2001JC000856.
- Kim, B. K., Joo, H., Song, H. J., Yang, E. J., Lee, S. H., Hahm, D., ... & Lee, S. H. (2015). Large seasonal variation in phytoplankton production in the Amundsen Sea. *Polar Biology*, 38(3), 319-331.
- Lee, S.H., Kim, B.K., Yun, M.S., Joo, H.T., Yang, E.J., Kim, Y.N., Shin, H.C., and Lee, S.H. (2012) Spatial distribution of phytoplankton productivity in the Amundsen Sea, Antarctica. *Polar Biol.*, 35: 1721-1733.
- Lee, S. H., Yun, M. S., Kim, B. K., Joo, H., Kang, S. H., Kang, C. K., & Whitley, T. E. (2013). Contribution of small phytoplankton to total primary production in the Chukchi Sea. *Continental Shelf Research*, 68, 43-50.
- Lee, S. H., Kim, B. K., Lim, Y. J., Joo, H., Kang, J. J., Lee, D., ... & Lee, S. H. (2017). Small phytoplankton contribution to the standing stocks and the total primary production in the Amundsen Sea. *Biogeosciences*, 14(15), 3705.
- Minas, H. J., Minas, M. and Packard, T. T. (1986) Productivity in upwelling areas deduced from hydrographic and chemical fields. *Limnol. Oceanogr.*, 31:71 1182-1206.
- Morán, X. A. G., LÓPEZ-URRUTIA, Á. N. G. E. L., CALVO-DÍAZ, A. L. E. J. A. N. D. R. A., & Li, W. K. (2010). Increasing importance of small phytoplankton in a warmer ocean. *Global Change Biology*, 16(3), 1137-1144.
- Rignot, E., Bamber, J. L., Van den Broeke, M. R., Davis, C., Li, Y. H., van de Berg, W. J. and van Meijgaard, E. (2008) Recent Antarctic ice mass loss from radar interferometry and regional climate modelling. *Nat.Geosci.*, 1 (2): 106-110.
- Siegenthaler, U. and Sarmiento, J. L. (1993) Atmospheric carbon dioxide and the ocean. *Nature*, 365: 119-125.

3.5. Acoustics

¹La, Hyoung Sul and ¹Son, Wuju

¹Korea Polar Research Institute

요약문

남극 아문젠해에 서식하는 중대형 동물플랑크톤의 분포를 파악하기 위해서 음향조사를 실시하였다. 음향시스템은 아라운에 설치된 과학 음향 탐지기 (scientific echo sounder) EK60을 사용하였으며 3개의 주파수 (38, 120, and 200 kHz) 1 msec 신호 길이를 이용하여 수심 1000 m 까지 체적음향산란강도 (S_v , dB re 1 m⁻¹)를 수신하였다. 정점 이동간 선속은 10 – 13 노트였으며 정선하여 연구를 수행하는 동안에도 시간에 따른 S_v 를 1 – 3초 간격으로 획득하였다. 수신된 S_v 의 음향 산란층 (sound scattering layer) 내 동물플랑크톤 종 구성을 파악하기 위해서 사각 네트 (1 m²) 를 활용하여 중대형 동물플랑크톤을 채집하였다. 본 리포트에서는 $S_{v120-38\text{ kHz}}$ 를 이용하여 음향 산란층 내 어류 ($S_{v120-38\text{ kHz}} < 2\text{ dB}$), 대형 동물플랑크톤 ($2 < S_{v120-38\text{ kHz}} < 18\text{ dB}$), 중형 동물플랑크톤 ($S_{v120-38\text{ kHz}} > 18\text{ dB}$)을 구분하였으며 생물량의 상대적인 분포 변화를 Nautical Area Scattering Coefficient (NASC, m² nmi⁻²) 로 확인하였다.

3.5.1. Introduction

The coastal polynya in the Southern Ocean is noted for sustaining enhanced levels of biological production and biogeochemical activity during because they are the first polar marine systems to be exposed to the increasing solar radiation during spring and summer (Arrigo, 2003). The coastal polynya is considered significant regions not only for the primary production but also zooplankton because highly deformed ice with many ridges provides a favorable habitat for zooplankton.

The Amundsen Sea coastal polynya is also well known for the rapid sea ice retreat (Jacobs and Comiso, 1997), as well as one of the most productive areas among 37 coastal polynyas in the Southern Ocean. It is responsible for >75% of total production in Antarctica (Arrigo, 2003). While a few biological investigations have conducted, little is known about the abundance and distribution of zooplankton throughout the Amundsen Sea because it is one of the most remote and least known continental shelf regions of the Southern Ocean (Jones, 1982).

The EK60 was run throughout ANA08B to collect information on the horizontal and vertical distribution of zooplankton and to derive estimates of zooplankton distribution in the Amundsen Sea. The overall purposes of acoustic observation are:

- To collect acoustic data to accompany all stations, transects, and net tows during the Amundsen Sea survey.
- To determine the temporal and spatial distribution of relative abundance of mid-trophic levels (Fish, macrozooplankton, and mesozoopalnkton)

3.5.2. Materials and methods

Acoustic data were collected using a multi-frequency echo sounder (EK60, Simrad) configured with down-looking 38, 120, and 200 kHz split-beam transducers mounted in the hull of the IBRV Araon (Figure 3.10. and Table 3.3). Because of instability of sync unit, there were continuous interference noise from ADCP and EM122 during the entire running time. Post processing will be followed to remove the non-biological signals (surface bubbles, ice fragments, false bottom echoes, frequency interference from other acoustic instruments) and background noise using virtual echogram (Myriax, Echoview software). The raw acoustic data will convert to raw volume backscattering strengths (S_v) binned into mean SV cells with an interval of 0.1 nautical mile (nmi) horizontal distance and a width of 1-m depth. The data will threshold to 100 dB at three frequencies. The contribution of other zooplankton such as copepod and amphipod could be negligible because of their low densities and low mean target strength. For example, target strength is about 103 dB for a 2 - 3 mm long copepod at 120 kHz (Stanton and Chu, 2000).

Simrad ER60 v.2.2.0 was used for ER60.raw data files, which were logged to extra hard drive using a USB cable. All raw data were collected to 1000 m and Echolog was run on the EK60 workstation. All raw data were saved in a general folder ANA08B/raw, all echolog data were saved in the folder ANA08B/data/EK60. All files were prefixed with ana08b. Calibration data were not additionally saved because calibration was not properly conducted during the cruise. The EK60 was run initially using previous settings, although the environmental settings were updated at the start of the cruise to a temperature of and salinity of these resulted in new settings for c and alpha. The transducer settings were reset to default and the gain settings setup with the last measured values during ANA02B. The EK60 was calibrated on the January 2012, and the calibration variables were applied to the all transducers.

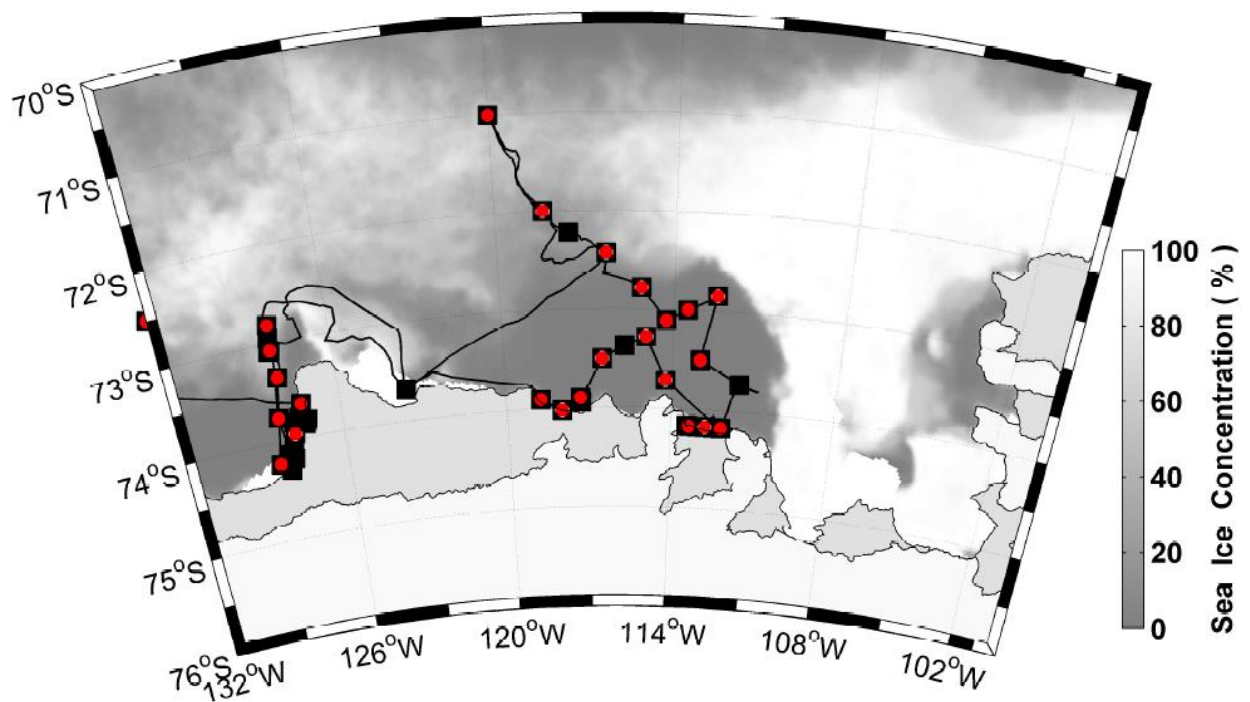


Figure 3.10. Study area on the bathymetry of Amundsen Sea showing the whole ship transect (black line) and locations of conductivity-temperature-depth (CTD) (black squares) and nets (red dots).

Table 3.3. EK60 data logger book

Station	Latitude (°N)		Longitude (°E)		EK60 Data (UTC)		Depth (m)
	D	M	D	M	Date	Time	
ARA8B-St.01	65	10.444	168	41.345	6-Aug-17	3:54 - 6:21	52
ARA8B-St.02	66	37.841	168	41.186	7-Aug-17	13:44 - 16:49	45
ARA8B-St.03	67	40.204	168	57.584	7-Aug-17	21:41 - 0:04	51
ARA8B-St.04	67	46.966	168	36.161	7-Aug-17	0:54 - 1:23	51
ARA8B-St.05	67	53.887	168	14.128	7-Aug-17	2:21 - 2:44	59
ARA8B-St.06	68	0.8	167	52.09	8-Aug-17	3:41 - 5:39	53
ARA8B-St.07	68	7.689	167	29.687	8-Aug-17	6:37 - 7:03	50
ARA8B-St.08	68	14.532	167	7.335	8-Aug-17	7:52 - 9:54	45
ARA8B-St.09	69	9.962	168	39.913	8-Aug-17	14:54 - 17:35	51
ARA8B-St.10	70	30.006	168	40.003	9-Aug-17	0:03 - 3:15	40
ARA8B-St.11	71	25.791	168	39.978	9-Aug-17	8:45 - 9:48	48
ARA8B-St.12	72	21.6	168	40	9-Aug-17	14:54 - 18:49	56
ARA8B-St.13	73	3.286	168	18.177	9-Aug-17	22:44 - 0:12	64
ARA8B-St.14	73	34.896	168	17.055	10-Aug-17	2:46 - 6:50	133
ARA8B-St.15	74	47.889	167	53.17	10-Aug-17	13:51 - 17:08	201.83
ARA8B-St.16	75	14.642	171	59.034	11-Aug-17	23:04 - 7:01	503
ARA8B-St.17	75	9.053	176	0.971	11-Aug-17	13:04 - 17:23	330
ARA8B-St.18	75	59.999	175	29.999	11-Aug-17	22:22 - 2:38	2100
ARA8B-St.19	76	59.992	174	59.95	12-Aug-17	8:53 - 12:28	2030
ARA8B-St.20	78	0.101	174	55.882	12-Aug-17	19:25 - 3:54	1690
ARA8B-St.21	77	42.554	179	59.977	15-Aug-17	9:47 - 12:51	1590
ARA8B-St.22	75	46.117	177	9.487	16-Aug-17	10:18 - 18:17	529
ARA8B-St.23	75	0.045	173	36.499	19-Aug-17	02:17 - 5:19	145
ARA8B-St.24	73	59.944	170	0.339	19-Aug-17	12:56 - 15:57	46
ARA8B-St.25	74	37.679	174	53.732	20-Aug-17	0:45 - 4:09	69.5
ARA8B-St.26	75	9.486	-179	59.54	20-Aug-17	13:17 - 15:20	526
ARA8B-St.27	77	0.03	-170	3.008	21-Aug-17	07:48 - 11:10	2200
ARA8B-St.28	76	0.001	-170	29.921	21-Aug-17	16:07 - 19:56	1300
ARA8B-St.29	75	41.482	-166	38.25	22-Aug-17	0:57 - 3:58	285
ARA8B-St.30	76	34.915	-165	22.698	22-Aug-17	08:27 - 12:46	1007
ARA8B-St.31	77	28.335	-164	7.099	22-Aug-17	17:22 - 20:28	271
ARA8B-St.32	77	30.007	-158	52.425	23-Aug-17	05:02 - 08:02	1640
ARA8B-St.33	76	31.531	-159	58.149	23-Aug-17	14:45 - 19:23	2130
ARA8B-St.34	75	30.019	-161	7.417	24-Aug-17	03:12 - 05:34	2068
ARA8B-St.35	74	30.014	-162	14.935	24-Aug-17	11:01 - 15:43	1528

3.5.3. Preliminary results

The preliminary results were summarized in Figure 3.11 in the Amundsen Sea. Photosynthetically active radiation (PAR), sea ice concentration (SIC), water temperature, salinity, and fluorescence could support the interpretation of temporal and spatial variation of sound scattering layers from fish, mesozooplankton, and macrozooplankton. S_A ($S_A=10\log_{10}NASC$, dB re 1 ($m^2 nmi^{-2}$)) of macrozooplankton was likely to be contributed by ice krill of the composition of all the rectangular net samples. The values were generally higher around the western Getz ice shelf than the values around the Eastern Getz and Dotson ice shelves. Relatively cold and low salinity waters were located throughout much of the eastern Getz ice shelf, and in the Dotson trough in the Amundsen Sea. On the other hand, the relatively high fluorescence was observed along the trough in the western Getz ice shelf. This indicated that the warm and high fluorescence water could cause the relatively high abundance of macrozooplankton such as ice krill in this regions.

There was a problem encountered. Interference from other acoustic instruments was continuously generated as the sync unit was not properly working to synchronise the ADCP and EM122. The sync unit has kept instruments (ADCP and EM122) into standby even if it does give the signals to work on them. As a result, we disable to use the sync unit to minimize the interference from other scientific instruments all triggering. We need a post processing technique to remove the interference noise of ADCP and EM122 from the echo integration data of EK60.

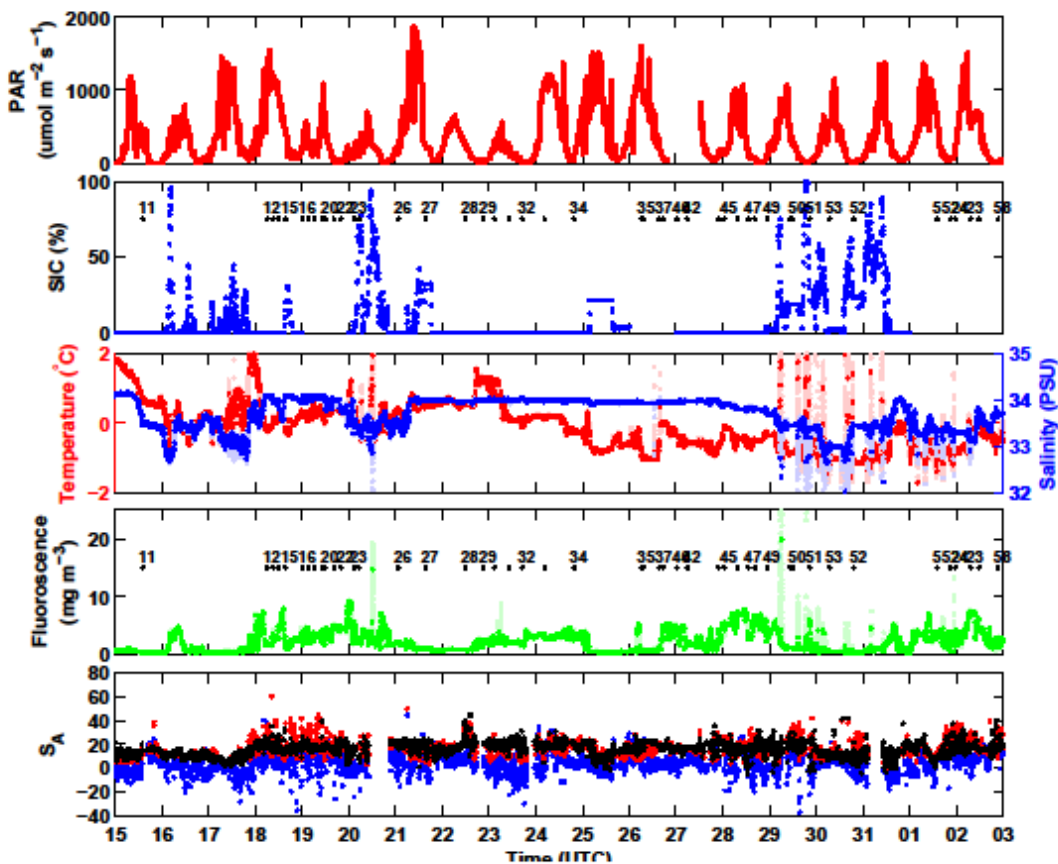


Figure 3.11. The preliminary results of Photosynthetically active radiation (PAR), sea ice concentration (SIC), water temperature, salinity, fluorescence, and S_A ($S_A=10\log_{10}NASC$, dB re 1 ($m^2 nmi^{-2}$)) from fish (blue dots), macrozooplankton (red dots), and mesozooplankton (black dots).

References

- Arrigo, K.R., and van Dijken, G.L., 2003. Phytoplankton dynamics within 37 Antarctic coastal polynya systems. *Journal of Geophysical Research* 108: 3271
- Jacobs, S.S., and Comiso, J.C. 1997. A climate anomaly in the Amundsen and Bellingshausen Seas. *J. Climate*, 10: 697-711.
- Jones, A.G.E. 1982. *Antarctica Observed*. Caedmon of Whitby, Yorkshire, UK. 118 pp.
- Stanton, T.K. and Chu, D. 2000. Review and recommendations for the modelling of acoustic scattering by fluid-like elongated zooplankton: euphausiids and copepods. *ICES J. Mar. Sci.*, 57 (4): 793-807.

3.6. Grazing impacts and community structure of heterotrophic protists

¹Youngju Lee, ¹Eun-Jin Yang and ¹Jung Kuk Moon

¹Korea Polar Research Institute, Incheon, 21990, Korea (ejyang@kopri.re.kr)

요약문

아문젠해 연안 해역에서 2018년 1월에 원생동물의 생물량, 군집구조, 식물플랑크톤 및 박테리아에 대한 섭식률 실험을 총 15개 정점에서 수행하였다. 원생동물의 생물량 분포 및 군집구조 분석은 현장에서 고정하여 실험실로 가져간 후 분석되어질 예정이다. 또한 해수희석법을 이용하여 측정된 식물플랑크톤과 박테리아에 대한 섭식률 측정은 2016년 자료와 비교하여 분석되어질 예정이다.

3.6.1. Background study

Heterotrophic protists ingest a broad size spectrum of prey, from bacteria to microphytoplankton, and are themselves important prey items for mesozooplankton. Many researches suggest that heterotrophic protists contribute to the trophic linkage between phytoplankton and mesozooplankton and are important in the pelagic food webs of many oceanic waters. The importance of heterotrophic protists in pelagic ecosystems has become increasingly evident in the past two decades, and trophic interaction between heterotrophic protists and phytoplankton has been reported in various marine. Studies of protozooplankton in the Southern Ocean have emphasized the importance of protozooplankton in microbial communities and their role as major consumers of phytoplankton (Burkill et al., 1995; Froneman and Perissinotto, 1996; Landry et al., 2001; Pearce et al., 2011; Safi et al., 2007; Selph et al., 2001). Overall, previous research has suggested that knowledge of the structure of the microbial community and protozoan grazing impacts, is central to developing an understanding of carbon flux in the Southern Ocean. However, comprehensive studies on protozooplankton assemblages have been generally limited to the Weddell Sea, Bellingshausen Sea, and the Atlantic and Indian sectors of the Southern Ocean, particularly the marginal ice-edge zone (Froneman et al., 2004; Klass, 1997; Safi et al., 2007). There is no information on the relative importance of heterotrophic protists in the pelagic ecosystem of the Amundsen Sea. The Amundsen Sea, which is historically known as a region of heavy ice, is undergoing sea ice recession within the last decades (Jacobs and Comiso, 1993), and extensive phytoplankton blooms near the coast have been observed (Smith and Comiso, 2008). In this study area, we investigated the meso-scale variations and structure of heterotrophic protist communities and grazing rates on phytoplankton in the various environmental conditions such as sea ice zone, polynya, and ice shelves. During this cruise, we investigated protozoa abundance, biomass and grazing rate in total 15 stations. This data will be compared to ANA06 data set.

3.6.2. Work at Sea

Abundance and community composition of heterotrophic protists

This study was conducted at total 15 stations (Figure 3.12). To determine the abundance of heterotrophic protists, a CTD-Niskin rosette sampler was used to take water samples from 4 depths in the upper 100m and 4~6 depths in the deeper 100m. For ciliates and sarcodina, 1,000 ml water from the vertical profiles was preserved with 1% acid Lugol's iodine solution and these samples were then stored in darkness. For heterotrophic nanoflagellates and heterotrophic dinoflagellates smaller than 20 μm , 500 ml of water was preserved with glutaraldehyde (0.5% final concentration) and stored at 4° C.

Grazing experiments

Grazing rates of heterotrophic protists were determined by the dilution method (Landry and Hassett 1982). Water for grazing experiments was collected from 3~5 depths of each station, and gently filtered through a 200- μm mesh. At each station, 50L seawater were collected in a Niskin bottle and transferred to a polycarbonate carboy. Part of this water was filtered through the 0.22- μm filtration system. Dilution series were set up in ten 1.3-l PC bottles. Ten bottles were used to establish a nutrient-enriched dilution series consisting of replicate bottles with 11, 28, 50, 75, and 100% natural seawater. The bottles were incubated on deck for 24 – 48 h at ambient sea surface temperatures and screened to the ambient light level with neutral density screening. Subsamples were collected from replicate bottles at 0 and 24-48h to determine chlorophyll-a concentrations and bacterial abundance.

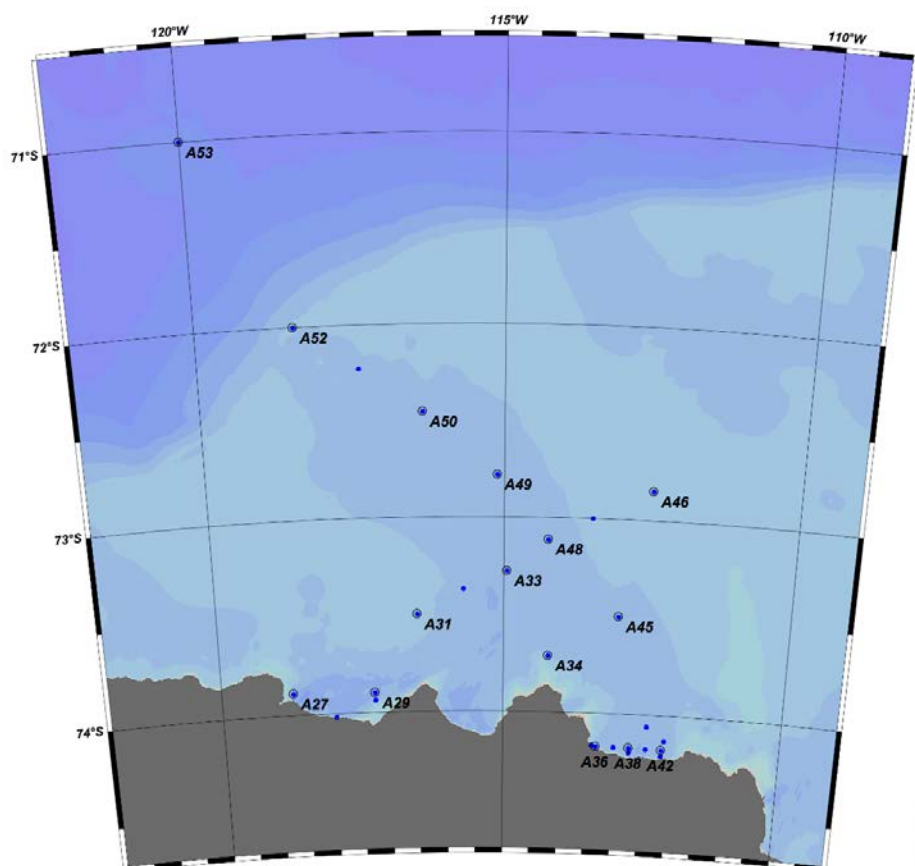


Figure 3.12. The sampling stations of protozoa community and grazing rate in the Amundsen Sea.

References

- Jacobs, S. S., Comiso, J. C. 1993. A recent sea-ice retreat west of the Antarctic Peninsula. *Geophysical Research Letters* 20: 1171-1174.
- Smith, W. O. Jr., Comiso, J. C. 2008. Influence of sea ice on primary production in the Southern Ocean: a satellite perspective. *Journal of Geophysical Research* 113 doi:10.1029/2007JC004251.
- Pearce, I., Davidson, A.T., Thomson, P.G., Wright, S., van den Enden, R., 2011. Marine microbial ecology in the sub-Antarctic Zone: Rate of bacterial and phytoplankton growth and grazing by heterotrophic protists. *Deep-Sea Res. Part II.* 58, 2248-2259.
- Safi, K.A., Griffiths, F.B., Hall, J.A., 2007. Microzooplankton composition, biomass and grazing rates along the WOCE SR3 line between Tasmania and Antarctica. *Deep-Sea Res. Part I.* 54, 1025-1041.
- Selph, K.E., Landry, M.R., Allen, C.B., Calbet, A., Christiansen, S., Bidigare, R.R., 2001. Microbial community composition and growth dynamics in the Antarctic Polar Front and seasonal ice zone during late spring 1997. *Deep-Sea Res. Part II.* 48, 4059-4080.
- Landry, M.R., Brown, S.L., Selph, K.E., Abbott, M.R., Letelier, R.M., Christensen, S., Bidigare, R.R., Casciotti, K., 2001. Initiation of the spring phytoplankton increase in the Antarctic Polar Front Zone at 170°W. *J. Geophys. Res.* 106(C7), 13,903-13,915.
- Froneman, P.W., 2004. Protozooplankton community structure and grazing impact in the eastern Atlantic sector of the Southern Ocean in austral summer 1998. *Deep-Sea Res. Part II.* 51, 2633-2643.
- Landry, M.R., Hassett, R.P., 1982. Estimating the grazing impact of marine microzooplankton. *Mar. Biol.* 67, 283-288. Froneman, P.W., Perissinotto, R., 1996. Structure and grazing of the microzooplankton communities of the subtropical convergence and a warm core eddy in the Atlantic sector of the Southern Ocean. *Mar. Ecol. Prog. Ser.* 135, 237-245.
- Burkill, P.H., Edwards, E.S., Sleigh, M.A., 1995. Microzooplankton and their role in controlling phytoplankton growth in the marginal ice zone of the Bellingshausen Sea. *Deep-Sea Res. Part II.* 42, 1277-1299.

3.7. Mesozooplankton community

¹La, Hyoung Sul and ¹Son, Wuju

¹Korea Polar Research Institute

요약문

중형동물플랑크톤은 남극 해양생태계의 하위 영양단계와 상위 영양단계를 연결하는 주요 연결 고리이다. 이 에 아문젠해역에 서식하는 중형동물플랑크톤의 공간 분포를 정량적으로 파악하고 해양환경 인자 (수온, 염분, 엽록소, 해빙 등)와의 비교를 통해서 중형동물플랑크톤의 생태계 특성을 이해하는 것이 필수적이다. 본 연구에서는 중형동물플랑크톤 분포를 파악하기 위해서 25개 정점에서 봉고네트와 사각네트를 이용하여 샘플을 채집 하였다. 크릴 샘플은 현장에서 길이 (body length) 분포를 측정하였고 향후 중형동물플랑크톤의 지역별 군집 특성과 군집 분포에 영향을 미치는 주요 해양환경 인자를 파악할 예정이다.

3.7.1. Introduction

Coastal Polynya, an area of open water surrounded by sea ice, is an important part of the coastal system in the Southern Ocean. Mesozooplankton taxon in Southern Ocean believed to play key roles in the planktonic food web consuming organic energy produced by primary producers and as energy linker to the higher trophic levels. The Amundsen Seas is one of the most productive areas of the Southern Ocean (Fragoso and Smith 2012), with annual primary production reaching up to 160 g C m^{-2} and chlorophyll concentrations exceeding $>10 \mu\text{g l}^{-1}$ (Arrigo and van Dijken 2003). Little is known about the abundance and community of zooplankton throughout the Amundsen Sea, because most biological investigations have focused on other trophic levels. Also, despite the numerical importance of mesozooplankton community, little studies have been conducted on their feeding ecology in the Amundsen Sea.

In this study the main goals are to quantify the mesozooplankton community and understand interactions among the environmental factors (i.e. seawater temperature, salinity and chlorophyll a concentration), protozoa and mesozooplankton community in the polynya and non-polynya area according to different water masses.

3.7.2. Materials and methods

Zooplankton samples were collected with a Bongo net (330 and 505 μm mesh) and rectangular net with a 1 m^2 opening (330 μm mesh) at 23 selected stations (Figure 3.13 and Table 3.4). Twenty-five Bongo net was towed vertically within the upper 200 m of water column. 330 μm mesh samples were split using a Folsom plankton splitter as follows: $\frac{1}{2}$ of each tow was immediately fixed and preserved with buffered formaldehyde (pH 8, final concentration ca. 5%) for quantitative analyses and $\frac{1}{2}$ was frozen in $-80 \text{ }^\circ\text{C}$ for further analysis such as Next Generation Sequencing (NGS) while $\frac{1}{2}$ of the samples from 505 μm mesh was used to examine the number of mesozooplankton and $\frac{1}{2}$ was preserved with buffered formaldehyde. Some of copepod and ice krill were taken and frozen in $-80 \text{ }^\circ\text{C}$ for separate analysis.

The ten rectangular nets within 200 m oblique trawls were used to characterise the mesozooplankton community around Amundsen Sea. The wire-up speed was 30 m min^{-1} and ship speed was about 2 – 2.5 knots for about 0.5 hour. The first of all, length measurements of krill were performed from the front of the eye to the tip of the telson (Morris et al., 1988). The length-frequency distributions were estimated based on more than 100 individuals each tow. The samples were also split using a Folsom plankton splitter as follows: $\frac{1}{2}$ of each tow was split and preserved in -80°C and $\frac{1}{2}$ was preserved in 10% buffered formalin for taxonomic identification.

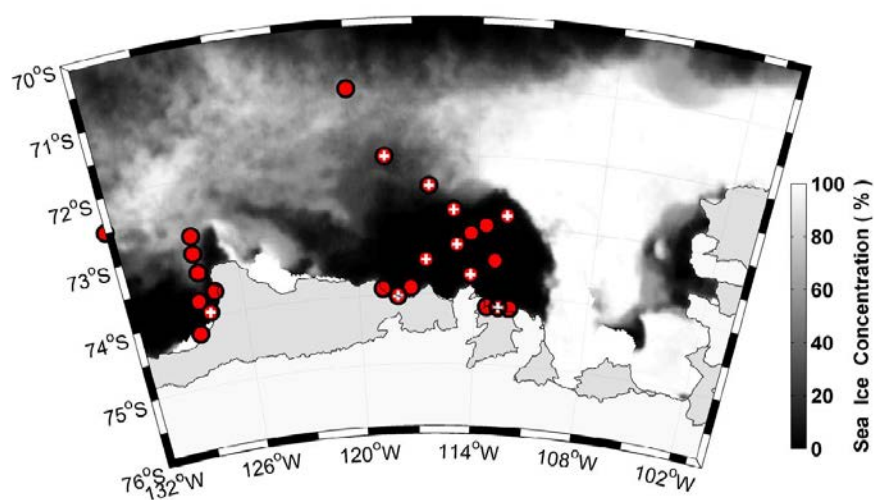


Figure 3.13. Mesozooplankton stations during ANA08B. Red dots and white crosses represent Bongo and rectangular net sampling stations, respectively.

Table 3.4. Sampling locations of zooplankton composition during ANA08B.

Station	Latitude (°S)		Longitude (°W)		Net Type	Sampling (UTC)		Flow meter	Depth (m)
	D	M	D	M		Date	Time		
ANA8B-St.11	66	27.955	155	44.198	BN	15-Jan-18	18:54 - 19:08	99061 -	194
ANA8B-St.11	66	27.955	155	44.198	BN	15-Jan-18	19:23 - 19:37	- 00399	194
ANA8B-St.12	73	39.513	127	24.127	BN	18- Jan -18	06:53 - 07:03	00400- 00807	127
ANA8B-St.18	73	56.720	127	48.435	BN	19- Jan -18	07:23 - 07:38	00807- 01430	192
ANA8B-St.18	73	56.723	127	48.428	RN	19- Jan -18	09:03 - 09:21	432505- 462683	215
ANA8B-St.22	74	13.614	128	33.462	BN	19- Jan -18	20:58 - 21:11	01432- 02036	191
ANA8B-St.27	73	54.280	118	44.836	BN	21- Jan -18	16:42 - 16:54	02037- 02938	192
ANA8B-St.28	74	01.149	117	58.712	BN	22- Jan -18	13:03 - 13:16	02938- 03603	193
ANA8B-St.28	74	00.770	117	56.378	RN	22- Jan -18	15:39 - 16:08	548721- 562864	76
ANA8B-St.29	73	53.774	117	17.742	BN	22- Jan -18	22:22 - 22:34	03603-04239	192
ANA8B-St.31	73	30.002	116	30.032	BN	23- Jan -18	12:31 -12:49	04239-05108	193
ANA8B-St.31	73	30.001	116	30.004	RN	23- Jan -18	14:43 -15:09	567159-612389	-
ANA8B-St.33	73	16.773	114	56.980	BN	24- Jan -18	05:37 - 05:50	05108-06209	193
ANA8B-St.33	73	16.944	114	57.688	RN	24- Jan -18	13:23 - 13:57	612401-670737	68
ANA8B-St.34	73	42.675	114	12.939	BN	24- Jan -18	20:38 - 20:52	06209-06811	192
ANA8B-St.34	73	42.678	114	12.920	RN	24- Jan -18	23:42 - 00:06	670741-732713	68
ANA8B-St.36	74	10.305	113	19.174	BN	26- Jan -18	08:15 - 08:27	06811-07473	192
ANA8B-St.38	74	10.440	112	43.457	BN	26- Jan -18	18:40 -18:53	07473-08135	194
ANA8B-St.38	74	10.440	112	43.457	BN	26- Jan -18	19:00 -19:07	08135-08420	96
ANA8B-St.38	74	10.434	112	43.438	RN	26- Jan -18	20:14 -20:42	732896-805201	103
ANA8B-St.42	74	10.577	112	08.081	BN	27- Jan -18	06:50 -07:02	08420-09061	192
ANA8B-St.45	73	30.001	112	59.996	BN	28- Jan -18	01:41 -01:52	09062-09762	-
ANA8B-St.46	72	51.001	112	29.973	BN	28- Jan -18	08:31 -08:43	09762-10391	192
ANA8B-St.46	72	51.044	112	29.989	RN	28- Jan -18	11:00 -11:18	805190-844347	87
ANA8B-St.47	73	00.001	113	30.006	BN	28- Jan -18	13:55 -14:07	10391-11069	192
ANA8B-St.48	73	06.782	114	14.999	BN	28- Jan -18	17:34 -17:46	11070-12356	192
ANA8B-St.49	72	46.918	115	07.499	BN	28- Jan -18	23:44 -23:55	12356-13659	191
ANA8B-St.49	72	46.961	115	07.392	RN	29- Jan -18	02:30 -02:46	844349-893148	69
ANA8B-St.50	72	25.876	116	20.328	BN	29- Jan -18	11:16 -11:27	13661-14326	193
ANA8B-St.50	72	26.471	116	27.603	RN	29- Jan -18	16:47 -17:04	893133-926822	94
ANA8B-St.53	71	00.005	120	00.012	BN	30- Jan -18	08:58 -09:10	14326-14972	194
ANA8B-St.52	71	59.999	118	25.005	BN	30- Jan -18	21:00 -21:11	14972-15623	194
ANA8B-St.52	72	00.345	118	27.501	RN	30- Jan -18	23:41 -23:55	926821-959631	88
ANA8B-St.55	72	50.884	128	04.017	BN	01- Feb -18	16:24 -16:36	15623-16294	194
ANA8B-St.24	73	04.508	128	08.014	BN	02- Feb -18	00:24 -00:35	16295-16974	194
ANA8B-St.23	73	21.258	128	03.082	BN	02- Feb -18	08:20 -08:31	16975-17633	193
ANA8B-St.23	73	21.258	128	03.082	BN	02- Feb -18	08:36 -08:39	17633-17793	47
ANA8B-St.57	73	45.817	128	18.182	BN	02- Feb -18	12:40 -12:51	17794-18811	194

3.7.3. Preliminary results

We used a 500- μm mesh net to count total number of mesozooplankton samples and copepods accounted more than 70 % of total mesozooplankton abundance. The abundance shows clearly the regional differences representing the relatively high number of mesozooplankton in the center of Dotson trough and the western Getz ice shelf (Figure 3.14). The highest values were recorded at Station 23.

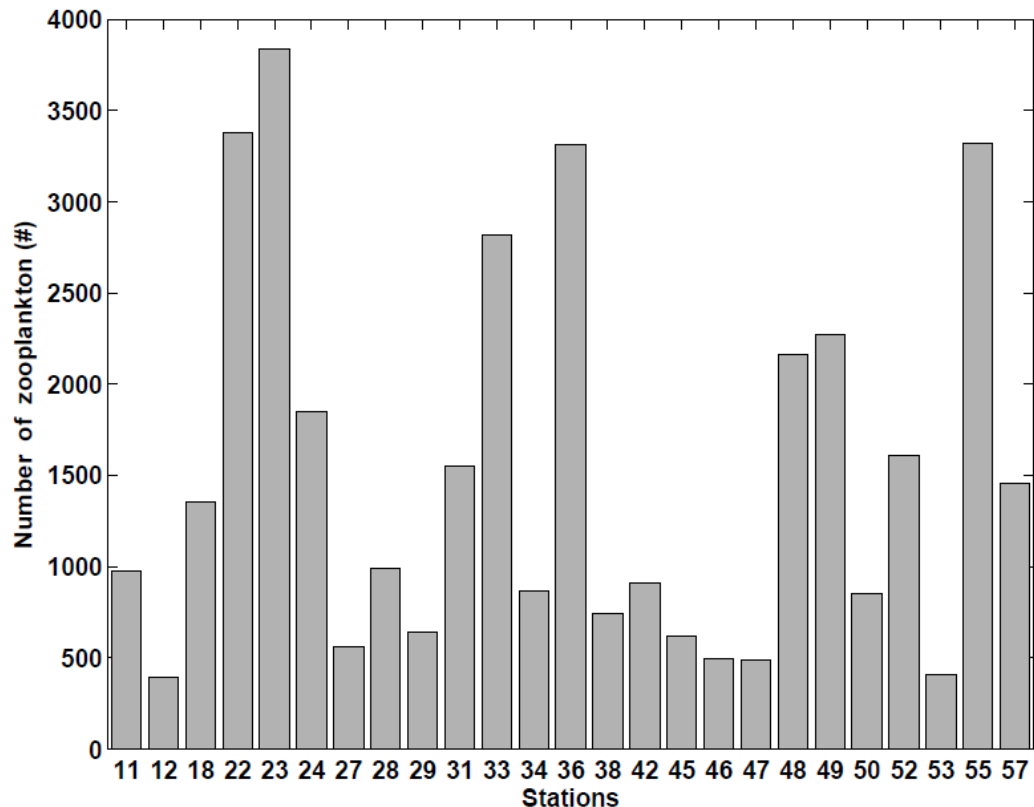


Figure 3.14. Regional distribution of mesozooplankton abundance.

Ice krill (*Euphausia crystallorophias*) were sampled to determine the variation in the structure of the population around the eastern Getz and Dotson ice shelves and to provide parameters required in the target strength model for krill biomass estimation. Ice krill samples were taken from oblique tow (surface to 200 m) samples using a rectangular net (1 m² mouth area, 330 μm mesh) where there were sufficient numbers of krill to select 100 decent state specimens for length frequency. The tows were conducted at a speed of 2 - 3 knots for about 0.5-h period while weather conditions were good during the all sets of transects. Krill total length was measured from the anterior edge of the eye to the tip of the telson, with measurements rounded down to the nearest millimetre. The ice krill length frequency for the whole net tows are shown in Figure 3.15 The mean length of ice krill was 12.3 mm (SD=5.3 mm) and varied from 2 to 37 mm.

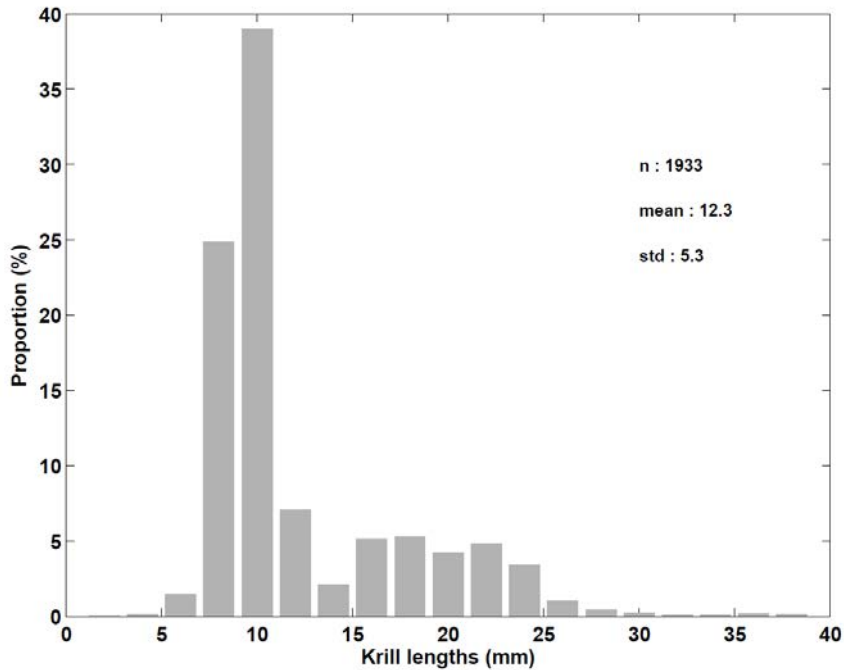


Figure 3.15. Length-frequency distribution of ice krill (Mean length: 12.3 (SD:5.3), N=1933).

References

- Arrigo KR, van Dijken GL (2003) Phytoplankton dynamics within 37 Antarctic coastal polynyas. *J Geophys Res* 108: doi:10.1029/2002JC001739.
- Fragoso GM, Smith WO (2012) Influence of hydrography on phytoplankton distribution in the Amundsen and Ross Seas, Antarctica. *J Mar Syst* 89:19-29.
- Morris, D.J., Watkins, J.L., Ricketts, C., Buchholz, F., Priddle, J., 1988. An assessment of the merits of length and weight measurements of Antarctic krill *Euphausia superba*. *Brit. Antarct. Surv. B.* 79, 27–50.

3.8. Samplings for isolation of dominant microorganisms

¹Chung, Taek-Soo and ¹Yu, Woon-Jong

¹Chungbuk National University, Korea

요약문

서남극해의 아문젠 해역 폴리냐는 여름철 1차 생산성이 높은 흥미로운 생태계환경이다. 2012-2014년 연구 탐사에서 얻은 자료를 통하여 아문젠해에는 *Pelagibacter*가 우점하고 있다는 사실을 알아냈다. *Pelagibacter*는 환경에서 우점하고 있는 세균이지만 배양은 쉽지 않다. *Pelagibacter*의 물질대사 중 흥미로운 사실은 이 미생물이 canonical metabolic pathway를 가지고 있지 않다는 점이다. 이는 *Pelagibacter*의 배양에는 환원된 형태의 N이나 S source가 필요하다는 것을 보여준다. Amino acid가 그러한 역할을 하는 것으로 생각되며, 배양을 하

는데 있어 중요한 요소이다. 이를 기반으로, amino acid를 기질로 이용하는 배양 조건을 구상했다. 또한 algae lysate (*Prochlorococcus marinus*)와 *Phaeocystis antarctica*를 이용, post-blooming 환경과 유사한 조성의 배지를 구상했다. 시료를 채취한 정점은 여름 아문젠 해역의 1차 생산이 활발히 일어나는 것으로 생각되는 폴리냐 중심부 및 주변부 그리고 Getz와 Dotson Ice shelf, 대양으로 선정하였다. 정점에서 배양을 시도하는 수심은 Surface Chlorophyll Maximum (SCM)과 일부 photic zone 그리고 해저이다. 또한 배양 실험의 대상을 *Pelagibacter*로 한정하지 않고, *Pelagibacter*와 유사하게 canonical metabolic pathway가 부분적으로 결손되어 있는 MGII나 Ant4D3와 같은 난배양성 미생물도 배양을 시도했다. 배양 방법은 enrichment culture와 High Throughput Culture (HTC) 기술인 serial dilution method를 이용하였으며, 추후에 flowcytometer, PCR을 통해 난배양성 미생물을 스크리닝할 계획이다. 또한 ice-core를 통해 얻은 ice algae에 대한 배양 실험을 계획 중이며, 조류와 원핵미생물의 공생배양(co-culture)을 통해 질소 순환에 대한 연구를 진행할 예정이다.

3.8.1. Objective

Polynya in the Amundsen Sea area of the West Antarctic Sea is an interesting ecosystem with high primary productivity during the summer season. It has been found that *Pelagibacter* are dominant in the Amundsen Sea through data obtained from research exploration in 2012-2014. *Pelagibacter* are dominant bacteria in the Antarctic Ocean, but it is hard to be cultivated.

Pelagibacter don't have a canonical metabolic pathway, which is the interesting factor of metabolism of this microorganism. Therefore, reduced forms of N and S sources are required for the cultivation of *Pelagibacter*. Amino acids are reduced forms as minimum nutrient sources and the essential factors for cultivation. Based on this, cultivation conditions were designed including amino acids as substrates. In addition, algae lysate (*Prochlorococcus marinus*) as a substrate and *Phaeocystis antarctica* as a strategy for co-culture were used on each complex medium with similar composition to the post-blooming conditions.

Water samples were collected from the center and margin of Polynya where the primary production of the summer Amundsen sea is considered to be active, and the others were the Getz, Dotson Ice shelf and open oceans. The sampling depths for cultivation were at the Surface Chlorophyll Maximum (SCM), some photic zones and the bottom of the sea. In addition, we tried to cultivate not only *Pelagibacter* but also unculturable microorganisms such as MGII and Ant4D3 which also don't have canonical metabolic pathway partially.

3.8.2. Sampling and Cultivation

Water samples from stations at a polynya (polynya center and margins), sea-ice, and ice-free open oceans were collected during the expedition, between 21 December, 2017 and 12 February, 2018 (Table 3.5). Cultivation was set up by using enrichment culture and serial dilution (High throughput culture (HTC) skills) methods at each station.

- For isolation of dominant bacteria and archaea such as *pelagibacter*, Ant4D3 and MGII, vertical water samples (4 liters each, depths at SCM, bottom and deep-sea) were collected at each station. The samples were stored at 4°C refrigerator.
- For enrichment, 10% 0.45um filtered water samples were suspended in 10ml of sterile artificial seawater medium (ASW) with sodium bicarbonate (3 mM), potassium phosphate (0.1 mM), 1x trace element mixture and 1x vitamin solution. For substrates, Amino acids were used as the minimum nutrient requirements on a defined medium. In addition, algae lysate (*Prochlorococcus marinus*) as a substrate and *Phaeocystis antarctica* as a strategy for co-culture were used on each complex medium. Cultivation conditions of substrates were shown below.

- 1) 20 amino acid mixtures (each 0.01mM) and 0.1mM pyruvate
- 2) *Prochlorococcus marinus* (lysate, 20% of total volume), 0.05mM pyruvate, 0.01mM Methionine, 0.05mM Leucine and 0.01mM Glycine
- 3) *Phaeocystis antarctica* (sea water samples filtered using 0.45um, 20% of total volume), 0.05mM pyruvate, 0.01mM Methionine, 0.05mM Leucine and 0.01mM Glycine

All cultures are incubated at 10°C.

- For serial dilution, all conditions are same with enrichment cultures except for total volume. Containers for serial dilution cultivation were different from enrichment cultures. 96 deep well plates were used for cultivation and its total volume for each well is 1ml.

3.8.3. Sampling for Ice-core

- Latitude : 73.04°S, Longitude : 126.11°W
- N cycle studies through the responses of marine bacteria to co-culture with ice-algae will be planned.

Further studies

- After cultivation in 96 well plates (serial dilution method), unculturable microorganisms will be screened by using flow cytometer and PCR. (Figure 3.16)

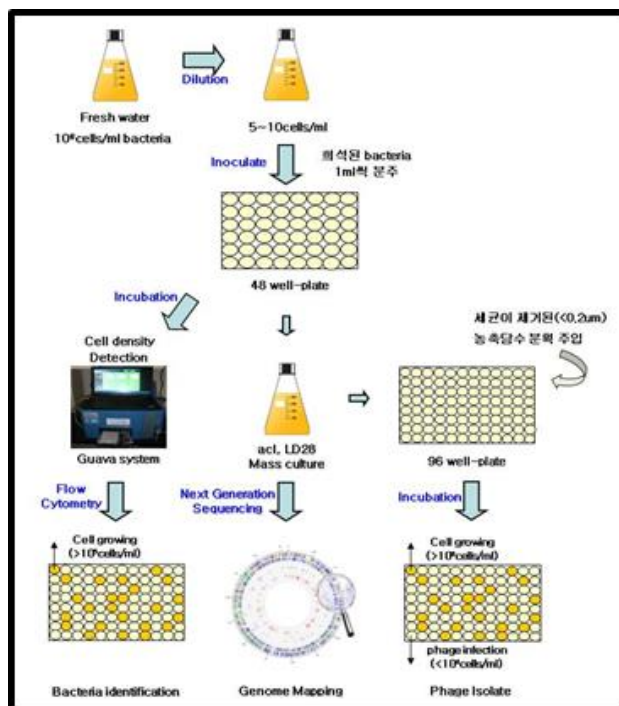


Figure 3.16. The module for cultivation of unculturable bacteria by using HTC

Table 3.5. Summary of sampling sites for isolation of dominant microorganisms

Station	Surrounding	Sampling Date	Sampling Depth (m)	Latitude (°S)	Longitude (°W)
7	open ocean	2017-12-29	20, 40, 100, 500, 1000, 2711	56.00	145.71
9	open ocean	2017-12-30	45, 100, 1200, 3010	56.99	147.39
22	Western Getz Ice shelf	2018-01-20	35, 725	74.22	128.55
27	Middle Getz Ice shelf	2018-01-22	270, 1011	73.88	118.72
31	Polynya center	2018-01-23	20, 358	73.50	116.50
33	Polynya center	2018-01-23	40, 812	73.27	114.94
38	Dotson Ice shelf	2018-01-24	22,1047	74.17	112.72
46	Polynya center	2018-01-28	10, 440	72.85	112.50
49	Polynya center	2018-01-29	40, 577	72.78	115.12
50	Polynya margin	2018-01-29	35, 528	72.45	116.35
52	Polynya margin	2018-01-31	40, 480	72.00	118.41
53	open ocean	2018-01-30	35, 2380	71.00	120.00

References

- Paul Carini, Laura Steindler, Sara Beszteri and Stephen J Giovannoni (2013) Nutrient requirements for growth of the extreme oligotroph 'Candidatus Pelagibacter ubique' HTCC1062 on a defined medium. *The ISME Journal* 7, 592–602
- J.-G. Kim, S.-J. Park, I.-T. Cha, S.-J. Kim, K.-H. Kim, E.-J. Yang, Y.-N. Kim, S.-H. Lee, S.-K. Rhee (2013) Unveiling abundance and distribution of planktonic Bacteria and Archaea in a Polynya in Amundsen Sea, Antarctica. *Environ Microbiol* 16(6), 1566-1578
- Mrinalini P. Nikrad, Matthew T. Cottrell and David L. Kirchman (2014) Growth activity of gammaproteobacterial subgroups in waters off the west Antarctic Peninsula in summer and fall. *Environ Microbiol* 16(6), 1513-15

CHAPTER 4

Biogeochemical Oceanography

4.1. Sediment trap

¹Yewon Kim, ²So-Young Kim

¹Korea Institute of Ocean and Science Technology, Korea

²Korea Polar Research Institute, Incheon 406-840, Korea

요약문

서남극 아문젠해는 최근 빙상·빙붕 및 해빙 면적의 급격한 감소와 해양생산성이 높은 폴리냐 환경의 상대적 증가로 인해, "biological pump"에 의한 CO₂의 해양 유입량 및 탄소 순환 기작의 상당한 변화가 예측되는 해역이다. 본 현장조사는 퇴적물포집기를 이용하여 아문젠해 침강입자 (유기탄소, 탄산칼슘, 생물기원 규소, 육상기원 쇄설물)의 시·공간적 변화를 알아보기 위해 수행하였다. 2016년 2월에 설치하였던 3대의 퇴적물포집기를 정점 27 (설치수심 427 m), 33 (설치수심 426 m), 34 (설치수심 443 m)에서 회수하였다. 정점 27의 퇴적물포집기에 약 2년 동안 수집된 시료들은 모두 사진으로 기록한 후, 밀봉하여 냉장보관 하였으며 향후 연구소에서 분석할 계획이다. 정점 33과 34에서는 포집기 내 다량의 해조류 밀집 등에 기인한 장비오작동으로 샘플 수집에 실패하였다. 추가로, 본 현장조사에서는 3대의 퇴적물포집기를 정점 33 (설치수심 440 m), 정점 36 (설치수심 455 m), 정점 30 (설치수심 566 m)에서 계류하였으며, 모두 약 2년 동안 여름·가을·봄은 20일 간격, 겨울은 2달 간격으로 샘플을 채집하도록 설정하였다.

4.1.1. Objectives

The Amundsen Sea is considered to be one of the most rapidly changing parts of the cryosphere in responding to global climate change (Shepherd et al., 2004; Scott et al., 2009; Katz and Worster, 2010). A particular concern is for dramatic signs of ice loss in coastal zones of the Amundsen Sea enhancing seasonal sea ice melting and CO₂ absorption which will directly affect the carbon cycling over this region. Flux of organic matters sinking from euphotic zone to deep sea not only represents new production, but also governs the ocean carbon inventory as well as removal of bioactive elements from the ocean. Despite its significant implication on both regional and global carbon cycles, this process has been poorly studied in the Amundsen Sea. The main objective of this sampling effort was to 1) quantify seasonal variations in the sinking fluxes of biogenic elements such as particulate organic carbon (POC), CaCO₃ and biogenic silica using a sediment trap device and 2) estimate the amounts of CO₂ removed from atmosphere into the ocean by "biological pump" in the Amundsen Sea.

4.1.2. Work at sea

All sediment traps were safely recovered from three mooring stations (St. 27, 33 and 34; Figure 4.1). The sediment trap recovered from St. 27 had worked during the deployment period, as scheduled (Figure 4.2). The collect trap samples were sealed and stored in the refrigerator for further analysis. However, the two sediment trap recovered from St. 33 and 34 had not rotated fully, but was stuck on the 2nd bottle. In the sediment trap recovered from St. 34, some biological growth was evident near the base of the funnel. For future recovery, three additional sediment traps were deployed at St. 30 and 36 (the polynya coastal), and St. 33 (the polynya center). Each sediment trap consists of 21 bottles, scheduled to operate the each bottle with time interval of 20 and 60 days during summer/autumn/spring and winter seasons, respectively (Table 4.1). After 2 year, the sediment trap will be recovered and analyzed to investigate annual flux of organic matters in the Amundsen Sea.

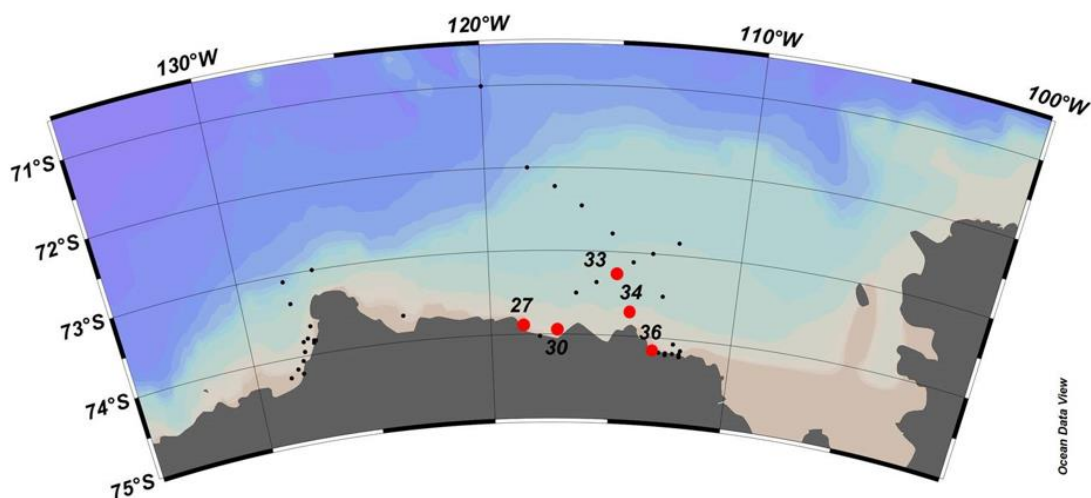


Figure 4.1. A station map of the sediment trap recovery and deployment.



Figure 4.2. Sediment trap samples collected from St. 27.

Table 4.1. Sediment trap time schedules

Bottle Number	St. 30	St. 33	St. 36
1	2018.01.25	2018.01.26	2018.01.28
2	2018.02.16	2018.02.16	2018.02.16
3	2018.03.10	2018.03.10	2018.03.10
4	2018.04.01	2018.04.01	2018.04.01
5	2018.06.01	2018.06.01	2018.06.01
6	2018.08.01	2018.08.01	2018.08.01
7	2018.10.01	2018.10.01	2018.10.01
8	2018.12.01	2018.12.01	2018.12.01
9	2018.12.21	2018.12.21	2018.12.21
10	2019.01.10	2019.01.10	2019.01.10
11	2019.01.30	2019.01.30	2019.01.30
12	2019.02.19	2019.02.19	2019.02.19
13	2019.03.11	2019.03.11	2019.03.11
14	2019.04.01	2019.04.01	2019.04.01
15	2019.06.01	2019.06.01	2019.06.01
16	2019.08.01	2019.08.01	2019.08.01
17	2019.10.01	2019.10.01	2019.10.01
18	2019.12.01	2019.12.01	2019.12.01
19	2019.12.21	2019.12.21	2019.12.21
20	2020.01.11	2020.01.11	2020.01.11
21	2020.02.01	2020.02.01	2020.02.01
Close	2020.03.01	2020.03.01	2020.03.01

References

- Katz, R.F., Worster, G., 2010. Stability of ice-sheet grounding lines. *Proceedings of the Royal Society* 466, 1597-1620.
- Scott, J.B.T., Gudmundsson, G.H., Smith, A.M., Bingham, R.G., Pritchard, H.D., Vaughan, D.G., 2009. Increased rate of acceleration on Pine Island Glacier strongly coupled to changes in gravitational driving stress. *The Cryosphere* 3, 125-131.
- Shepherd, A., Wingham, D., Rignot, E., 2004. Warm ocean is eroding West Antarctic ice sheet. *Geophysical Research Letters* 31 (L23402).

4.2. Sediment coring

¹Minkyong Kim, ²So-Young Kim, ²Wuju Son, ³Taecksoo Chung, ³Woonjong Yu

¹Seoul National University, Korea

²Korea Polar Research Institute, Incheon 406-840, Korea

³Chungbuk National University, Korea

요약문

서남극 아문젠해는 최근 빙상·빙붕 및 해빙 면적이 급격하게 감소함에 따라, 해양생산성이 높은 폴리냐 환경의 증가가 예상되는 해역이다. 식물플랑크톤 일차생산을 통해 형성되어 침강입자 형태로 수주에서 저층으로 제거되는 입자성 유기탄소는 "biological pump"의 중요한 부분으로, 폴리냐 환경에서의 CO₂ 흡수량 및 전지구적 탄소순환 효율을 결정한다. 본 연구는, 1) 해양퇴적물의 총 유기탄소 및 질소 함량, 식물플랑크톤 색소 분석을 통해 수층 식물플랑크톤 생산력 변화에 따른 해저 유기물 공급량 및 에너지 흐름 변동을 이해하고, 2) 방사성 탄소동위원소 및 바이오마커 분석을 통해 과거 유기탄소 퇴적 변동 및 그 순환 기작을 이해하기 위한 목적으로 수행되었다. 현장조사를 통해, 폴리냐 해역을 포함한 총 4개 정점에서 박스코어 퇴적물채집기를 이용하여 해양퇴적물 시료를 채취하였다. 채집한 시료는 각 항목 별로 전처리를 한 후, 향후 실험실 분석을 위해 냉동 및 냉장 보관하였다.

Objectives

The Amundsen Sea has shown dramatic signs of ice loss over the last few decades including a rapid shrinkage of ice shelves, glaciers and sea ice coverage (Rignot et al., 2012; Stammerjohn et al., 2012), leading some to suggest that more extensive areas of polynya environments in the Amundsen Sea will be possible in near future. As the polynya regions exhibit high primary productivity (Becquevort and Smith Jr., 2001; Arrigo and van Dijken, 2003), CO₂ absorption controlled by the biological pump in this region may hold a substantial impact on global carbon cycling. Therefore, it is of pivotal importance to better document and understand past variability of organic carbon accumulations in the Amundsen Sea, which cannot be fully understood by short-term instrumental observations alone, but entail investigation on longer time series using sedimentary records. During the ANA08B cruise, a sediment coring program was conducted: i) to obtain integrated sedimentary records of organic carbon accumulation rate and radiocarbon chronology from the Amundsen shelf sediments, and ii) to attain data on past changes in chemical compositions of seafloor sediments assessing natural instabilities in biogeochemical processes in this region.

Work at sea

Sediment coring was performed with a box corer consisting of a headstand weighing ca. 350 kg attached to the top of a rectangular steel tube (30×40×60 cm) at 7 stations (Table 4.2). The coring tool was deployed from the A frame in the stern using the Deep Sea Traction (DST) winch with spectra rope. Once on deck the top centimeter of sediments captured in the steel tube was skimmed for organic geochemical determinations. Despite some general problems of lost core material (Figure 4.3), coring was successful. The sediment in the box core was subsampled into a cylindrical push core and the rest of the material left in the box was examined for megafauna presence and then discarded.

Table 4.2. Locations of box coring

Date	Station	Recovery (cm)	Location		Water depth (m)
			Latitude	Longitude	
2018.01.19	20	-	74°8.4702'S	128°12.2437'W	568
2018.01.20	25	-	72°59.6588'S	126°58.4301'W	270
2018.01.21	26	31	73°40.9102'S	123°34.7121'W	580
2018.01.24	33	51	73°16.771'S	114°56.994'W	827
2018.01.29	50	42	72°25.8752'S	116°20.3249'W	537
2018.01.30	51	-	72°13.3913'S	117°35.4862'W	521
2018.02.03	57	37	73°45.8168'S	128°18.1817'W	711



Figure 4.3. Box coring at St. 20, 25 and 51 was performed unsuccessfully due to high gravel contents.

Preliminary results

Surface sediments were taken from box corer at 4 stations with water depths varying between 537 and 821 m. Surface sediments were photographed and then the uppermost 1cm sediments were sub-sampled in plastic bottles for biogeochemical and microfossil analyses. The characteristics of surface sediments are summarized in Table 4.3.

Table 4.3. Characteristics of surface sediments recovered by box corer

Stations	Water depth (m)	Color and lithology		Remarks
26	580	brownish silty clay mud		soft sediment, bioturbated, benthic organisms
33	827	brownish mud		soft sediment
50	537	brownish sandy mud		coarse sediment, high gravel content, bioturbated, benthic organisms
57	711	brownish silty clay mud		soft sediment, bioturbated, benthic organisms

The recovery of the box core sediments taken at 4 stations varied from 31 to 51 cm (Table 4.2). Push core subsamples (10 cm in diameter) for geochemical properties were collected, labeled, and immediately moved to a refrigerated container (Figure 4.4. A). Sediment cores for radiocarbon and biomarker analyses were sliced into 1–2 cm thick subsamples on board and stored in pre-baked 4 oz glass jar (Wheaton) and kept frozen until further analyses (Figure 4.4. B).

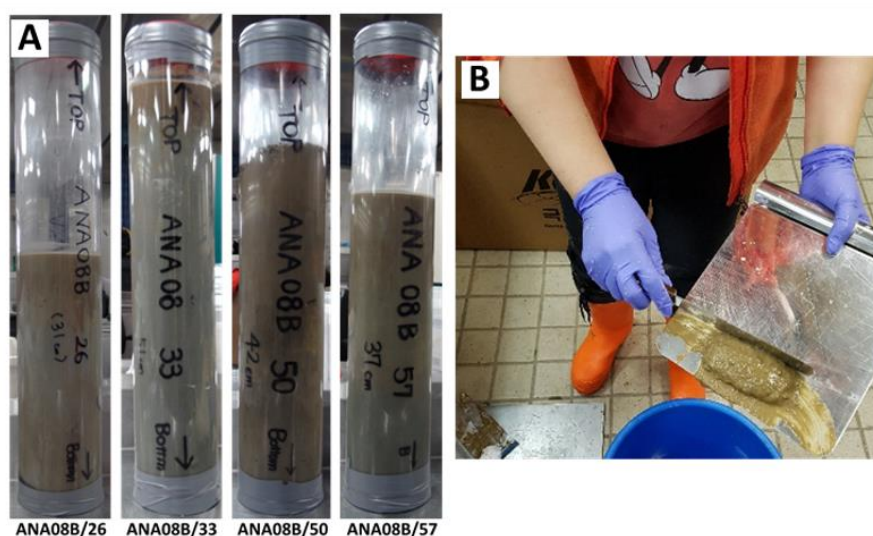


Figure 4.4. A) Box core sediments were collected in a plastic tube during ANA08B and B) subsampled for radiocarbon and biomarker analyses.

Summary and future analyses

The sediment coring program during the ANA08B cruise was generally successful in managing to retrieve cores from stations that were considered high priority for this expedition. A successful series of core recovery yielded 4 tubes of sediment will be used to study biological and biogeochemical processes taking place in the Amundsen ice shelf environments. Detailed investigation will be performed at KOPRI and SNU.

References

- Arrigo, K.R., van Dijken, G.L., 2003. Phytoplankton dynamics within 37 Antarctic coastal polynya systems. *J. Geophys. Res.* 108, 3271.
- Becquevort, S., Smith Jr., W.O., 2001. Aggregation, sedimentation and biodegradability of phytoplankton-derived material during spring in the Ross Sea, Antarctica. *Deep-Sea Res. II* 48, 4155–4178.
- Rignot, E., Bamber, J.L., Van Den Broeke, M.R., Davis, C., Li, Y., Van De Berg, W.J., Van Meijgaard, E., 2008. Recent Antarctic ice mass loss from radar interferometry and regional climate modelling. *Nat. Geosci.* 1, 106–110.
- Stammerjohn, S., Massom, R., Rind, D., Martinson, D., 2012. Regions of rapid sea ice change: An inter-hemispheric seasonal comparison. *Geophys. Res. Lett.* 39, L0501.

Chapter 5

Trace metals

5.1. Sampling using the Titan sampling system for trace metals

¹Rob Middag, ¹Hung-An Tian, ¹Charlotte Eich, ¹Mathijs van Manen, ¹Sven Pont and ²Scott McCain

¹Royal Netherlands Institute for Sea Research

²Dalhousie University, Halifax, Canada

5.1.1. Introduction

The production of oceanic phytoplankton that form the base of the marine food web depends on the availability of sunlight and nutrients, typically nitrogen and phosphorus (and silicate for diatoms). In the Southern Ocean, an important high nutrient low chlorophyll (HNLC) area (Bruland et al., 2014; Moore et al., 2013), iron (Fe) affects the amount of atmospheric CO₂ sequestered in deep ocean waters and ocean sediments via the biological pump (De La Rocha, 2007), with far reaching implications for global climate and the local ecosystem (Arrigo et al., 2008; Boyd and Ellwood, 2010; Moore et al., 2013). Yet, it is becoming increasingly clear that the situation is more complex, and controlled by factors beyond just the scarcity of Fe. New insights highlight the importance of other trace-metals (Morel et al., 2014), co-limitation by two or more nutrients (Arrigo, 2005; Middag et al., 2013; Middag et al., 2011; Saito et al., 2008) and variability in nutrient requirements between species and environmental conditions (Arrigo and van Dijken, 2003; Klunder et al., 2014; Moore et al., 2013). Notably for Fe, its solubility and probably also its availability depends strongly on the Fe-binding dissolved organic ligands (Boye et al., 2005; Croot et al., 2004; Hassler et al., 2011; Maldonado et al., 2005; Thuroczy et al., 2010). Microbial community composition as well as microbial and viral interactions impact the production and cycling of metals and metal-binding ligands (Bonnain et al., 2016; Slagter et al., 2016).

In the open ocean surrounding Antarctica, the amount of phytoplankton that can be sustained is lower than expected due to the very low availability of trace metals, notably iron. In contrast, in the coastal seas around Antarctica very dense phytoplankton blooms occur every year when the sea ice opens up. These ‘blooms’ support Antarctica’s key higher organisms and take up a large amount of atmospheric CO₂, but the extent depends on which species is blooming. Which species becomes dominant, and its ability to bloom, likely depends on the availability of macro-nutrients, iron and light, as different species have different requirements. However, much is still unknown about these requirements and the processes that control the availability and cycling of iron in the marine environment. Additionally, grazing and death through viral lysis control the standing stock of the phytoplankton. Viral lysis is a thus far understudied loss factor for phytoplankton, particularly in the Southern Ocean. The coastal region of Antarctica is currently experiencing dramatic changes as temperatures are rising and glaciers are melting rapidly. Glaciers are a source of iron, but much is still unknown about the importance of this source of iron for phytoplankton, the spatial extent and how this is likely to change.

5.1.2. Objectives

Currently, much is still unknown about the sources of Fe and other bio-active metals to the Antarctic ecosystem. Western Antarctic glaciers and ice sheets are a relatively unquantified source of Fe and other metals that can fuel phytoplankton blooms (De Jong et al., 2015; Gerringa et al., 2012; Wadham et al., 2013). These glaciers and ice sheets are rapidly melting (Joughin et al., 2014; Rignot et al., 2014), potentially increasing this source (Alderkamp et al., 2012). Furthermore, little is known about the spatial extent of Fe fertilisation via Antarctic

ice or the delivery of other metals from this source as the largest fraction of metals is delivered in the particulate phase and will quickly settle to the seafloor unless it can be solubilised and stabilised by organic ligands (Buck and Bruland, 2007). Moreover, other sources such as upwelling and the continental margin cannot be ignored either (De Jong et al., 2015; Gerringa et al., 2015; Middag et al., 2013; Middag et al., 2012). After entry and solubilisation into the ocean, the fate of Fe depends on the presence of ligands and the cycling through the microbial community and we are only just starting to understand how the cycling of Fe is affected by microbial actions, and in turn affects phytoplankton growth. Thus a closer look at sources of Fe, Fe-binding ligands and the interaction with the microbial community under changing conditions is critical.

5.1.3. Work at sea

The concentrations of metals in seawater are vanishingly low. In the case of iron (our main interest), the concentrations are equivalent to 1 paperclip dissolved in 40 billion liters of seawater, or 15 Olympic sized swimming pools. Utmost care needs to be taken not to contaminate the samples. We collected our samples using Titan, the ‘ultra-clean’ sampling system for trace metals and biology. Traditional CTD sampling systems cannot be used as the metal in these systems or the cable used for deployment, would contaminate the samples. The Titan system is deployed on a Dyneema cable and is made out of titanium and plastics, allowing us to collect uncontaminated samples. The grey polypropylene samplers are light proof to protect the phytoplankton from sudden exposure to light when the system comes out of the water. The entire sampling system is parked inside a clean room container. The air inside of this container is filtered over HEPA filters to keep the environment free of dust and other contamination and we dress up in dust free clean room suits when collecting our samples from the Titan system. Using this system, we collected water on 19 stations (maximum depth 1000 m due to length of cable) and at three stations both a deep and shallow cast were performed. The three shallow casts were done to start a bio-assay experiment in temperature controlled incubators where we contrasted temperature (in situ seawater and + 2 °C) and iron concentrations (in situ and + 2 nM). Station locations are displayed in Table 5.1

Table 5.1. Locations and maximum depths for the 19 stations sampled with Titan. The stations with numbers in bold were the stations where a bio-assay was started.

Station	Latitude (degrees S)	Longitude (degrees west)	month	day	year	max depth (m)
1	51.00	143.83	12	27	2017	473
4	54.00	143.83	12	29	2017	1013
10	58.00	147.50	01	01	2018	1015
11	66.47	155.74	1	15	2018	1009
31	73.50	116.50	1	23	2018	334
33	73.28	114.95	1	24	2018	768
34	73.71	114.22	1	24	2018	542
36	74.17	113.32	1	26	2018	654
42	74.18	112.13	1	27	2018	769
45	73.50	113.00	1	28	2018	507
46	72.85	112.50	1	28	2018	437
48	73.11	114.25	1	28	2018	592
49	72.78	115.13	1	29	2018	572
50	72.45	116.35	1	29	2018	505
52	72.00	118.42	1	30	2018	483
53	71.00	120.00	1	30	2018	1015
55	72.82	128.02	2	1	2018	1019
24	73.08	128.19	2	2	2018	553
57	73.76	128.30	2	2	2018	706

5.2. Trace metal sampling and analysis

¹Hung-An Tian, Mathijs van Manen and ¹Rob Middag

¹Royal Netherlands Institute for Sea Research

5.2.1. Introduction

At all 19 trace metal stations (1, 4, 10, 11, 24, 31, 33, 34, 36, 42, 45, 46, 48, 50, 52, 53, 55 and 57) and all depths (maximum 14) and during three bio-assays samples were collected for shipboard dissolved iron determination, total dissolvable metals (unfiltered water), dissolved metals (0.2 µm filtered). The last two are taken back to the shore based laboratory for Multi-Element (ME) determination that will give the concentrations of Cd, Co, Cu, Fe, Mn, Ni, Zn, Ti, Y, La, Pb and Ga. At all stations (with exception of station 46) samples for particulate metals and particulate carbon and nitrogen were collected at a maximum of 12 depths. Additionally, samples were collected for Particulate organic carbon (POC) and nitrogen (PON), iron binding ligands, ligand characterisation and particulate metals at most stations (Table 5.2).

5.2.2. Results

Dissolved Fe

Work at sea

Dissolved iron (DFe) concentrations of 19 stations with a maximum of 14 depths were mostly measured directly on board by an automated Flow Injection Analysis (FIA) after a modified method of De Jong et al. 1998.

Material and Methods

Filtered (0.2µm) and acidified (pH 1.8, 2ml/L 12M Baseline grade Seastar HCl) seawater was concentrated on a column containing aminodiacetic acid (IDA). This material binds only transition metals and not the interfering salts. After washing the column with ultrapure water, the column is eluted with diluted hydrochloric acid. After mixing with luminol, peroxide and ammonium, the oxidation of luminol with peroxide is catalyzed by iron and a blue light is produced and detected with a photon counter. The amount of iron is calculated using a standard calibration line, where a known amount of iron is added to low iron containing seawater. Using this calibration line a number of counts per nM iron is obtained. Samples were analyzed in triplicate and average DFe concentrations and standard deviation are given.

Preliminary results

Concentrations of DFe measured during the Amundsen cruise ranged from 0.053nM at the surface up to more than 2nM in the Amundsen polynya. Since samples containing less than 0.06nM DFe values are near the detection limit of the system; the standard deviation of these measurements were higher than the average value. The consistency of the FIA system over the course of the day was verified using a drift standard. Drift has been observed and seemed to be variable from day to day. All data will be corrected for this daily drift after the cruise and all results so far are not corrected. A certified SAFe standard (Johnson et al. 2007) for the long term consistency and absolute accuracy was measured on a regular basis.

In the Figure 5.1 below three depth profiles of station 10, 11 (open ocean) and 31 (Amundsen polynya) are depicted. In the polynya DFe in the upper water (below 200 meter) compared to the open ocean stations. Towards the surface concentrations of DFe at all three stations decreased till concentrations around 0.1 nM.

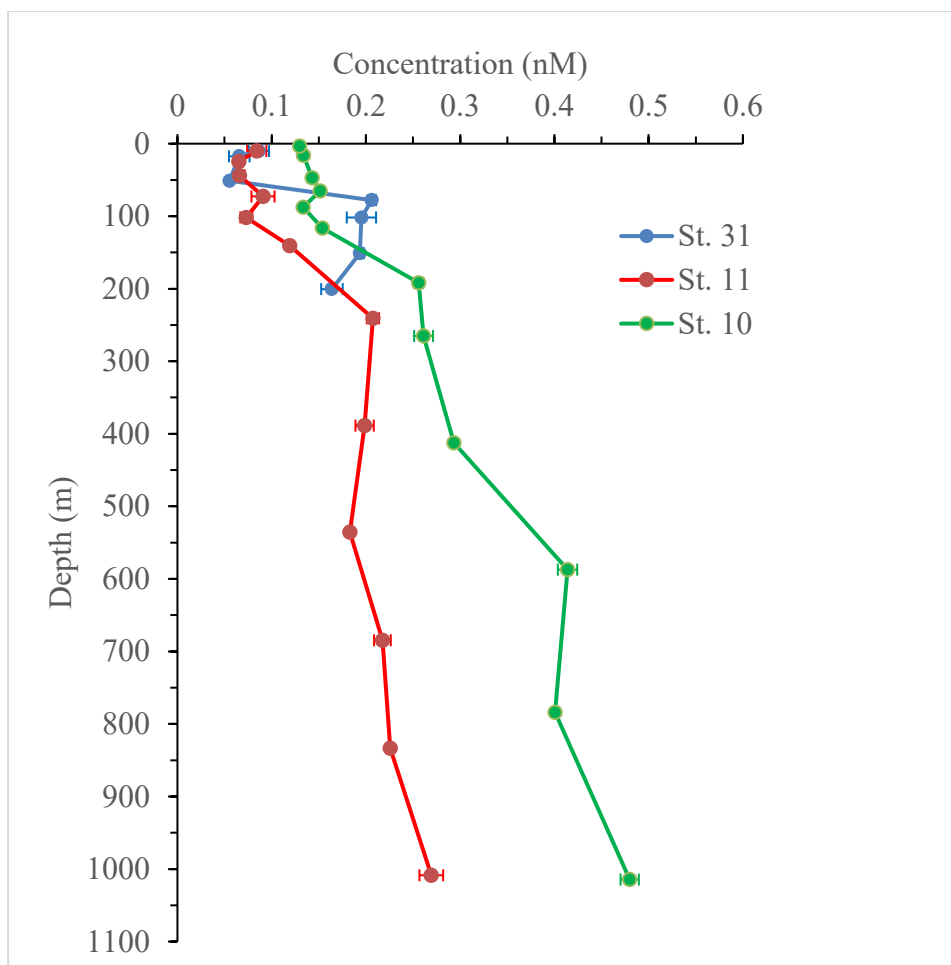


Figure 5.1. Three depth profiles (station 10, 11 and 31) of dissolved iron. Error bars are presenting the standard deviation [0.00082-0.01 nM], small values are falling within the size of the symbol.

Fe isotopes

Due to the isotopic signatures caused by fractionation in different Fe sources, Fe isotopes have been used as a promising tool for identifying Fe sources and quantifying these sources during recent years (Conway et al., 2014). For this expedition, Fe isotopes were sampled to identify the dissolved Fe sources and quantify their contribution to the dissolved Fe pool in the Amundsen Sea and nearby Southern Ocean. Dissolved Fe isotopes samples were sampled at all stations and all depths. Due to anticipated low Fe concentration in surface water, 4L filtered (0.2 μm) sea water was sampled for surface water (shallower than 100m), whereas 1L filtered sea water was sampled for the remaining, deeper depths. These samples were acidified to pH \sim 1.8 using ultrapure HCl (12M, Baseline grade Seastar HCl) on the ship after sampling and will be taken back to our shore based laboratory for further metal isotope analysis. In total, there were 250 Fe isotopes samples collected from 19 stations (12-14 for each station) during this cruise.

Particulate organic carbon (POC) and nitrogen (PON)

For POC and PON sampling, 5L unfiltered sea water was collected from 12 depths of 18 stations (Table 5.2). These samples were stored in dark bottles and further filtered by glass microfiber filters (GF/F, 0.7 μm). The filters were wrapped in aluminum foil and stored in $-20\text{ }^{\circ}\text{C}$. In addition to normal cast samplings, POC and PON samples were also collected from bio-assay experiments. 2L unfiltered water were sampled from bio-assay and filtered by 0.3 and 0.7 μm GF/F filters (1L for each pore size). The procedure was the same as above. The C/N analysis will be conducted in the shore based laboratory.

Particulate metals

For particulate metals sampling six liter of unfiltered seawater was collected from 11 depths of 18 stations (Table 5.2). The samples were filtered on a PES filter (Supor, 0.4 μm). After filtration samples were stored in LDPE bags and stored in -20 °C. Beside normal stations, PM samples were also collected at the end of the three bio-assays. PM analysis will be performed on the home institute.

Ligand concentration and characterization

The presence of dFe at concentrations beyond the inorganic solubility of Fe is thought to be facilitated by organic complexation of Fe with stabilizing ligands, which buffer dFe in seawater against hydrolysis and ensuing precipitation (Hunter and Boyd, 2007). Electrochemical measurements of bulk Fe(III) ligand concentration and binding strength suggest that this ligand pool ranges from 1 to 2nM and complexes over 99% of dissolved iron in the ocean. However, the molecular structures, sources, and fates of these ligands are currently unknown (Boiteau et al., 2013).

At a total of eight stations (Table 5.2) and three bio-assays samples for ligand concentration (0.2 μm filtered) were taken at a maximum of 12 depths. Samples were immediately stored at -20 degrees and will be taken home for home based analysis using cathodic stripping voltammetry (Gledhill and Van den Berg, 1994). This method gives information about the bulk concentration of ligands, defined in two classes; L1 (strong binding ligands) and L2 (weak binding ligands).

Beside taking samples for this bulk concentration measurement, we took samples for ligand characterization on six stations (11 depths; Table 5.2), at the end of three bio-assays (11 samples) and surface samples during the transect from Lyttelton towards the Amundsen sea (10 samples). For this analysis a maximum of four litre of seawater was collected (0.2 μm filtered). Immediately after sampling ligands were extracted using a SPE-cartridge with an average flow-rate of 6ml/min. After extraction samples were placed in geochemical bags and stored at -20°C for later analysis at the home institute using High-Performance Liquid Chromatography–Inductively Coupled Plasma–Mass Spectrometry (Boiteau et al, 2013). With the use of this technique siderophores (a group of strong binding ligands) can be detected and quantified.

Table 5.2. Overview of samples taken from the trace metal stations; X denotes samples taken for given parameter.

STATION	DfE	DM	TM	ISO	LIB	C/N	PM	FEL	LIG. CHAR
1	X	X	X	X	X	X	X		
4	X	X	X	X	X	X	X		
10	X	X	X	X	X	X	X		
11	X	X	X	X	X	X	X	X	X
24	X	X	X	X	X	X	X		
31	X	X	X	X	X	X	X	X	X
33	X	X	X	X	X	X	X	X	
34	X	X	X	X	X	X	X	X	X
36	X	X	X	X	X	X	X	X	X
42	X	X	X	X	X	X	X	X	X
45	X	X	X	X	X	X	X	X	X
46	X	X	X	X	X				
48	X	X	X	X	X	X	X		
49	X	X	X	X	X	X	X	X	X
50	X	X	X	X	X				
52	X	X	X	X	X	X	X	X	X
53	X	X	X	X	X	X	X		
55	X	X	X	X	X	X	X		
57	X	X	X	X	X	X	X		

5.3. Trace Metal Biogeochemistry and Proteomics

¹James Scott Patrick McCain

¹Dalhousie University, Halifax, Canada

5.3.1. Introduction

We aimed to examine the relationship between trace metals and microbial community physiology. To assess physiological status of the microbial communities, we will use quantitative proteomics and mass spectrometry to identify biomarkers of nutrient stress. For example, the expression of the iron-free protein flavodoxin, as opposed to the iron-containing ferredoxin, is indicative of iron stress in phytoplankton (LaRoche et al., 1996).

5.3.2. Work at sea

During this expedition, we collected size-fractionated samples (0.2µm, 3.0µm, and 12.0µm pore size) on polycarbonate filters at 21 different stations, for a total of 238 filters (Table 5.3). Most samples were collected with the trace-metal clean CTD ‘Titan’ (232/238), and immediately filtered via peristaltic pump. The different size fractions were for distinct microbial communities; the largest size fraction (>12.0µm) was used to target *Phaeocystis antarctica* colonies, the intermediate size fraction was used to target diatoms and other phytoplankton species <12.0µm and >3.0µm, and the smallest size fraction (<3.0µm and >0.2µm) was designated for smaller phytoplankton and bacteria. We will use a combination of exploratory, global proteomics and targeted proteomic approaches to quantify nutrient limitation biomarkers (e.g. Bertrand et al., 2012). Importantly, these trace-metal stress biomarker data are coupled to trace metal sampling, and to metal-binding ligand sampling, of the same water masses.

In addition to the station sampling, we performed multiple ‘bioassay’ experiments with temperature-controlled incubators. Our main experiments examined the combined influence of iron limitation and temperature on microbial community composition and physiology. We also conducted smaller experiments to examine potential colimitation of iron, manganese, and vitamin B₁₂ in the Amundsen Sea polynya.

We also collected large surface water samples from the underway pump system for exploratory microbial proteomics and genomics (Table 5.4). These large-volume samples have enough biomass to use for metaproteomics, via high resolution and mass accuracy mass spectrometry (i.e. with an Orbitrap VelosPro).

Table 5.3. Stations sampled for proteomics

Date	Station	Total Samples
2017-12-27	1	12
2017-12-29	4	12
2018-01-01	10	12
2018-01-16	11	16
2018-01-18	18	3
2018-01-19	22	3
2018-01-24	31	12
2018-01-24	33	12
2018-01-25	34	12
2018-01-27	36	12
2018-01-28	42	12
2018-01-28	45	12
2018-01-29	46	12
2018-01-29	48	12
2018-01-29	49	12
2018-01-30	50	12
2018-01-31	53	12
2018-01-31	52	9
2018-02-02	55	9
2018-02-02	24	12
2018-02-03	57	15

Table 5.4. Locations of underway sampling locations for proteomics

Date	Latitude	Longitude
2017-12-25	48 3 88 S	161 39 37 W
2017-12-26	49 12 57 S	154 50 09 W
2017-12-27	50 36 43 S	146 43 07 W
2017-12-27	51 01 01 S	144 43 01 W
2017-12-28	53 59 99 S	143 49 5 W
2017-12-30	54 55 61 S	143 46 69 W
2017-12-31	56 0 31 S	145 42 18 W
2018-01-03	61 49 905 S	133 46 21 W
2018-01-04	60 55 22 S	140 30 05 W
2018-01-05	60 11 65 S	150 37 32 W
2018-01-06	58 27 13 S	161 54 69 W
2018-01-07	56 19 26 S	170 23 63 W
2018-01-07	56 11 75 S	170 12 31 W
2018-01-08	52 39 75 S	176 45 20 W
2018-01-08	52 35 75 S	176 50 38 W
2018-01-09	48 3 18 S	177 50 63 W
2018-01-09	47 58 41 S	177 44 69 W
2018-01-11	46 33 71 S	173 31 58 W
2018-01-11	46 40 86 S	173 32 52 W
2018-01-12	51 54 72 S	174 19 98 W
2018-01-12	51 58 85 S	174 28 24 W
2018-01-13	55 45 61 S	178 56 07 W
2018-01-13	55 51 05 S	178 46 03 W
2018-01-13	57 31 70 S	175 37 06 W
2018-01-14	59 44 14 S	171 12 64 W
2018-01-15	63 32 91 S	162 52 95 W
2018-01-16	66 27 95 S	155 49 19 W
2018-01-17	70 12 23 S	145 24 89 W
2018-01-19	73 49 76 S	127 30 76 W
2018-01-20	74 13 61 S	128 33 46 W
2018-01-23	73 42 67 S	114 12 91 W
2018-01-30	73 38 19 S	123 20 24 W

5.4. Viral ecology

¹Charlotte Eich and ¹Sven Pont

¹Royal Netherlands Institute for Sea Research

Microbes (viruses, heterotrophic prokaryotes, phytoplankton and zooplankton) make up more than 95% of the ocean's biomass and are essential for the cycling of biogeochemical elements (e.g. Suttle, 2007). Furthermore, phytoplankton that are responsible for about 50% of the Earth's oxygen production, form the base of most of the pelagic food chains in the seas. Phytoplankton production is regulated by physicochemical variables such as light, temperature and nutrients. In the HNLC Southern Ocean, chlorophyll-a concentrations are relatively low as compared to the concentrations of macronutrients (nitrogen, phosphorus and silicate) largely due to iron deficiency. At the same time, primary production is controlled by predation and recently also viral lysis has been shown a significant loss factor (Mojica et al., 2016). The main focus of our sampling was to determine viral lysis rates of the microbial community and study the community composition of potential microbial host and viruses, along a natural iron gradient as well as during bioassay experiments (iron additions and with temperature increase).

Samples were collected using the Titan sampling system. We sampled for microbial abundances and community composition, as well as for viral lysis rates of microbial hosts and metagenomic analysis of microbial host community as well as the pelagic virus community.

Microbial abundances were sampled from seven depths: the surface mixed layer, top DCM, DCM, bottom DCM, chlorophyll-a minimum layer and two depths between bottom DCM and chlorophyll-a minimum; phytoplankton samples were fixed using formaldehyde/hexamine (18%/10% v/w; 100µl per 3.5ml sample). Bacterial and viral abundances were fixed in glutaraldehyde (0.5% final concentration). All fixed samples were flash frozen in liquid nitrogen after fixation for 30 min at 4°C, and stored at -80°C. Phytoplankton abundances were also counted fresh using the benchtop BD FACSCalibur flow cytometer (488nm Argon laser). The trigger was set on chlorophyll-a red autofluorescence and phytoplankton populations were discriminated based on their red (Chl-a), orange (phycoerythrin-containing cyanobacteria, and cryptophytes) and scatter characteristics.

Filtrations for pigment analysis from specific depths (used for viral lysis of phytoplankton) were conducted for 2 fractions (total and <20 µm). Chlorophyll-a will be used as an indicator for algal biomass, whereas specific marker pigments will reveal the presence of specific taxonomic groups (using the CHEMTAX program). Analysis of samples will be performed in the home laboratory (NIOZ-Texel).

Samples for microscopic analysis of larger-sized phytoplankton (and zooplankton) were collected in 100 mL brown glass bottles and fixed with Lugol solution, whenever viral lysis of phytoplankton was performed (except Station 34). Samples will be stored with our Korean collaborators and will be shipped to NIOZ only when further analysis is needed, depending on the previous results.

Samples for metagenomics of prokaryotic and eukaryotic microbial community (using 0.2 µm pore-size Sterivex filters) as well as for viruses (using 0.02 µm Anotop filters, and using the FeCl₃ precipitation method) were collected at each station where viral lysis rates of the microbial hosts were determined (see Table 5.5).

Viral lysis and microzooplankton grazing rates of phytoplankton were determined simultaneously using the modified dilution method (Evans et al., 2003) in combination with flow cytometry (fresh counts mainly). Either the DCM was sampled or otherwise the mixed layer (appr. 3% light depth). Samples were protected from light and processed at low temperature (1°C) and dimmed light. The principle of the method is that the removal of predators (grazers and viruses) by dilution allows algal cells to increase in standing stock over the incubation time of 24h. The difference in algal concentration over the period; therefore, provides an estimate of algal growth rate. Plotting the growth rate against the dilution, the slope of the linear regression represents the loss rate. Depending on the type of diluent (either grazer-free or grazer and virus-free) the microzooplankton grazing rate and the viral lysis rate can be obtained. From the difference between the two dilutions series the actual virally mediated algal mortality rate can be calculated. Grazer-free diluent was prepared using a 0.45 µm Sartopore filter (by gravity filtration), and the grazer and virus-free diluent was prepared using a 30 kDa tangential flow cartridge (Vivaflow 200) after prefiltration through 0.45 µm. The dilutions aimed for were 20,

40, 70 and 100% whole water (triplicate 1L PC bottles for each dilution factor and series; see Figure 2). The filled bottles (no air bubbles) were incubated on a slow turning wheel at in-situ temperature and light conditions. From each bottle, a T0h and T24h sample for phytoplankton was obtained, and either counted fresh or fixed with formaline/hexamine.

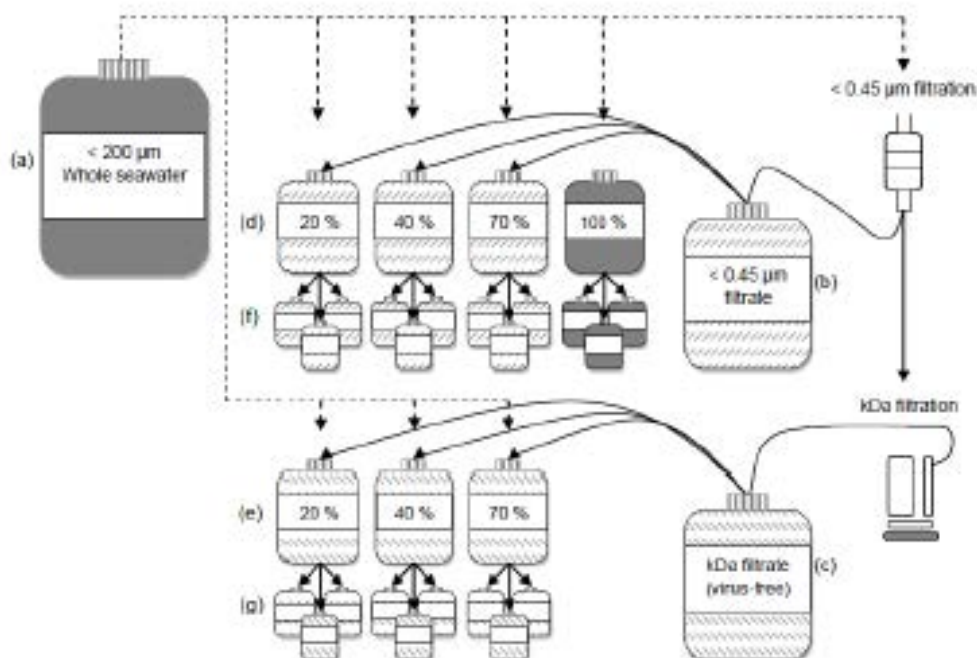


Figure 2: Experimental design of the modified dilution approach. Mesoplankton-free whole seawater (a) was combined with either < 0.45 μm filtrate (b) or 30 kDa filtrate (c) in the correct proportions to create the parallel to dilution series: < 0.45 μm series, with reduced grazing mortality (d) kDa series, with reduced grazing and viral mortality (e). Replicate sample bottles from the < 0.45 μm and kDa dilution series were then created (f and g) and incubated under experimental conditions.

Besides viral lysis rates of phytoplankton, we also determined viral lysis rates of the bacterial hosts (Winget et al., 2015). Here the principle of the method is based on the increase of newly released viruses (from the bacterial hosts) over time. Using this viral production assay, the natural viruses present were washed out after which the newly produced viruses released from formerly infected bacteria were counted over time. From the production rate, the infection rate of bacteria can be calculated. Additionally, rates of lysogenic infection were determined by addition of Mitomycin C to initiate the lytic phase of any lysogenic viruses that have infected the bacterial population. Filtrations and incubations were performed in a temperature controlled room at 1°C under low light conditions and darkness, respectively. Subsamples for viruses were taken after 0, 3, 6, 9, 12, and 24h and fixed with glutaraldehyde (0.5% final conc) after which they were flash frozen in liquid nitrogen and stored at -80°C . Samples will be analysed in the home lab (NIOZ).

Besides sampling along a natural gradient in nutrient concentrations (iron), we also sampled for fine sediments from shelf ice melt. Since sediment can act as a nucleation point for viruses, sediment filtrations were conducted for most stations where also sampling for viral lysis rates of bacteria was performed.

Additionally to sampling using the ultraclean CTD on stations, microbial abundances and metagenomics sampling were performed during the transit (surface samples were sampled from the ship's internal surface-seawater supply; see Table 5.4). We also took sea-ice samples at the sea-ice camp.

For the bioassays the sampled parameters were microbial abundances (daily), viral lysis of microbes (start and end), phytoplankton pigments (start and end).

Table 5.5: Stations sampled for viral lysis rate measurements and viral production. Additional viral lysis measurements were conducted at the end of bioassay incubations. Bioassay starting stations are marked with an asterix.

Station #	Viral lysis	Viral production
1	X	X
4	X	X
10	X	X
11*	X	X
12		X
18		X
22		X
31*	X	X
33	X	X
34		X
36	X	X
42	X	X
45	X	X
46		X
49	X	X
53	X	X
52*	X	X
55	X	X
55 ice		X
24		X
56	X	X

References

- Arrigo, K.R., 2005. Marine microorganisms and global nutrient cycles. *Nature* 437, 349-355.
- Arrigo, K.R., van Dijken, G.L., 2003. Phytoplankton dynamics within 37 Antarctic coastal polynya systems. *Journal of Geophysical Research-Oceans* 108.
- Arrigo, K.R., van Dijken, G., Long, M., 2008. Coastal Southern Ocean: A strong anthropogenic CO₂ sink. *Geophys. Res. Lett.* 35.
- Bertrand, E.M. *et al.* 2012. Influence of cobalamin scarcity on diatom molecular physiology and identification of a cobalamin acquisition protein. *PNAS*. 109: 1762-1771
- Boiteau, R.M., Fitzsimmons, J.N., Repeta, D.J., Boyle, E.A., 2013. Detection of Iron Ligands in Seawater and Marine Cyanobacteria Cultures by High-Performance Liquid Chromatography-Inductively Coupled Plasma-Mass Spectrometry. *Anal. Chem.* 85, 4357-4362.
- Bonnain, C., Breitbart, M., Buck, K.N., 2016. The Ferrojan Horse Hypothesis: Iron-Virus Interactions in the Ocean. *Frontiers in Marine Science* 3.
- Boyd, P.W., Ellwood, M.J., 2010. The biogeochemical cycle of iron in the ocean. *Nature Geoscience* 3, 675-682.
- Boye, M., Nishioka, J., Croot, P.L., Laan, P., Timmermans, K.R., de Baar, H.J.W., 2005. Major deviations of iron complexation during 22 days of a mesoscale iron enrichment in the open Southern Ocean. *Mar. Chem.* 96, 257-271.
- Bruland, K.W., Middag, R., Lohan, M.C., 2014. Controls of Trace Metals in Seawater, in: Holland H.D, a.T.K.K. (Ed.), *Treatise on Geochemistry* 2nd edition, pp. 19-55.
- Buck, K.N., Bruland, K.W., 2007. The physicochemical speciation of dissolved iron in the Bering Sea, Alaska. *Limnol. Oceanogr.* 52, 1800-1808.

- Croot, P.L., Andersson, K., Öztürk, M., Turner, D.R., 2004. The distribution and speciation of iron along 6°E in the Southern Ocean. *Deep Sea Research Part II: Topical Studies in Oceanography* 51, 2857-2879.
- De Baar, H.J.W., Timmermans, K.R., Laan, P., De Porto, H.H., Ober, S., Blom, J.J., Bakker, M.C., Schilling, J., Sarthou, G., Smit, M.G., Klunder, M., 2008. Titan: A new facility for ultraclean sampling of trace elements and isotopes in the deep oceans in the international Geotraces program. *Mar. Chem.* 111, 4-21.
- De Jong, J.T.M., den Das, J., Bathmann, U., Stoll, M.H.C., Kattner, G., Nolting, R.F., de Baar, H.J.W., 1998. Dissolved iron at subnanomolar levels in the Southern Ocean as determined by ship-board analysis. *Anal. Chim. Acta* 377, 113-124.
- De Jong, J.T.M., Stammerjohn, S.E., Ackley, S.F., Tison, J.L., Mattielli, N., Schoemann, V., 2015. Sources and fluxes of dissolved iron in the Bellingshausen Sea (West Antarctica): The importance of sea ice, icebergs and the continental margin. *Mar. Chem.* 177, Part 3, 518-535.
- De La Rocha, C.L., 2007. 6.04 - The Biological Pump, in: Holland, H.D., Turekian, K.K. (Eds.), *Treatise on Geochemistry*. Pergamon, Oxford, pp. 1-29.
- Evans C, Archer SD, Jacquet S, Wilson WH (2003) Direct estimates of the contribution of viral lysis and microzooplankton grazing to the decline of a *Micromonas* spp. Population. *Aquat Microb Ecol* 30:207-219
- Gerringa, L.J.A., Alderkamp, A.-C., Laan, P., Thuroczy, C.-E., De Baar, H.J.W., Mills, M.M., van Dijken, G.L., van Haren, H., Arrigo, K.R., 2012. Iron from melting glaciers fuels the phytoplankton blooms in Amundsen Sea (Southern Ocean): Iron biogeochemistry. *Deep-Sea Research Part II-Topical Studies in Oceanography* 71-76, 16-31.
- Gerringa, L.J.A., Laan, P., van Dijken, G.L., van Haren, H., De Baar, H.J.W., Arrigo, K.R., Alderkamp, A.C., 2015. Sources of iron in the Ross Sea Polynya in early summer. *Mar. Chem.* 177, Part 3, 447-459.
- Gledhill, M., 1994. Determination of complexation of iron(III) with natural organic complexing ligands in seawater using cathodic stripping voltammetry. *Mar. Chem.* 47, 41-54.
- Hassler, C.S., Schoemann, V., Nichols, C.M., Butler, E.C.V., Boyd, P.W., 2011. Saccharides enhance iron bioavailability to Southern Ocean phytoplankton. *Proceedings of the National Academy of Sciences* 108, 1076-1081.
- Hunter, K.A., Boyd, P.W., 2007. Iron-binding ligands and their role in the ocean biogeochemistry of iron. *Environmental Chemistry* 4, 221-232.
- Johnson, K.S., Elrod, V., Fitzwater, S., Plant, J., Boyle, E., Bergquist, B., Bruland, K., Aguilar-Islas, A., Buck, K., Lohan, M., Smith, G.J., Sohst, B., Coale, K., Gordon, M., Tanner, S., Measures, C., Moffett, J., Barbeau, K., King, A., Bowie, A., Chase, Z., Cullen, J., Laan, P., Landing, W., Mendez, J., Milne, A., Obata, H., Doi, T., Ossiander, L., Sarthou, G., Sedwick, P., Van den Berg, S., Laglera-Baquer, L., Wu, J.-f., Cai, Y., 2007. Developing standards for dissolved iron in seawater. *Eos, Transactions American Geophysical Union* 88, 131-132.
- Alderkamp, A.-C., Mills, M.M., van Dijken, G.L., Laan, P., Thuroczy, C.-E., Gerringa, L.J.A., de Baar, H.J.W., Payne, C.D., Visser, R.J.W., Buma, A.G.J., Arrigo, K.R., 2012. Iron from melting glaciers fuels phytoplankton blooms in the Amundsen Sea (Southern Ocean): Phytoplankton characteristics and productivity. *Deep-Sea Research Part II-Topical Studies in Oceanography* 71-76, 32-48.
- Joughin, I., Smith, B.E., Medley, B., 2014. Marine Ice Sheet Collapse Potentially Under Way for the Thwaites Glacier Basin, West Antarctica. *Science* 344, 735-738.
- Klunder, M.B., Laan, P., De Baar, H.J.W., Middag, R., Neven, I., Van Ooijen, J., 2014. Dissolved Fe across the Weddell Sea and Drake Passage: impact of DFe on nutrient uptake. *Biogeosciences* 11, 651-669.
- LaRoche, J., *et al.* 1996. Flavodoxin as an *in situ* marker for iron stress in phytoplankton. *Nature*. 382: 802-805.
- Maldonado, M.T., Strzepek, R.F., Sander, S., Boyd, P.W., 2005. Acquisition of iron bound to strong organic complexes, with different Fe binding groups and photochemical reactivities, by plankton communities in Fe-limited subantarctic waters. *Global Biogeochem. Cycles* 19.
- Middag, R., de Baar, H.J.W., Laan, P., Cai, P.H., van Ooijen, J.C., 2011. Dissolved manganese in the Atlantic sector of the Southern Ocean. *Deep-Sea Research Part II-Topical Studies in Oceanography* 58, 2661-2677.
- Middag, R., de Baar, H.J.W., Laan, P., Huhn, O., 2012. The effects of continental margins and water mass circulation on the distribution of dissolved aluminum and manganese in Drake Passage. *Journal of Geophysical Research-Oceans* 117.
- Middag, R., de Baar, H.J.W., Klunder, M.B., Laan, P., 2013. Fluxes of dissolved aluminum and manganese to the Weddell Sea and indications for manganese co-limitation. *Limnol. Oceanogr.* 58, 287-300.

- Mojica, K. D. A., Huisman, J., Wilhelm, S. W. & Brussaard, C. P. D. (2016) Latitudinal variation in virus-induced mortality of phytoplankton across the North Atlantic Ocean. *ISME J* 10, 500-513
- Moore, C.M., Mills, M.M., Arrigo, K.R., Berman-Frank, I., Bopp, L., Boyd, P.W., Galbraith, E.D., Geider, R.J., Guieu, C., Jaccard, S.L., Jickells, T.D., La Roche, J., Lenton, T.M., Mahowald, N.M., Maranon, E., Marinov, I., Moore, J.K., Nakatsuka, T., Oschlies, A., Saito, M.A., Thingstad, T.F., Tsuda, A., Ulloa, O., 2013. Processes and patterns of oceanic nutrient limitation. *Nature Geoscience* 6, 701-710.
- Morel, F.M.M., Milligan, A.J., Saito, M.A., 2014. 8.5 - Marine Bioinorganic Chemistry: The Role of Trace Metals in the Oceanic Cycles of Major Nutrients, in: Holland, H.D., Turekian, K.K. (Eds.), *Treatise on Geochemistry (Second Edition)*. Elsevier, Oxford, pp. 123-150.
- Rignot, E., Mouginot, J., Morlighem, M., Seroussi, H., Scheuchl, B., 2014. Widespread, rapid grounding line retreat of Pine Island, Thwaites, Smith, and Kohler glaciers, West Antarctica, from 1992 to 2011. *Geophys. Res. Lett.*, n/a-n/a.
- Saito, M.A., Goepfert, T.J., Ritt, J.T., 2008. Some thoughts on the concept of colimitation: Three definitions and the importance of bioavailability. *Limnol. Oceanogr.* 53, 276-290.
- Slagter, H.A., Gerringa, L.J.A., Brussaard, C.P.D., 2016. Phytoplankton Virus Production Negatively Affected by Iron Limitation. *Frontiers in Marine Science* 3.
- Suttle, C (2008) Marine viruses — major players in the global ecosystem. *Nature Reviews Microbiology* 5: 801 – 812
- Thuroczy, C.E., Gerringa, L.J.A., Klunder, M.B., Middag, R., Laan, P., Timmermans, K.R., de Baar, H.J.W., 2010. Speciation of Fe in the Eastern North Atlantic Ocean. *Deep-Sea Research Part I-Oceanographic Research Papers* 57, 1444-1453.
- Wadham, J.L., De'ath, R., Monteiro, F.M., Tranter, M., Ridgwell, A., Raiswell, R., Tulaczyk, S., 2013. The potential role of the Antarctic Ice Sheet in global biogeochemical cycles. *Earth and Environmental Science Transactions of the Royal Society of Edinburgh* 104, 55-67.
- Winget, D. M., Williamson, K. E., Helton, R. R. & Wommack, K. E. (2005) Tangential flow diafiltration: an improved technique for estimation of virioplankton production. *Aquat. Microb. Ecol.* 41, 221-232

Appendix I. Cruise participants and contact information

	Name	Affiliation	Email
1	SangHoon Lee	Korea Polar Research Institute, Korea	shlee@kopri.re.kr
2	Kyoung-Ho Cho	Korea Polar Research Institute, Korea	kcho@kopri.re.kr
3	Tae-Wan Kim	Korea Polar Research Institute, Korea	twkim@kopri.re.kr
4	Taewook Park	Korea Polar Research Institute, Korea	twpark@kopri.re.kr
5	Jinyoung Jung	Korea Polar Research Institute, Korea	jinyoungjung@kopri.re.kr
6	Hyoung Sul La	Korea Polar Research Institute, Korea	hsla@kopri.re.kr
7	Hyuung Min Joo	Korea Polar Research Institute, Korea	hmjoo77@kopri.re.kr
8	Youngju Lee	Korea Polar Research Institute, Korea	yjulee@kopri.re.kr
9	So-Young Kim	Korea Polar Research Institute, Korea	kimsy@kopri.re.kr
10	Hee Won Yang	Korea Polar Research Institute, Korea	yhw@kopri.re.kr
11	Eunho Ko	Korea Polar Research Institute, Korea	ehko@kopri.re.kr
12	Yeonggi Kim	Korea Polar Research Institute, Korea	ygkim@kopri.re.kr
13	Wuju Son	Korea Polar Research Institute, Korea	swj5753@kopri.re.kr
14	Jineui Son	Korea Polar Research Institute, Korea	bourne0@kopri.re.kr
15	Jong Kuk Moon	Korea Polar Research Institute, Korea	jkmoon@kopri.re.kr
16	Chang Jin Lee	Korea Polar Research Institute, Korea	eoqh14@nate.com
17	Min-kyung Kim	Seoul National University, Korea	mini324@snu.ac.kr
18	Ye Won Kim	Korea Institute of Ocean Science and Technology	yewonkim@kiost.ac.kr
19	Woon-Yong Yu	Chungbuk National University, Korea	blueplussj@naver.com
20	Taxoo Chung	Chungbuk National University, Korea	vitav@naver.com
21	Doshik Hahm	Pusan National University, Korea	hahm@pusan.ac.kr
22	Dong-youb Shin	Pusan National University, Korea	ehdduq5662@gmail.com
23	Yu Jung Lim	Pusan National University, Korea	yjlim@pusan.ac.kr
24	You Dong Cho	Korean Alpine Club	youdong@hanmail.net
25	Suk Hyun Haam	NEOSEA Tec.	Haam6481@gmail.com
26	Thomas G. Richter	University of Texas at Austin, USA	Tom.richter@utexas.edu
27	Dillon Buhl	University of Texas at Austin, USA	dillon.buhl@utexas.edu
28	Lucas Beem	University of Texas at Austin, USA	lhbeem@gmail.com
29	Jason Gobat	University of Wansington, USA	jgobat@uw.edu
30	Jhon Mojica	NYU Abu Dhabi Campus, USA	jfm11@nyu.edu
31	Johan Rolandsson	University of Gothenburg, Sweden	johan.rolandsson@mmt.se
32	Karen Assmann	University of Gothenburg, Sweden	karen.assmann@marine.gu.se
33	Isabelle Durand	LOCEAN, Museum of Natural History, France	idurand@mnhn.fr
34	Pierre Dutrieux	Columbia University. USA	pierred@ldeo.columbia.edu
35	Rob Middag	Royal Netherlands Institute for Sea Research, Netherlands	rob.middag@nioz.nl
36	Sven Hubertus	Royal Netherlands Institute for Sea Research, Netherlands	sven.pont@gmail.com
37	Matis van Manen	Royal Netherlands Institute for Sea Research, Netherlands	Mathijs.van.manen@nioz.nl
38	Hung-An Tian	Royal Netherlands Institute for Sea Research, Netherlands	hatian1018@gmail.com
39	Charlotte Eich	Royal Netherlands Institute for Sea Research Netherlands	maria.eich@nioz.nl
40	James McCain	Dalhousie University, Canada	j.scott.mccain@dal.ca

Appendix II. Group photo

